TECHNISCHE UNIVERSITÄT MÜNCHEN

Lehrstuhl für Bioverfahrenstechnik

Protein Crystallization
in Stirred-Tank Reactors

Dirk Peter Hebel

Vollständiger Abdruck der von der Fakultät für Maschinenwesen der Technischen

Universität München zur Erlangung des akademischen Grades eines

Doktors der Naturwissenschaften

genehmigten Dissertation.

Acknowledgements

Table of contents

1 Introduction

Biotechnology has unknowingly been applied by mankind, e.g., for the production of cheese, curd, or beer, long before the term was actually coined by an Hungarian engineer in 1917 (Rao, 2008). Starting in the 19th century, the foundation was laid for modern biotechnology by research including Mendel's laws of inheritance, Koch's work with bacteria and Fleming's discovery of antibiotics. Subsequently, continuous research efforts led to the availability of various versatile tools for modern biotechnology, e.g., for the alteration and cloning of genes (Figure 1.1) (Verma *et al.*, 2011).
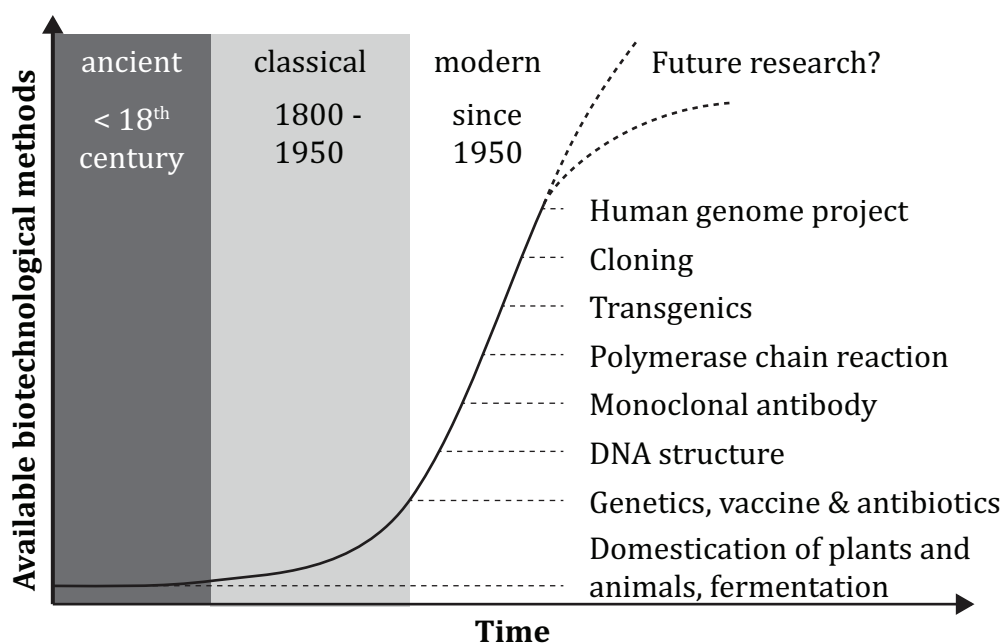
Figure 1.1: Schematic illustration of the history of biotechnology, highlighting important developments (modified from Verma *et al.*, 2011).

With increasing complexity, biotechnology was divided into branches according to the respective applications as listed in Table 1.1.

Table 1.1: Branches of modern biotechnology.

Application	Color code
Industrial biotechnology	white
Pharmaceutical biotechnology	red
Environmental biotechnology and/or waste processing	brown / grey
Agricultural biotechnology	green
Food biotechnology	yellow
Marine biotechnology	blue

Economically, two branches of biotechnology are of special interest: red and white biotechnology. For red biotechnology, the classical product line of low-molecular drugs can be augmented by protein-based drugs, with research focused on antibodies in the last decade. These proteins originate from the immune system of vertebrates and can be tailored to neutralize specific targets using modern biotechnology tools (Chowdhury and Wu, 2005). For white biotechnology, two major applications are of importance. First, biocatalyses often exhibit higher enantioselectivities than traditional chemical syntheses and can consequently be used to increase yields and to reduce the formation of unwanted byproducts (Müller *et al.*, 2005). Next, white biotechnology provides an alternative for the sustainable production of bulk chemicals and fine chemicals. The proposed biorefineries use renewable ressources, whereas the current petrochemical industry heavily relies on fossil materials with limited availability, i.e., oil, gas and coal (Kamm and Kamm, 2007).

2   Thesis motivation and objectives

The worldwide demand for high-valued biotechnologically produced proteins has increased over the past years and is expected to grow significantly in the future (Strohl and Knight, 2009). In order to satisfy this increasing demand, the production processes for proteins, especially for therapeutic proteins, have been optimized with regard to higher protein concentrations over the past years. However, this development created a bottleneck in the subsequent downstream processing which currently heavily relies on costly preparative chromatography steps (Shukla and Thömmes, 2010). Hence, alternative purification technologies need to be established (Kelley, 2009; Low *et al.*, 2007). Current research on alternative purification technologies follows diverse approaches, e.g., aqueous two-phase extraction, magnetic adsorbent particles, membrane-based techniques, and protein crystallization (Asenjo and Andrews, 2012; Franzreb *et al.*, 2006; Saxena *et al.*, 2009).

Crystalline proteins offer advantages regarding product activity and product stability. Therefore, protein crystallization can also overcome some drawbacks of the current protein formulations, i.e., primarily aqueous solutions or amorphous precipitated lyophilisates (Basu *et al.*, 2004; Manning *et al.*, 2010; Yang *et al.*, 2003). A significant cost reduction is expected compared to conventional preparative chromatography methods. While protein crystallization is best known for its use in protein structure determination, the technical-scale application for protein purification is limited to very few examples. The most prominent one is the stirred batch crystallization of the polypeptide insulin with volumes up to 500 L (Basu *et al.*, 2004; Harrison *et al.*, 2003; Schlichtkrull, 1957).

For larger biomolecules, the feasibility of protein purification by large-scale protein crystallization has been demonstrated in a limited number of research projects (Astier and Veesler, 2008; Jacobsen *et al.*, 1998; Judge *et al.*, 1995; Lee *et al.*, 2000; Matthews and Bean, 2006; Schmidt *et al.*, 2005; Takakura *et al.*, 2006). Only few of these studies were performed in well-defined, scalable stirred vessels. In addition, low yields and rather long process times were often observed. Hence, more research is necessary in order to establish large-scale protein crystallization as a viable alternative to common purification techniques.

This thesis investigates the crystallization of five different proteins from pure solutions in scalable stirred-tank reactors. The aim was to first evaluate the transfer of the usually used µL-scale vapor diffusion and/or microbatch crystallization conditions into parallel operated 5 mL-scale stirred-tank reactors. Afterwards, the crystallization processes should be characterized and improved regarding the crystallization yield and the crystallization kinetics using the 5 mL-scale reactors. The effects of new crystallization additives on protein crystallization from pure solutions should be investigated. Subsequently, the optimized crystallization conditions should be scaled up to 100 mL- and 1 L-scale stirred-tanks.

The individual tasks of this thesis were to:

- Design scaled-down 5 mL- and 100 mL-scale versions of a commercially available 1 L-scale stirred-tank reactor for the characterization of protein crystallization processes;
- Screen for and/or validate crystallization conditions for five structurally different proteins (lysozyme, lipase, xylanase, glucose isomerase, and a Fab fragment) in µL-scale vapor diffusion and/or microbatch crystallization experiments;
- Use screening to derive phase diagrams for the crystallization of the proteins under study;
- Transfer suitable crystallization conditions for each protein into the 5 mL-scale stirred-tank reactors to characterize and improve the crystallization yield and the crystallization kinetics on the 5 mL-scale;
- Evaluate new crystallization additives, e.g., ionic liquids, to study their effect on the crystallization yield and the crystallization kinetics;
- Transfer the improved crystallization processes into the 1 L-scale stirred-tank reactor; and
- Characterize and remove impurities from protein crystals.

3   Theoretical background

3.1   Proteins

3.1.1 Fundamentals

Proteins are a class of biological macromolecules. They are polypeptides built from 20 different amino acids, with the largest protein known so far, titin, consisting of over 30 000 residues (Bang *et al.*, 2001). While most proteins are way smaller with an average length of 361 residues for eukaryotes and 267 residues for bacteria (Brocchieri and Karlin, 2005), they still offer a vast structural and functional diversity. The availability of modern molecular tools for the cloning and the engineering of proteins has further increased this diversity. Proteins from organisms, that are difficult to cultivate or produce undesirable by-products, can be cloned into and expressed in common host organisms like *Escherichia coli* or Chinese hamster ovary (CHO) cells. The nucleotide sequence encoding the amino acid sequence of a protein can be altered in order to obtain new variants of a protein, e.g., featuring a higher activity, a higher stability or improved binding characteristics.

Today, proteins are becoming increasingly important for the industry. White biotechnology focuses on the use of enzymes as catalysts for biochemical reactions, whereas red biotechnology hopes to find promising therapeutic proteins for diseases that cannot be cured so far. Common applications in white biotechnology rely on whole-cell biocatalysis or rudimentarily purified protein solutions. In contrast, therapeutic proteins have to be free of contaminants for their application on a patient. Furthermore, therapeutic proteins need to be stored without significant loss of activity. Current and future techniques for the purification, formulation, and storage of proteins are detailed in the following chapters.

3.1.2 Purification techniques

Usually, biotechnologically produced proteins need to be separated from cell debris and components of the cells including nucleic acids, lipids, carbohydrates, and other proteins present in the culture broth. This often requires a cascade of different purification steps ranging from simple filtration techniques to costly, highly-selective chromatographic methods. An overview of the methods used in the different stages of downstream processing is given in Figure 3.1.
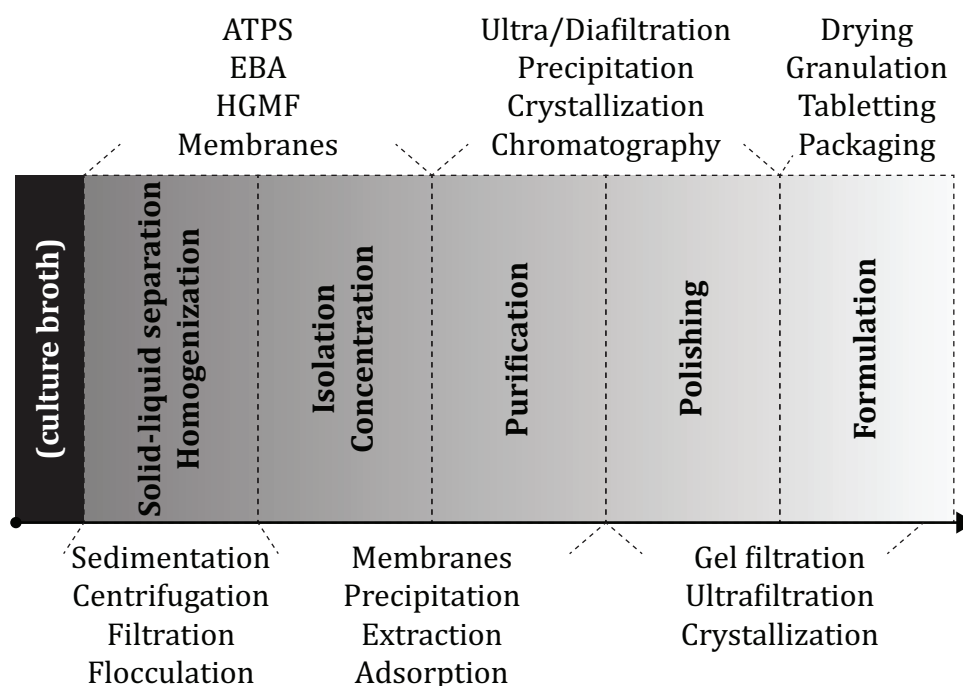
Figure 3.1: Overview of the techniques usually employed in the different stages of downstream processing (modified from Hubbuch and Kula, 2007). **ATPS:** aqueous two-phase separation; **EBA**: expanded bed adsorption; **HGMF:** high-gradient magnetic fishing.

While some proteins for the white biotechnology are only rudimentarily purified, high purities are imperative for therapeutic proteins, e.g., monoclonal antibodies (Low *et al.*, 2007; Shukla and Thömmes, 2010; Shukla *et al.*, 2007). Thus, the costs for downstream processing can take up to 90 % of the total production costs (Farid, 2007; Kasche and De Boer, 2000). The number of reviews outlining recent trends in the downstream processing of proteins, especially of therapeutic proteins like monoclonal antibodies, reflects the importance of this field of research (Gagnon, 2012; Hubbuch and Kula, 2007; Kelley, 2007; Przybycien *et al.*, 2004; Shukla and Thömmes, 2010; Shukla *et al.*, 2007; Weuster-Botz *et al.*, 2007). The following paragraphs give an overview over the current large-scale purification techniques as well as some promising future concepts.

Chromatography

Chromatography operations are commonly used for the initial purification and the subsequent polishing of proteins. This type of purification is based on the (preferably selective) binding of a portion of the proteins to the chromatography medium, while the remainder flows through the column. Subsequently, the proteins bound to the matrix can be eluted from the column by changing the mobile phase. A variety of chromatography media allow for different modes of purification to be employed using the same hardware. Common chromatography modes include gel filtration, ion exchange, hydrophobic interaction, and reverse phase chromatography (Gagnon, 2012). In gel filtration, the proteins do not bind to the column, but are separated by their molecular volume. Ion exchange chromatography separates the molecules by their charge. Depending on the functional groups of the chromatography medium, cations or anions bind to the column. Additionally, the charge of the proteins can be influenced by the pH of the mobile phase. The mode of separation in hydrophobic interaction chromatography is based upon the hydrophobic effect, which drives the adsorption of hydrophobic areas of the protein to the hydrophobic solid phase. More specialized chromatography media are derivatized with functional ligands allowing for highly-selective affinity chromatography, e.g., protein A chromatography for the purification of monoclonal antibodies.

All chromatography processes are usually limited by mass-transport, as the proteins need to diffuse into the pores of the chromatography medium in order to bind. The time needed for a complete cycle including the loading of the crude material, the elution of the target protein and the subsequent cleaning and equilibration of the column is rather long. This limits the throughput of chromatography processes and multiple chromatography columns are needed for the purification of larger amounts of protein. Also, the long-term use of chromatography media may lead to inferior results due to a deteriorated chromatography bed. Thus, chromatography media need to be exchanged regularly, which causes high costs, especially for affinity chromatography media (Hekmat *et al.*, 2011; Shukla and Thömmes, 2010; Weuster-Botz *et al.*, 2007).

Recent developments focused on overcoming some of the current drawbacks of chromatography processes. For example, expanded bed chromatography allows for the fast adsorption of proteins from unclarified crude material. Several applications

including the pilot-scale recovery of a protein are reported (Bermejo and Ramos, 2012; Yap *et al.*, 2010). Despite of these efforts to accelerate chromatography processes, diffusion into the pores remains the limiting step. The lifetime of the matrix may be reduced due to the necessity of more aggressive cleaning in place (CIP) procedures (Curbelo *et al.*, 2003). Also, protein A affinity chromatography, which currently plays a key role in the downstream processing of monoclonal antibodies, has undergone a number of improvements over the past years. Both the dynamic binding capacity and the lifespan of protein A chromatography media has been significantly improved (Brorson *et al.*, 2003; Jiang *et al.*, 2009; Rogers *et al.*, 2009). The use of monoliths instead of conventional chromatography beds offers some advantages, e.g., a lower backpressure at high flow-rates (Roberts *et al.*, 2009). However, no large-scale applications of protein purification using monoliths have been reported so far (Weuster-Botz *et al.*, 2007).

Membrane adsorbers or membrane chromatography is a special method of chromatography using functionalized membranes instead of packed beds. Thus, membrane chromatography enables the rapid processing of large volumes of dilute feedstreams, either as initial purification or as polishing step (Brandt *et al.*, 1988; Gottschalk, 2005; Hubbuch and Kula, 2007; Knudsen *et al.*, 2001). Even though, the applications are limited either to the polishing of concentrated protein solutions or the capture and concentration of a protein.

Aqueous two-phase separation

Aqueous two-phase separation (ATPS) is based on the different distribution of proteins in two liquid phases according to their partition coefficients (Equation 1).

$$K = \frac{c_T}{c_B} \hspace{3cm} \textit{(Equation 1)}$$

with	*K*	*partition coefficient*	-
	c_T	*concentration in the top phase*	*g L⁻¹*
	c_B	*concentration in the bottom phase*	*g L⁻¹*

Usually, aqueous polymer two-phase systems based on polyethylene glycol (PEG) and a salt, e.g., a sulfate, are used. For enzymes, no loss of activity is reported (Albertsson, 1961). The existence of mathematical models and continuous settlers allow for the

scale-up of this technology (Asenjo and Andrews, 2011, 2012). Rosa *et al.* (2009) reported the purification of a monoclonal antibody with 89 % yield and 75 % purity in a multi-stage ATPS process. A prominent example for the large-scale application of ATPS is the isolation of insulin-like growth factor I (IGF1) from cellular biomass with a cumulative yield of 70 % and a purity of 97 % (Hart *et al.*, 1994).

Magnetic adsorbent particles

Due to their unique properties, magnetic particles can be rapidly and highly selective removed from solutions. As magnetic particles can be derivatized with ligands already used in chromatography, they can be applied in many different stages of downstream processing. Protein purification using magnetic adsorbents in combination with high-gradient magnetic separation is known as high-gradient magnetic fishing (HGMF) (Hubbuch *et al.*, 2001). First, batch-based adsorption and elution of the target proteins was used, and pilot plants for volumes up to 100 L were built (Holschuh and Schwämmle, 2005). More recent work focused on continuous magnetic separation in combination with aqueous micellar two-phase systems (AMTPS) and the recycling of the magnetic particles (Fischer and Franzreb, 2011a, 2011b, 2012; Lee *et al.*, 2011). In 2006, the technology was expected to be commercially employed within the next 5 to 10 years. However, current disadvantages, especially the high price of today's generations of commercial adsorbents, limit the large-scale use of this technology (Franzreb *et al.*, 2006).

Foam fractionation

While foam formation is undesirable for many bioprocesses (Vardar-Sukan, 1998), it can be used for protein capture from crude material containing low protein concentrations (Maruyama *et al.*, 2007). Therefore, the feed solution is usually aerated, leading to the adsorption of surface-active substances to the gas-liquid interface. The bubbles formed during this process emerge into a foam fractionation column. The enriched foam is collected at the top of the column and collapsed in order to receive a solution containing the target molecule (Linke *et al.*, 2005). Approaches for continuous foam fractionation have been studied (Merz *et al.*, 2011). However, protein denaturation at the gas-liquid interface has sometimes been observed (Maruyama *et al.*, 2007) and, as of now, only laboratory-scale foam fractionation setups are described in the literature.

Filtration

Many stages in the downstream processing can be performed using various filtration techniques. Some methods for the initial protein capture require the removal of the cells from the crude material. Also, the purified protein solution is often sterile filtrated prior to formulation and, for therapeutic proteins, virus particles can be removed by filtration. Classical tangential-flow microfiltration is employed in favor of dead-end filtration. However, initial cell removal is often achieved using disk separators. Ultrafiltration and diafiltration can be employed for the concentration of protein solutions and buffer exchange, respectively (Bolton *et al.*, 2005; Hubbuch and Kula, 2007; van Reis and Zydney, 2001). A specialized application of filtration is the use of membrane adsorbers which is often described as a variant of chromatography. Thus, this technique is discussed in the paragraph regarding chromatography.

Precipitation

Precipitation is the transfer of a substance from a solution to a solid form. Therefore, precipitation can be used for protein separation, yielding a solid phase of very high protein concentration. While precipitation-based concentration steps have been often replaced by ultrafiltration for environmental reasons (Hubbuch and Kula, 2007), the method is still of interest as initial capture step due to its purification potential. The resulting high protein concentrations can have benefits for the subsequent purification steps (Gagnon, 2012; Low *et al.*, 2007). McDonald *et al.* (2009) reported the capture of an antibody with 82 % recovery and about 80 % removal of host cell protein. Tscheliessnig *et al.* (2009) purified 9 monoclonal immunoglobulin Ms (IgMs) by a combination of PEG precipitation and anion exchange chromatography with purities > 95 % for 7 immunoglobulin Ms (IgMs). A model for the calculation of the precipitation efficiency of proteins using PEGs was recently proposed (Sim *et al.*, 2012). One drawback of precipitation is the need for expensive centrifuges for the separation of the precipitate (Gagnon, 2012; McDonald *et al.*, 2009).

Protein crystallization

The special case of precipitation with the formation of a crystalline solid phase is referred to as protein crystallization. Similar to precipitation, low-cost crystallization agents, e.g., salts or PEGs, are used to generate supersaturation, thus reducing the costs for downstream processing. As crystalline proteins feature a very high purity, protein

crystallization can substitute purification and polishing steps (Przybycien *et al.*, 2004; Weuster-Botz *et al.*, 2007). The first technical application of protein crystallization was the stirred batch crystallization of the polypeptide insulin with volumes up to 500 L (Basu *et al.*, 2004; Harrison *et al.*, 2003; Schlichtkrull, 1957). For larger biomolecules, the feasibility of protein purification by large-scale protein crystallization has been demonstrated in a limited number of research projects (Astier and Veesler, 2008; Jacobsen *et al.*, 1998; Judge *et al.*, 1995; Lee *et al.*, 2000; Matthews and Bean, 2006; Schmidt *et al.*, 2005; Takakura *et al.*, 2006). However, only few of these studies were performed in well-defined, scalable stirred vessels. In addition, low yields and rather long process durations were often observed. The mechanisms and methods for protein crystallization shall be further discussed in chapter 3.2.

Concluding remarks

Most proteins are purified using well established chromatography methods with high yields and purities. Especially for therapeutic proteins, filtration steps and membrane-based techniques often complement the chromatographic purification. As the protein concentrations obtained in production processes increase, it is unclear, whether conventional packed bed chromatography will be able to deal with the increased protein load. Hence, some of the alternative purification techniques presented in this chapter may be employed in the future, the most promising being ATPS, (selective) precipitation, membrane chromatography and protein crystallization (Shukla and Thömmes, 2010). Due to the previously described limitations of precipitation and membrane chromatography, ATPS and protein crystallization remain as viable alternative purification methods.

3.1.3   Formulation and storage

Currently, proteins are usually stored as concentrated aqueous solutions or amorphous precipitated lyophilisates. An ultrafiltration/diafiltration setup is the method of choice for the buffer exchange into the formulation buffer and the subsequent concentration. For some therapeutic proteins, high dosages require the use of high protein concentrations, thus causing problems with an increased viscosity and protein aggregation. Moreover, the storage of large volumes of protein solution at -80 °C is very costly. The lyophilisates are obtained using spray drying or freeze drying. For both aqueous solutions and lyophilisates, additives or excipients are commonly used to

increase the stability of the product and its shelf life. Nevertheless, a reduction of activity is often observed and excipients may be unfavorable for pharmaceutical applications (Andya *et al.*, 2003; Hubbuch and Kula, 2007; Manning *et al.*, 2010; Shukla *et al.*, 2007; Weuster-Botz *et al.*, 2007). Some reagents, i.e., sulfate, should not be included in formulation buffers, as they lead to an increased aggregation of proteins over a wide concentration range (Lewus *et al.*, 2010).

Crystalline proteins offer advantages regarding product activity and product stability, as the protein structure is stabilized in the crystal lattice and the protein molecules are still surrounded by solvent channels. As protein molecules are tightly packed in the crystals, higher concentrations can be obtained at lower viscosities. This is beneficial both for therapeutic applications and protein storage. Hence, protein crystallization is a promising alternative for protein formulation in addition to its possible application for protein purification (Basu *et al.*, 2004; Elkordy *et al.*, 2002, 2004; Margolin and Navia, 2001; Shenoy *et al.*, 2001; Weuster-Botz *et al.*, 2007; Yang *et al.*, 2003).

3.2   Protein crystallization

The process of transferring a substance from a supersaturated solution to a solid crystalline state is called crystallization. Hence, protein crystallization refers to the precipitation of proteins in a crystalline form. Due to the nature of proteins, some techniques employed for obtaining supersaturated solutions of low-molecular substances, e.g., evaporative crystallization, cannot be used for protein crystallization. This chapter details the mechanisms of protein crystallization, the effects of different crystallization agents, additives, and other variables, and techniques for protein crystallization.

3.2.1   Mechanisms

The process of protein crystallization can be divided into the formation of crystal nuclei and their subsequent growth. Consequently, a prerequisite for protein crystallization is the existence of a nucleation zone in the phase diagram of the protein of interest (Figure 3.2). Phase diagrams present an overview of the different states of a protein solution relative to an adjustable parameter, e.g., the temperature or a salt concentration. A comprehensive overview of these parameters is given in chapter 3.2.2. Under conditions below the solubility curve, proteins remain stable in an undersaturated solution. If the

protein concentration and/or the adjustable parameter are varied, the solution may enter supersaturation. Solutions with only a slight supersaturation remain in a metastable state without the occurrence of crystal nucleation or precipitation. However, existing crystal nuclei would continue to grow until the equilibrium at the solubility curve is reached. In the nucleation zone, which may vary in size depending on the protein and the adjustable parameter(s), new crystal nuclei are formed. If the supersaturation is further increased, precipitate formation occurs.
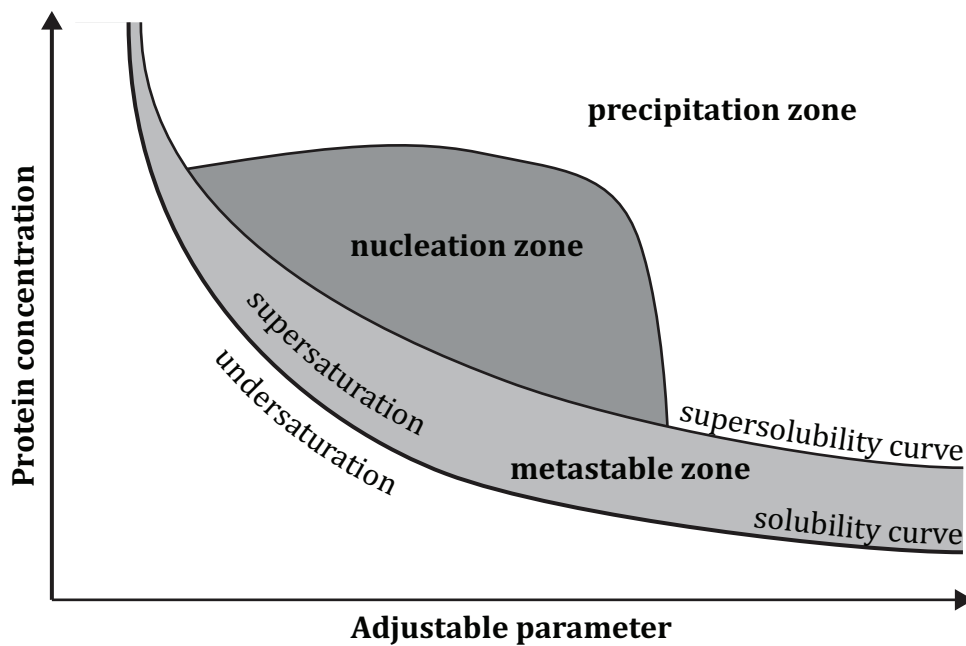
Figure 3.2: Schematic illustration of a protein crystallization phase diagram (modified from Chayen, 2005).

The thermodynamics of protein crystallization and the critical process of crystal nucleation will be further discussed in the following paragraphs.

Thermodynamics of protein crystallization

Protein crystallization is, as any process in nature, governed by ΔG^0, the change of Gibbs free energy. The Gibbs-Helmholtz equation describes the change of ΔG^0_{cryst} as the net effect of the enthalpy ΔH^0_{cryst} and the entropy ΔS^0_{cryst} (Equation 2).

$$\Delta G^0_{cryst} = \Delta H^0_{cryst} - T\Delta S^0_{cryst} \qquad \text{(Equation 2)}$$

For protein crystallization, ΔH^0_{cryst} is often only slightly negative or, in some cases, even positive. For example, a large positive enthalpy of 155 kJ mol^{-1} has been reported for the crystallization of human hemoglobin C. Consequently, the entropy term ΔS^0_{cryst} has to be

positive in order to generate a negative Gibbs free energy. The integration of large protein molecules into the crystal lattice itself causes a reduction of degrees of freedom. Subsequently, the entropy change for the protein molecules is negative. On the contrary, the release of water molecules from the hydration layer of the protein molecules was reported to be largely positive. It is suggested, that water molecules bound to hydrophobic patches of the protein molecules gain entropy upon their release into the bulk water. Hence, the entropy gain of water seems to be the driving force for most protein crystallization processes (Derewenda and Vekilov, 2006; Navarro *et al.*, 2009; Vekilov, 2003). Although a negative Gibbs free energy is an essential prerequisite, it is not the only requirement for protein crystallization. For successful crystal growth, an energy barrier has to be overcome to achieve nucleation.

The role of protein pair interactions

For protein crystallization, protein molecules have to integrate into the crystal lattice. Consequently, the protein molecules get in close contact with each other. The second virial coefficient B_{22} is an integral measure for the strength of these protein pair interactions. Repulsive interactions are reflected by positive values of B_{22}, whereas negative values stand for attractive interactions (Bhamidi *et al.*, 2005). Mild attractive interactions with B_{22} values between $-1 \cdot 10^{-4}$ and $-8 \cdot 10^{-4}$ mol mL g^{-2} were reported as *crystallization slot* (George *et al.*, 1997). A system with B_{22} does not necessarily guarantee crystallization, but the probability of success increases for B_{22} values within this range (Liu *et al.*, 2011). The strength of protein pair interactions can be influenced by many variables including the pH, the crystallization agents and their concentrations, as well as the temperature (Wanka and Peukert, 2011). The effects of different crystallization agents, additives and other variables will be described in chapter 3.2.2.

Classical nucleation theory

Initially developed for the condensation of vapor to liquid, classical nucleation theory (CNT) assumes crystal nuclei to grow continuously. As this does not apply to small protein crystal nuclei, the nucleation rates calculated from equation 3 using the supersaturation and the protein concentration are only valid for larger nuclei (Bhamidi *et al.*, 2002; Erdemir *et al.*, 2009; Galkin and Vekilov, 2001).

$$J = A \cdot c \cdot \exp\left(\frac{-B}{\sigma^2}\right) \qquad \text{(Equation 3)}$$

with J nucleation rate $L^{-1} s^{-1}$
        A model coefficient A s^{-1}
        B model coefficient B   -
        c protein concentration $g\ L^{-1}$
        σ thermodynamic supersaturation   -

The pre-exponential model coefficient A is difficult to determine and related to the uptake of molecules into the nucleus. Consequently, it is related to the molecular mobility and exhibits significant temperature dependence. Values of 10^{-15} to 10^{-18} have been reported for A (Erdemir *et al.*, 2009; Galkin and Vekilov, 2001). Bhamidi *et al.* (2002) found a correlation of A with the osmotic second virial coefficient B_{22}.
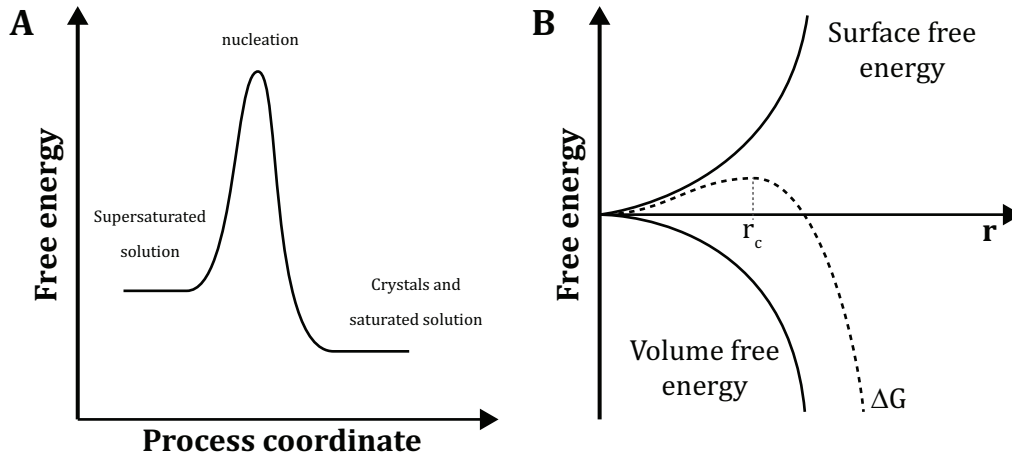
Figure 3.3: A) Schematic illustration of the free energy during crystal nucleation (modified from Rupp, 2010); **B)** Free energy diagram for crystal nucleation (modified from García-Ruiz, 2003). **ΔG:** change of the Gibbs free energy; **r:** size of the crystal nucleus; **r$_c$:** critical nucleus size.

Model coefficient B relates to the thermodynamic barrier for the formation of a critical spherical cluster, which is schematically depicted in Figure 3.3. B can be calculated from equation 4:

$$B = \frac{16\pi}{3}\frac{\Omega^2\gamma^3}{(k_\mathrm{B}T)^3} \qquad \text{(Equation 4)}$$

with Ω molecular volume of the protein in the crystal m^3
        γ surface free energy of the critical cluster $J\ m^{-2}$
        k_B Boltzmann constant $J\ K^{-1}$
        T temperature K

The thermodynamic supersaturation σ is calculated from equation 5:

$$\sigma = \ln\frac{c}{c_{eq}}$$ *(Equation 5)*

with σ *thermodynamic supersaturation*   -
      c *protein concentration* $g\ L^{-1}$
      c_{eq} *protein concentration at equilibrium* $g\ L^{-1}$

Despite the correlation of the two factors A and B with real-world effects, classical nucleation theory was found to perform poorly for the calculation of protein crystal nucleation. In contrast to the condensation of vapor to liquid, factors other than the local density and the size of the nucleus are important for protein crystallization. For example, the orientation of the large molecules has to be accounted for, as only periodic structures can form regular crystals (Erdemir *et al.*, 2009; Galkin and Vekilov, 2001; Vekilov, 2012).

Two-step mechanism of crystal nucleation

Recent research on protein nucleation suggests a two-step mechanism for the formation of nuclei in protein crystallization. Crystal nuclei are presumed not to form directly from the protein solution, but from an intermediate phase of local density fluctuations. The rate of transition from this intermediate phase to the final phase, i.e., the crystals, is improved. Nevertheless, rate of nucleation can also be negatively affected under certain conditions limiting the transfer of protein molecules to the intermediate phase. The two-step mechanism was shown to describe data from many experiments with good agreement (Erdemir *et al.*, 2009; Nicolis and Nicolis, 2003; Vekilov, 2012). A schematic illustration of this two-step mechanism is depicted in Figure 3.4.
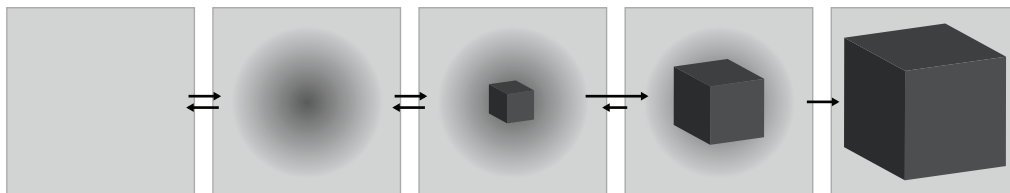

Figure 3.4: Two-step mechanism for the nucleation of crystals. Initially, an instable dense liquid cluster is formed. A stable crystal nucleus may form within this cluster (modified from Vekilov, 2012).

For the two-step mechanism, the nucleation rate J can be calculated using equation 6:

$$J = \frac{k_2 c_c T \exp\left(-\frac{\Delta G_2^*}{k_B T}\right)}{\eta(C_1, T)\left[1 + \frac{U_1}{U_0} exp\left(\frac{\Delta\mu_C}{k_B T}\right)\right]}$$ *(Equation 6)*

with	J	nucleation rate	$L^{-1} s^{-1}$
	c_c	protein concentration inside the clusters	$g\ L^{-1}$
	ΔG_2^*	barrier for nucleation inside the clusters	J
	k_2	constant scaling the nucleation rate of crystals inside the clusters	$Pa\ g^{-1}\ K^{-1}$
	k_B	Boltzmann constant	$J\ K^{-1}$
	$\Delta\mu_c$	chemical potential of a protein molecule inside the cluster	J
	η	viscosity inside the clusters	$Pa\ s$
	T	temperature	K
	U_1	effective rate of decay of clusters	-
	U_2	effective rate of formation of clusters	-

The numerator of the equation has a number of features in common with the classical nucleation theory (Equation 3), as the model still has to account for the formation of a crystal nucleus. As this nucleation occurs within a dense liquid cluster, the equation also includes terms in its denominator for the viscosity η of the dense liquid cluster as well as for the transfer of protein molecules into these clusters.

Vekilov (2012) notes that metastable liquid clusters have been demonstrated for several protein systems, but, nevertheless, might not be existent in all protein systems. Systems without such clusters probably feature direct formation of nuclei from the protein solution according to the classical nucleation theory.

Concluding remarks

In contrast to the crystallization of low-molecular substances, the driving force for protein crystallization is the entropy gain of water released from hydrophobic patches of the protein molecules. In addition to the negative Gibbs free energy, an energy barrier has to be overcome for nucleation to occur. Despite the availability of models for the two-step nucleation mechanism and increasing insight into the role of protein pair interaction, protein crystallization still remains a largely empirical technology.

3.2.2 Effects of crystallization agents, additives and other variables

A number of different physical, chemical and biochemical factors can affect crystallization. The most important factors are listed in Table 3.1.

Table 3.1: The most important physical, chemical, and biochemical factors affecting protein crystallization (Taken from McPherson, 2004).

Physical	Chemical	Biochemical
Temperature	pH	Purity of the protein
Properties of the medium (e.g. viscosity)	Crystallization agent(s) and its/their concentration	Post-translational modifications
Mechanical perturbations	Specific ions	Source of the protein
Surfaces	Degree of supersaturation	Isoelectric point
	Protein concentration	

Some of these factors, e.g., the post-translational modifications or the source of the protein, cannot be influenced without substantial work. The protein can be purified to some extent prior to crystallization. The isoelectric point pI of a protein cannot be changed, but the relation of the pH and the pI have an influence on interactions between the protein molecules and crystallization agents and/or other protein molecules. The properties of the medium and the supersaturation are a function of the temperature, the protein concentration and the crystallization agent(s), which remain as adjustable factors for protein crystallization. The different methods for protein crystallization will be described in chapter 3.2.3.

Temperature and protein concentration

The temperature is a very important variable for protein crystallization. On the one hand, the temperature influences the solubility and the stability of proteins. Similar to salts, a large number of proteins exhibit a temperature-dependent solubility which is reduced at lower temperatures. Others feature a retrograde temperature-dependent solubility, i.e., a lower solubility at higher temperatures. The solubility of some proteins, however, was shown to be temperature-independent (Christopher *et al.*, 1998). Additionally, irreversible protein denaturation occurs above protein-specific critical temperatures (Scharnagl *et al.*, 2005).

On the other hand, the formation of crystal nuclei and the crystal growth rate are affected by the temperature. Both classical nucleation theory and the two-step mechanism of crystal nucleation include terms for the temperature or terms depending on the temperature. At lower temperatures, the mobility of protein molecules decreases and the viscosity of local dense liquid clusters increases. Studies regarding the growth rate of lysozyme crystals at different temperatures confirmed the temperature-dependency of the growth rate. The growth rates exhibited maxima depending on the protein concentration (Sanamaría-Holek *et al.*, 2011; Vekilov, 2012).

Similar to the temperature, the protein concentration affects both, the nucleation rate and the protein stability. At very low protein concentrations, the number of protein molecules is insufficient for the formation of crystal nuclei, whereas the increasing viscosity of local dense liquid clusters limits the nucleation rate for very high protein concentrations (Vekilov, 2012). Also, very high protein concentrations may lead to the aggregation of protein molecules due to crowding effects and an increased chance of association, thus lowering the protein stability (Wang *et al.*, 2010).

pH and isoelectric point of the protein

While the isoelectric point pI is an intrinsic property of a protein, the pH of the crystallization buffer can be adjusted. The net charge of the protein molecules is a result of the pI and the pH. A pH below the pI results in a positive net charge, whereas a pH above the pI results in a negative net charge. At the pI, the protein solubility is the lowest and aggregation is often observed (Chi *et al.*, 2003). While the optimal pH for crystallization cannot be predicted, a few trends were observed. A statistic evaluation of reports of successful protein crystallization showed pH range from 4 - 10 with a maximum between pH 7 and pH 8 for both, acidic and basic proteins. Acidic proteins were frequently crystallized 0 - 2.5 pH units above their pI, whereas basic proteins were frequently crystallized 0.5 - 3 pH units below their pI. There is no evidence of a favorable protein net charge (Kantardjieff and Rupp, 2004; Kantardjieff *et al.*, 2004).

Crystallization agents and additives

A number of different crystallization agents are frequently used to generate supersaturated protein solutions for protein crystallization, including ammonium sulfate, sodium chloride or polyethylene glycol (McPherson, 2004). Nevertheless, this

might be biased, as common screens for crystallization conditions are based on previous successful crystallization experiments rather than on rational designs. Consequently, it is often necessary to perform a screening for crystallization conditions using a great variety of crystallization agents and additives. These reagents can be categorized in four groups: salts, polymers, organic solvents, and ionic liquids.

Salts

Salts can influence the solubility of proteins in two different ways, a direct and an indirect one. The indirect effect is based on the change of the surface water tension caused by the salt, leading to a preferential exclusion of the salt from the protein surface. Consequently, the protein surface is preferentially hydrated, subsequently stabilizing the protein. The ability of salts to cause these stabilizing effects is described in the Hofmeister series. The effect of the anions is usually dominant (Baldwin, 1996; Hofmeister, 1888; Shimizu *et al.*, 2006; Zhang and Cremer, 2006). An excerpt of the Hofmeister series is depicted in Figure 3.5.

Anions: $[SO4]^{2-} > [dhp]^- > [ac]^- > F^- > Cl^- > Br^- > I^- > [SCN]^-$

Cations: $Cs^+ > K^+ > Na^+ > Li^+ > Mg2^+ > Al3^+$

stabilizing   destabilizing

Figure 3.5: The Hofmeister series ranks anions and cations according to their protein-stabilizing efficiency (Collins and Washabaugh, 1985; Hofmeister, 1888; Weingärtner *et al.*, 2012). **[dhp]⁻:** dihydrogenphosphate; **[ac]⁻:** acetate.

The direct effect on the solubility of proteins is caused by the fact that salts are electrolytes. Consequently, salts contribute to the ionic strength of the crystallization buffer and modulate the strength of electrostatic interactions. As the charges on the protein surface depend on the pH, the effect of salts on protein solubility is rather complex (Chi *et al.*, 2003; Collins, 2004).

Polymers

Examples for polymers frequently used for protein crystallization are polyethylene glycol (PEG) and PEG monomethyl ether (PEG MME) (McPherson, 2004). Polyethylene glycols bind water, effectively reducing its activity and raising the effective protein concentration. This effect is schematically depicted in Figure 3.6.
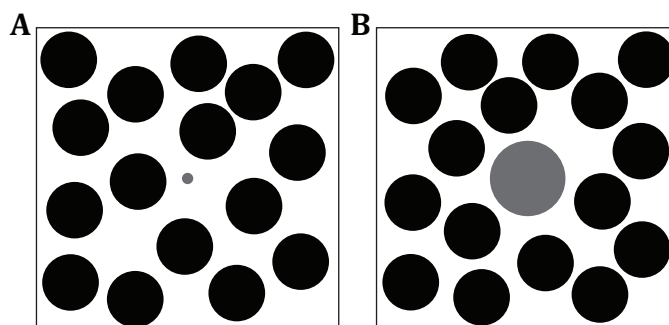
Figure 3.6: While the water between the large PEG molecules is **A)** available for low-molecular substances, it is **B)** unavailable for large protein molecules (modified from Chebotareva, 2007). Consequently, the effective protein concentration is raised. Black circles denote PEG molecules, whereas the grey circles represent a low-molecular substance and a protein molecule, respectively.

PEGs are often used in combination with metal salts. Both increase hydrophobic interactions between the hydrated protein molecule surfaces (Atha and Ingham, 1981; Jion *et al.*, 2006; Reid and Rand, 1997; Timasheff, 2002).

Organic solvents

Frequently used organic solvents are alcohols like ethanol, propanol, isopropanol, 1,3-propanediol, and 2-methyl-2,4-pentanediol (McPherson, 2004). Organic solvents reduce the electric fields mediating protein-protein interactions in solution through their polar groups. Hydrophobic groups of the organic solvents may disrupt intramolecular hydrophobic interactions. Consequently, the attraction between protein molecules increases and the protein solubility is reduced (Englard and Seifter, 1990; McPherson, 2004).

Ionic liquids

Ionic liquids are organic salts with a melting point below 100 °C, which are increasingly used as additives for protein crystallization. The use of ionic liquids for protein crystallization shall be further detailed in chapter 3.3.

3.2.3 Crystallization methods

A number of methods for protein crystallization are described in the literature. The different pathways through the phase diagram are schematically depicted in Figure 3.7.
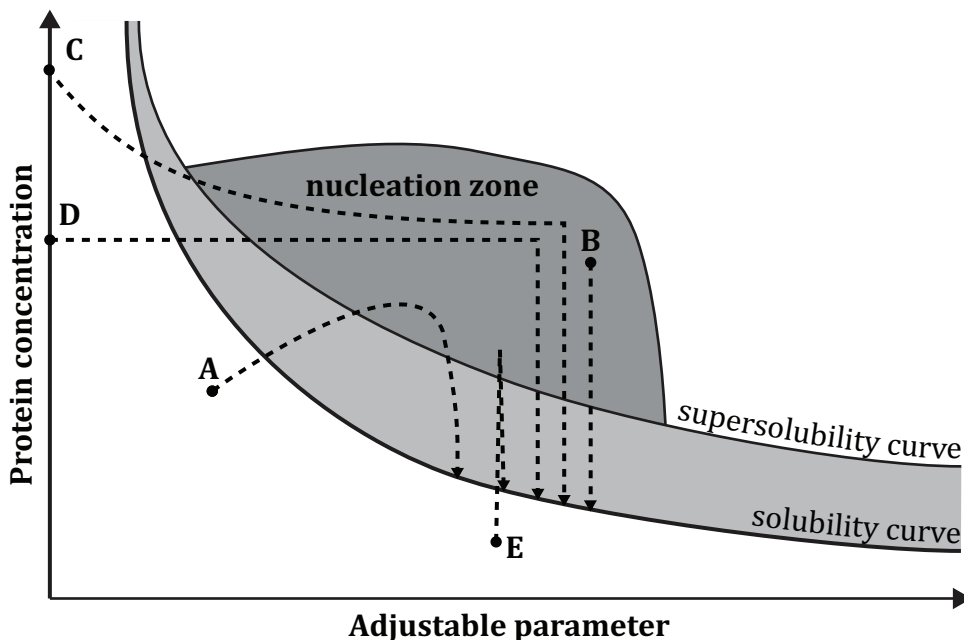

Figure 3.7: Schematic illustration of a protein crystallization phase diagram. The lines indicate exemplary pathways used in different crystallization methods: **A)** vapor diffusion crystallization; **B)** batch crystallization; **C)** free interface diffusion crystallization; **D)** microdialysis crystallization; **E)** ultracentrifugal crystallization (modified from Chayen, 2005). For a more detailed description of phase diagrams, see Figure 3.2.

Vapor diffusion crystallization

Classical vapor diffusion crystallization is usually employed for the initial screening for crystallization conditions. Three different methods for vapor diffusion crystallization are schematically depicted in Figure 3.8. Both, hanging drop and sitting drop vapor diffusion crystallization are frequently used for manual crystallization experiments and robotic high-throughput crystallization (Stevens, 2000).   Sandwich drop vapor diffusion crystallization, however, is a niche application and only used for specific problems (Sun *et al.*, 2010).
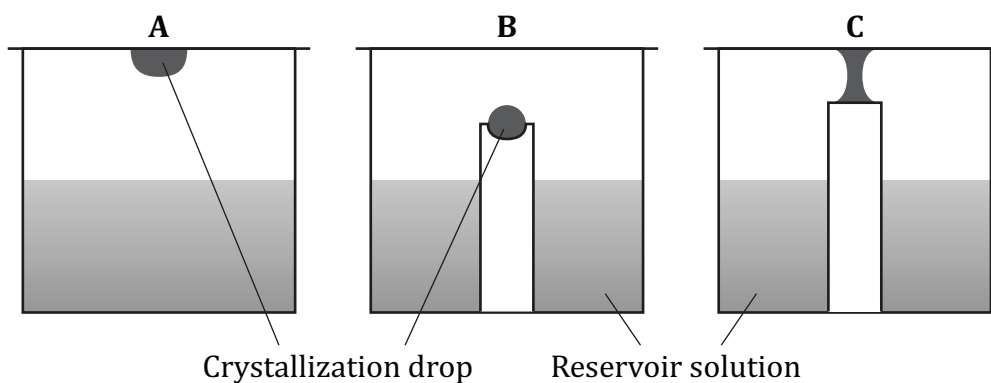
Crystallization drop   Reservoir solution

Figure 3.8: Schematic illustration of different vapor diffusion crystallization methods. The crystallization drop is placed next to a reservoir solution within a sealed compartment. **A)** hanging drop; **B)** sitting drop; **C)** sandwich drop (modified from Bergfors, 1999).

The crystallization drop, containing both the protein and the crystallization agents, is placed next to a reservoir solution within a sealed compartment. The reservoir solution contains increased concentrations of the crystallization agents (usually 2-fold). Water diffuses from the crystallization drop through the saturated atmosphere in the headspace into the reservoir due to the concentration gradient. Consequently, the concentrations of both the protein and the crystallization agents increase during vapor diffusion crystallization. This slow increase of the concentrations can be beneficial for the growth of large monocrystals. However, vapor diffusion crystallization is an inadequate starting point for technical-scale protein crystallization, as the exact conditions under which the crystallization occurred are unknown. Also, vapor diffusion itself cannot be scaled up (Bergfors, 1999; McPherson, 2004; Schmidt *et al.*, 2005).

Batch crystallization

Similar to vapor diffusion crystallization, batch crystallization is often used for the initial screening of crystallization conditions and in automated high-throughput crystallization systems (Stevens, 2000). However, batch crystallization exhibits disadvantages for the initial screening. In contrast to vapor diffusion crystallization, where a wide range of crystallization conditions is encountered for every single drop, batch crystallization is performed under well-defined conditions. The crystallization drop comprising the protein and the crystallization agents is placed under a layer of paraffin, consequently inhibiting evaporation. A schematic illustration of a batch crystallization setup is depicted in Figure 3.9.
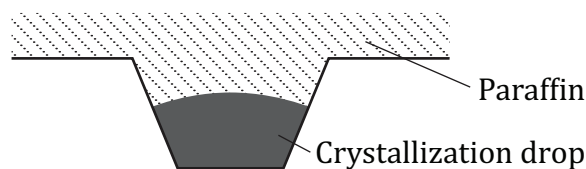
Figure 3.9: Schematic illustration of batch crystallization. The crystallization drop sits in a well of a Terasaki plate. The plate is sealed with paraffin (modified from Bergfors, 1999).

Nevertheless, the aforementioned drawback of batch crystallization for the initial screening renders batch crystallization as a favorable starting point for subsequent technical-scale protein crystallization processes. The well-defined crystallization conditions are presumed to be transferable into technical-scale batch crystallizers (Bergfors, 1999; Schmidt *et al.*, 2004). As this is the focal point of this work, it will be described separately in chapter 3.2.4.

Free interface diffusion crystallization

Using free interface diffusion crystallization, a whole range of crystallization conditions can be evaluated within one test tube. The protein and the crystallization agent solutions are carefully layered into the test tube, preferably separated by a permeable membrane, and the tube is sealed. Over time, a concentration gradient is generated via diffusion (Chayen, 2004; Salemme, 1972). A schematic illustration of a free interface diffusion crystallization setup is depicted in Figure 3.10.
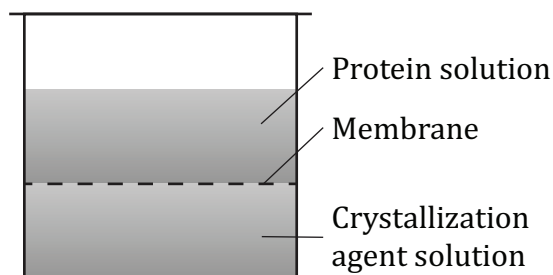

Figure 3.10: Schematic illustration of free interface diffusion crystallization (modified from Salemme, 1972).

Free interface diffusion crystallization is useful for the initial screening of crystallization conditions, especially since the development of microfluidic systems. These systems allow for a large number of parallel reactions (currently 144 per microfluidic chip) using only 10 nL of protein solution per crystallization condition (Hansen *et al.*, 2002).

Microdialysis crystallization

Similar to free interface diffusion crystallization, a protein-rich phase and a protein-free phase containing the crystallization agents are brought in contact for microdialysis crystallization. However, a semipermeable membrane is used instead of a permeable membrane. Consequently, the protein molecules are confined to the microdialysis button and the protein concentration remains constant throughout the process (Hampton, 2001). A schematic illustration of a setup for microdialysis crystallization is depicted in Figure 3.11.
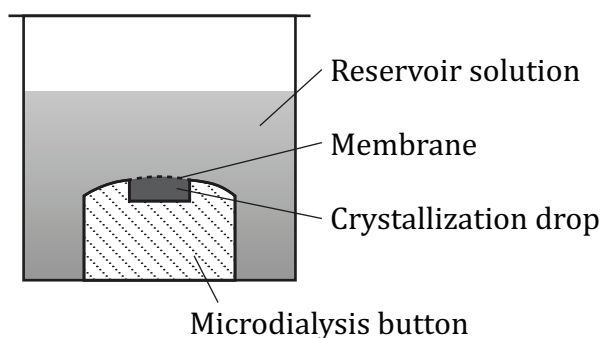
Figure 3.11: Schematic illustration of microdialysis crystallization (modified from Hampton, 2001).

The scale-up of both, free interface diffusion crystallization and microdialysis crystallization, is not feasible and both methods do not provide exact crystallization conditions for the technical-scale batch crystallization of proteins.

Ultracentrifugal crystallization

Ultracentrifugation can be used to locally increase the protein concentration, thus generating supersaturation (Behlke and Knespel, 1997; Lenhoff *et al.*, 1997; Pitts, 1992; Wyckoff and Corey, 1936). The crystal growth rate for some proteins was faster when using ultracentrifugation. Also, the separation and subsequent crystallization of a protein in the presence of a 1000-fold molar excess of another protein was recently demonstrated (Dimitrov and Nanev, 2006; Lorber, 2008). While this crystallization technique may be used to accelerate crystallization processes and to separate proteins from impure solutions, it is non-scalable and therefore not applicable for the use in large-scale downstream processing.

3.2.4   Technical-scale protein crystallization

For decades, structure determination via protein crystallography has been the only application for protein crystallization. Recently, the application of technical-scale protein crystallization for the purification of proteins has been proposed. Since the polypeptide insulin was successfully crystallized using stirred batch crystallization with volumes up to 500 L (Basu *et al.*, 2004; Harrison *et al.*, 2003; Schlichtkrull, 1957), a similar approach shall be followed for the technical-scale crystallization of proteins. As shear flow was shown to positively affect the nucleation of protein crystals (Penkova *et al.*, 2006; Roberts *et al.*, 2010), the stirred batch crystallization of proteins is feasible.

Additionally, early research work on technical-scale protein crystallization exists. Judge *et al.* (1995) reported the successful purification of ovalbumin with a purity greater than 99 % in 1 L stirred batch crystallizers. Jacobsen *et al.* (1998) and Lee *et al.* (2000) crystallized fungal lipases from clarified concentrated fermentation broths using seed crystals on 225 mL- and 500 mL-scale bottles, respectively. Two isoforms of an undisclosed protein were separated in stirred tanks with volumes up to 100 mL (Schmidt *et al.*, 2005). While the crystallization kinetics showed only a slight dependency on the stirrer speed, lower stirrer speeds resulted in the formation of larger crystals. Takakura *et al.* (2006) purified L-methionine γ-lyase from a pretreated crude enzyme solution in a 100 L stirred tank with a yield of 87 %. An undisclosed therapeutic protein was crystallized within 8.5 h using a temperature ramp on a 1 L- and on a 800 L-scale (Matthews and Bean, 2006). The impact of secondary nucleation, i.e., crystal splinters serving as crystal nuclei, on the agitated 250 mL-scale crystallization of lysozyme was studied. The increased secondary nucleation rates for higher stirrer speeds were most likely caused by the increased frequency and the increased magnitude of crystal collisions, while the fluid shear forces played a minor role (Tait *et al.*, 2009).

3.2.5   Properties of protein crystals

Crystals of macromolecules are usually very soft and fragile (modulus of elasticity E = 0.1 - 0.5 GPa; Chernov, 2003). Protein crystals contain 25 - 90 % water. A solvent content of 70 % was estimated for all proteins in this work. Most of it is not bound as crystal water, but surrounding the individual protein molecules. Crystallization agents are embedded into the solvent channels during crystallization. The solvent channels allow for the diffusion of substances into and out of crystals (Cvetkovic *et al.*, 2005;

McPherson, 2004). A schematic illustration of the protein molecules bound in the crystal lattice surrounded by solvent channels is shown in Figure 3.12.
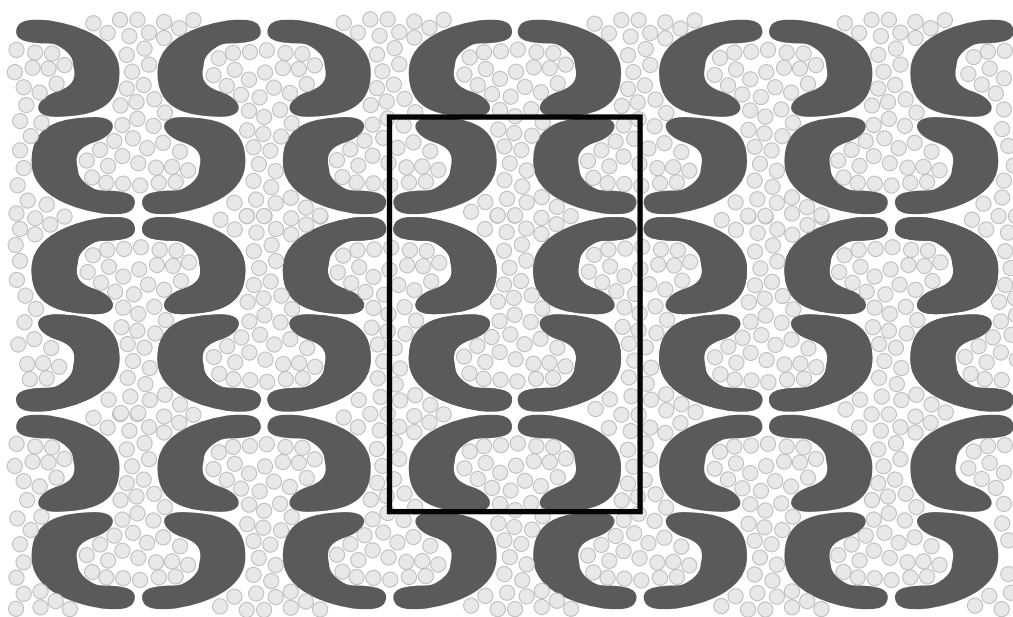

Figure 3.12: Schematic illustration of protein molecules bound in the crystal lattice. The protein molecules (dark, bean-shaped) are surrounded by water molecules in the solvent channels (grey). The black box denotes an unit cell of the crystal lattice (modified from Takayama and Nakasako, 2011).

Depending on the protein and the crystal form, the structure of the protein may be very similar to the one in solution. However, the crystal packing has been reported to influence the protein structure in some cases (Eyal *et al.*, 2005; McPherson, 2004). Crystalline proteins were reported to feature a higher stability than proteins in solution. Also, crystals of therapeutic proteins release their activity over a prolonged period compared to aqueous protein solutions (Basu *et al.*, 2004; Hallas-Moller *et al.*, 1952; Margolin and Navia, 2001; Takakura *et al.*, 2006).

3.2.6 Proteins under study

This chapter briefly portrays the four enzymes and the therapeutic antigen-binding antibody fragment crystallized in this work. All proteins were previously crystallized for structure determination and available either commercially or through the cooperation partner Merck KGaA (Darmstadt, Germany).

Lysozyme from *Gallus gallus* (LYS)

Lysozyme (LYS) is a peptidoglycan *N*-acetylmuramoylhydrolase (EC 3.2.1.17) which breaks up peptidoglycan linkages in bacterial cell walls, thus acting as an antimicrobial agent (Fleming, 1922; Phillips, 1967). It has been used as a model protein for crystallization for almost three decades despite of its uncommon properties as its high isoelectric point of 11.1 or its low molecular size of 14.6 kDa (Durbin and Feher, 1986; Peng *et al.*, 2005). Both LYS and its crystallization have been studied intensively, and datasets on the influence on the NaCl concentration and the temperature on the solubility of LYS are available (Howard *et al.*, 1988). The common crystal forms are known (Bhamidi *et al.*, 2001). Phase diagrams for the crystallization of LYS using NaCl in sodium acetate buffer are reported (Hekmat *et al.*, 2007b; Wanka and Peukert, 2011). A phase diagram based on the data from the two aforementioned reports is shown in Figure 3.13.
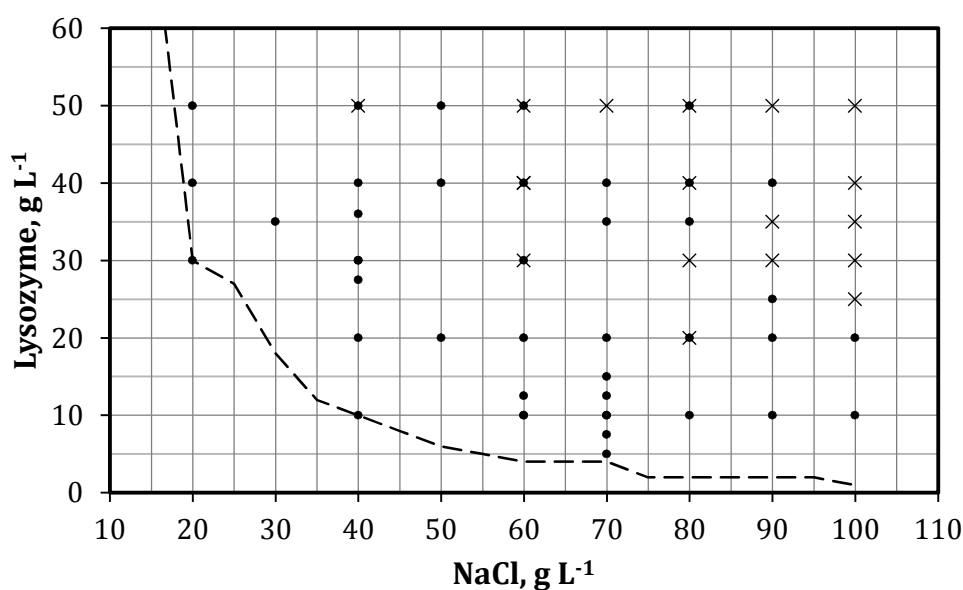
Figure 3.13: Phase diagram for the crystallization lysozyme in sodium acetate buffer pH 4 created from the qualitative data presented in Hekmat *et al.* (2007b) and Wanka and Peukert (2011). • crystal growth; × precipitate formation. The solubility data represented by the dashed line was taken from (Howard *et al.*, 1988). The line is included for visualization and is not the result of a simulation.

While LYS might not represent the majority of proteins, e.g., due to its unusually high pI, it is still regularly used for benchmarking new crystallization techniques, not least because of its commercial availability. For example, LYS was the first protein to be crystallized using an ionic liquid, ethylammonium nitrate (EAN), as additive (Garlitz *et al.*, 1999). Hekmat *et al.* (2007a, 2008) reported the crystallization of 50 g L^{-1} LYS using 40 g L^{-1} NaCl, 25 mM sodium acetate buffer pH 4.0, and optionally 100 g L^{-1} ionic liquid in vapor diffusion and 5 mL-scale stirred-batch experiments. A yield of 82 % was achieved within 8 h. No details regarding the crystallization kinetics are given for the 5 mL-scale crystallization process. The ionic liquids under study were 2-hydroxyethylammonium formate (2-HEAF), EAN, bis-(2-methoxyethyl)-ammonium acetate, *N,N*-dimethylethanolammonium glycolate, and choline dihydrogenphosphate (CDHP). The fastest crystallization kinetics in vapor diffusion experiments were observed using 2-HEAF with a 5.5-fold increase compared to the crystallization without the addition of ionic liquids. The structure of LYS is shown in Figure 3.14.

Lysozyme

from *Gallus gallus*

UniProt P00698; PDB 2LYZ

14 kDa, 147 AA, pI 11.1

hydrolase (EC 3.2.1.17)

Figure 3.14: Structure (Diamond, 1974) and key data of LYS. UniProt (Universal Protein Resource; http://www.uniprot.org/; Aug 2012; Uniprot Consortium, 2012), PDB (Protein Data Bank; http://www.pdb.org/; Aug 2012; Berman *et al.*, 2000).

Lipase from *Thermomyces lanuginosus* (LIP)

Since the structure of the lipase from *Thermomyces (humicola) lanuginosus* (LIP) was solved (Derewenda *et al.*, 1994), LIP has become a common ingredient of washing agents for the degradation of fats. LIP hydrolyzes triglycerides into fatty acids and glycerol (EC 3.1.1.3), enabling their removal from fabrics (Brzozowski *et al.*, 2000; Jaeger and Reetz, 1998). LIP consists of 291 amino acids, has a molecular weight of 29 kDa and a pI of 5.0. For this work, a commercially available LIP formulation, Lipolase 100L, was used. The vapor diffusion crystallization of LIP with and without the addition of ionic liquids has been described in the literature using the following crystallization conditions: 2.5 - 10 g L^{-1} NaCl, 50 mM sodium acetate buffer pH 4.0 - 4.35, and optionally 0 - 40 g L^{-1} choline dihydrogenphosphate (Hekmat *et al.*, 2008). The structure of LIP is shown in Figure 3.15.

Lipase

from *Thermomyces lanuginosus*

UniProt O59952; PDB 1TIB

29 kDa, 291 AA, pI 5.0

hydrolase (EC 3.1.1.3)

Figure 3.15: Structure (Derewenda *et al.*, 1994) and key data of LIP. UniProt (Universal Protein Resource; http://www.uniprot.org/; Aug 2012; Uniprot Consortium, 2012), PDB (Protein Data Bank; http://www.pdb.org/; Aug 2012; Berman *et al.*, 2000).

Xylanase II from *Trichoderma reesei* (XYL)

The Xylanase II from *Trichoderma reesei* (XYL) hydrolyzes beta-1,4-xylosidic bonds in xylans (EC 3.2.1.8). Xylanases are primarily employed for the cleavage of xylans in the pulp and paper industry (Beg *et al.*, 2001). More recent applications include the use of xylanases in enzyme cocktails for the hydrolysis of lignocellulose (Viikari *et al.*, 2007). XYL is commercially available from Hampton Research, Aliso Viejo, CA, USA as a protein crystallization standard. XYL consists of 190 amino acids, has a molecular weight of 20.8 kDa and a pI of 9 (Hampton, 2010; Tenkanen *et al.*, 1992). Two vapor diffusion crystallization conditions are reported in the literature: A) $5 - 15$ g L^{-1} XYL, $100 - 150$ g L^{-1} ($\approx 0.76 - 1.14$ M) ammonium sulfate, 25 mM sodium acetate buffer pH 4.2 (Törrönen *et al.*, 1993); B) $2 - 17$ g L^{-1} XYL, $0.6 - 1.4$ M sodium potassium phosphate pH $7.0 - 8.2$ (Hampton, 2010). The structure of XYL is shown in Figure 3.16.
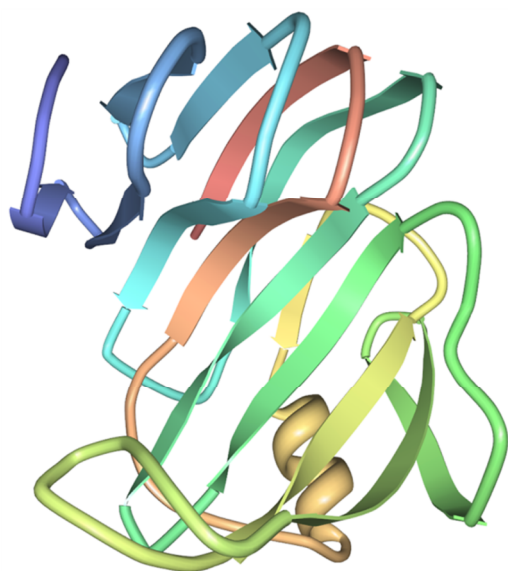
Xylanase II

from *Trichoderma reesei*

UniProt P36217; PDB 2DFC

20.8 kDa, 190 AA, pI 9

hydrolase (EC 3.2.1.8)

Figure 3.16: Structure (Watanabe *et al.*, 2006) and key data of XYL. UniProt (Universal Protein Resource; http://www.uniprot.org/; Aug 2012; Uniprot Consortium, 2012), PDB (Protein Data Bank; http://www.pdb.org/; Aug 2012; Berman *et al.*, 2000).

Glucose isomerase from *Streptomyces rubiginosus* (GLU)

Glucose isomerases or xylose isomerases (EC 5.3.1.5) catalyze the isomerization from glucose to fructose. A prominent large-scale application for this enzyme class is the high fructose corn syrup (Bhosale *et al.*, 1996). Glucose isomerase from *Streptomyces rubiginosus* (GLU) is commercially available from Hampton Research, Aliso Viejo, CA, USA as a protein crystallization standard. GLU consists of 388 amino acids and has a molecular weight of 43.2 kDa and a pI of 3. In solution, GLU forms a homotetramer with a total molecular weight of 172.8 kDa. No phase diagrams are reported for GLU. However, a number of crystallization conditions are available in the literature for both vapor diffusion and batch crystallization, including the following: A) 1.5 - 2.5 M ammonium sulfate, pH 7.0; B) 100 - 150 g L^{-1} PEG 4000 - 8000 in 200 mM ammonium sulfate, pH 7.0; C) 0.6 - 1.0 M sodium citrate, pH 8.0. The structure of GLU was solved in 1994 by crystallography (Carrell *et al.*, 1994; Hampton, 2012) and is shown in Figure 3.17.
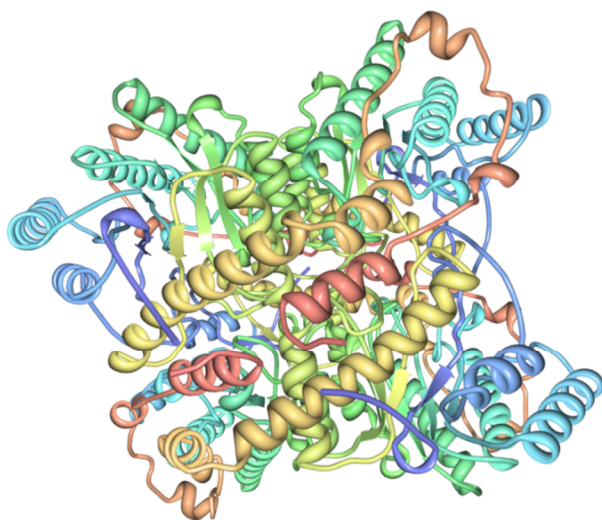
Glucose isomerase

from *Streptomyces rubiginosus*

UniProt P24300; PDB 1XIB

monomer: 43.2 kDa, 388 AA, pI 3

tetramer: 172.8 kDa, pI 3

isomerase (EC5.3.1.5)

Figure 3.17: Structure (Carrell *et al.*, 1994) and key data of GLU. UniProt (Universal Protein Resource; http://www.uniprot.org/; Aug 2012; Uniprot Consortium, 2012), PDB (Protein Data Bank; http://www.pdb.org/; Aug 2012; Berman *et al.*, 2000).

Antigen-binding fragment of cetuximab (FAB)

This antigen-binding fragment (Fab) is generated by papain digestion of cetuximab. Cetuximab is a chimeric monoclonal IgG1-type antibody. It is also known as C225-03, IMC-C225, C225, and ch225. Cetuximab is the active agent of *Erbitux*. The variable region of this antibody binds to the active site of the epidermal growth factor receptor (EGFR), which is thereby inhibited. The EGFR is frequently overexpressed in cancer cells (Arteaga, 2001; Li *et al.*, 2005). The structure and function of antibodies shall be described briefly before details on the Fab fragment of cetuximab (FAB) are given.

IgG-type antibodies are heterodimeric proteins with two light and two heavy polypeptide chains (Fleischman *et al.*, 1963; Pain, 1963). Four IgG subclasses are defined based on differences of the heavy chains, IgG1 being the most common one (Jazwinska *et al.*, 1988). The schematic structure of an IgG molecule is depicted in Figure 3.18.
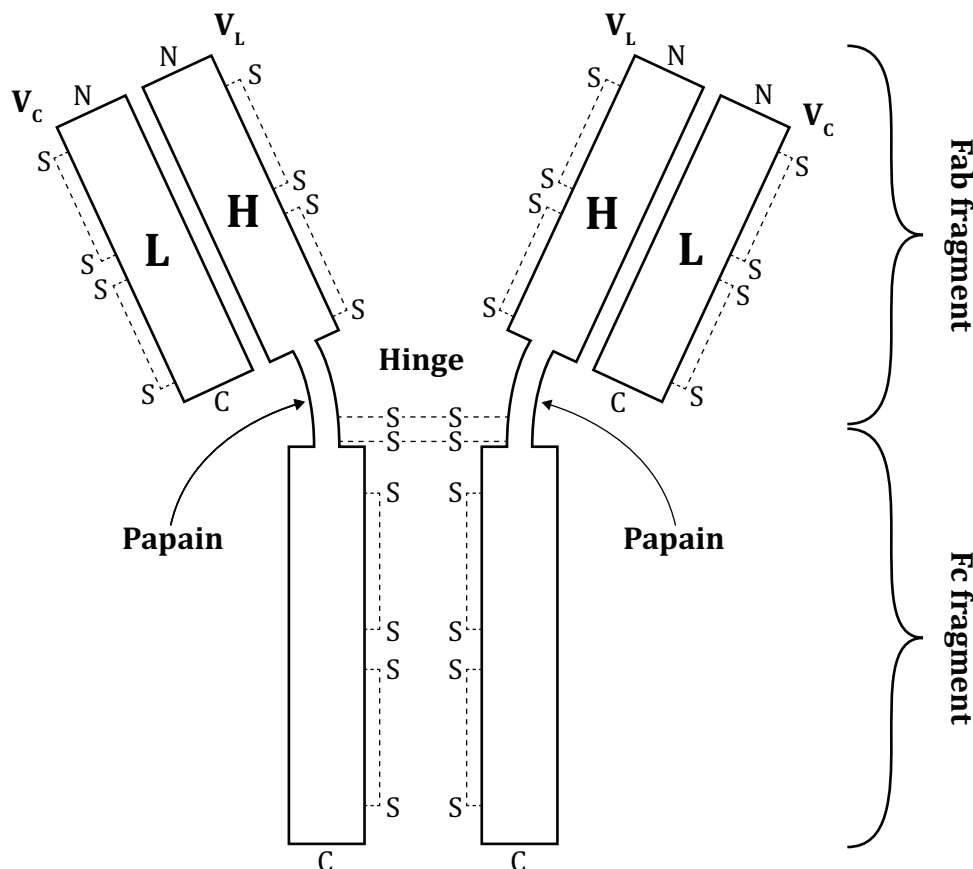
Figure 3.18: Schematic structure of an IgG molecule (modified from Schroeder and Cavacini, 2010). **H:** heavy chain; **L:** light chain; **V$_x$:** variable domain; **N:** amino terminus; **C:** carboxy terminus; **s-s:** disulfide bridge.

The very flexible hinge region between the constant (Fc) region and the two Fab regions allow the two Fab regions to bind to epitopes in variable orientations. Upon the binding of antigens, the antibody-antigen complex triggers a number of reactions using the Fc region of the antibody leading to the neutralization of the antigen, e.g., via the complement system (Schroeder and Cavacini, 2010). However, this flexibility and the glycosylation of the Fc region render the crystallization of antibodies very difficult (Arnold *et al.*, 2007; Low *et al.*, 2007). Antibodies can be split into Fab and Fc fragments in the hinge region using the proteolytic enzyme papain. The Fab fragments lack the ability to induce effector functions, but are still able to bind to antigens without cross-linking (Mage, 1980; Zappacosta *et al.*, 1968).

Similar to the full-length antibody cetuximab, FAB binds to the active site of the EGFR. FAB thereby prevents the binding of the epidermal growth factor to the receptor. It inhibits the dimerization of the receptor molecules which would activate the signal cascade leading to, among other things, the proliferation of the tumor cells and angiogenesis (Dutta and Maity, 2007; Li *et al.*, 2005; Yarden, 2001). FAB was crystallized using the following vapor diffusion crystallization conditions for structure determination: 11 g L^{-1} FAB, 0.9 M ammonium sulfate, 50 mM NaCl, 50 mM sodium citrate pH 6.25, and 5 mM Tris-HCl pH 8.5. NaCl and Tris-HCl were residuals from the protein A-based purification (Li *et al.*, 2005). The structure of FAB is shown in Figure 3.19.
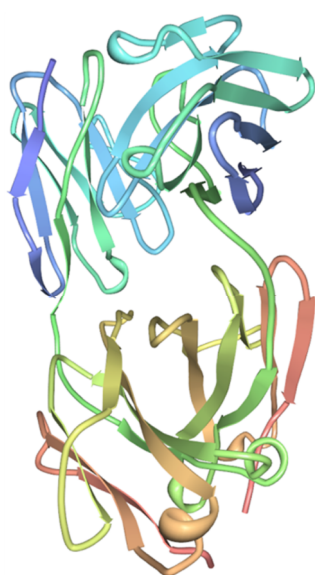
Fab fragment of cetuximab

(Fab fragment of a chimeric monoclonal IgG1 antibody)

PDB 1YY8

46.9 kDa, 434 AA, pI 8.7

Figure 3.19: Structure (Li *et al.*, 2005) and key data of FAB. PDB (Protein Data Bank; http://www.pdb.org/; Aug 2012; Berman *et al.*, 2000).

3.3   Ionic liquids and proteins

While the term *ionic liquid* generally describes all salts in the liquid state, it is commonly used for salts with a melting point below 100 °C. Ionic liquids (ILs) with a melting point below 20 °C are called room temperature ILs (RTILs). Most of these ILs consist of an organic cation and an inorganic polyatomic anion. The vast diversity of cation/anion combinations allows for ILs with many different properties. Consequently, a number of different applications exist, including the following:

- ILs as green designer solvents (Earle and Seddon, 2000)
- ILs as electrolytes in Li-ion batteries (Lewandowski and Świderska-Mocek, 2009).
- Water-immiscible ILs as a biocompatible second phase for whole-cell biocatalysis (Bräutigam *et al.*, 2009; Dennewald *et al.*, 2011; Pfruender *et al.*, 2004, 2006; Weuster-Botz, 2007).
- ILs as additives for protein refolding (Buchfink *et al.*, 2010; Lange *et al.*, 2005).
- ILs as additives for protein crystallization (Garlitz *et al.*, 1999; Hekmat *et al.*, 2007a; Pusey *et al.*, 2007).

As a complete description of all applications for ILs would exceed the scope of this work, only the effects of ILs in protein-related applications as biocatalysis, refolding and crystallization will be discussed in the following.

Effects on protein stability and enzyme activity

Many ILs were reported to enhance the stability of proteins and the activity of enzymes. As the molecular-level solubility of proteins in pure ILs is low (Fujita *et al.*, 2005, 2007; Sate *et al.*, 2007), ILs are commonly used as additives to aqueous protein solutions. ILs can form an ionic network when used at high concentrations or as pure solvent. However, this ionic network breaks up in solutions with low IL concentrations (Moreno *et al.*, 2008). Consequently, Weaver *et al.* (2012) suggested that the IL choline dihydrogenphosphate (CDHP) should be considered as an osmolyte similar to other water-soluble compounds such as sugars and salts when used at low concentrations. Hence, it is not surprising, that the effects of ILs on protein stability correlate well with the Hofmeister series for the classification of anions and cations (Endres, 2010; Hofmeister, 1888; Weingärtner *et al.*, 2012; Yang, 2009).

As for salts, ILs with highly charged and/or small anions were shown to stabilize the native protein conformation. Depending on the cation, which, in ILs, is usually destabilizing, ILs are more or less denaturing. In addition to the ion-specific indirect effects, the direct interactions between ions and macromolecules specific to a protein-ion-combination are of importance (Baldwin, 1996; Collins and Washabaugh, 1985; Weingärtner *et al.*, 2012; Zhang and Cremer, 2006). When used at low concentrations, most ionic liquids were shown to have no detrimental effect on the protein structure (Kennedy *et al.*, 2011). Similar to the protein stability, the activity of enzymes is also affected by the Hofmeister series. It was proposed that the activity-inhibiting effects of a salt are a result of its structure-disrupting effects, as the protein structure determines enzyme activity and its specifity. This was shown to apply for ILs as well, e.g., by a correlation of the enzymatic efficiency to the Hofmeister series. In contrast, the apparent binding constant K_m of the substrate (Michaelis constant) and the turnover number k_{kat} could not be correlated to the Hofmeister series and is believed to be affected by the specific effects of protein-ion-combinations (Warren *et al.*, 1966; Weibels *et al.*, 2012; Weingärtner *et al.*, 2012).

Effects on protein crystallization

ILs were reported to positively influence protein crystallization, resulting in faster kinetics, a more compact crystal morphology, and an increased protein stability in small-scale vapor-diffusion and microbatch experiments (Chen *et al.*, 2010; Garlitz *et al.*, 1999; Judge *et al.*, 2009; Kennedy *et al.*, 2011; Pusey *et al.*, 2007). For lysozyme, the crystallization kinetics were increased up to 5.5-fold by the addition of the IL 2-HEAF. Crystal polymorphism and spontaneous precipitation were reduced even at higher crystallization agent concentrations (Hekmat *et al.*, 2007a, 2008).

For protein crystallization, the ILs are often used in low concentrations (Kennedy *et al.*, 2011). Consequently, the effects of the ILs are most likely caused by the individual ions of the ILs, as previously described for the stabilization of proteins and for biocatalysis. For some crystallization experiments, the ILs may have acted as the primary crystallization agent, which is a further hint for the similarity of IL solutions and salt solutions (Kowacz *et al.*, 2012; Pusey *et al.*, 2007).

The ILs are usually not bound in the crystal structure. Nevertheless, one case of both ions of the IL choline acetate binding in the crystal structure of LYS was reported. The

two ions form a bridge of hydrogen bonds in one of the cavities of the LYS structure (Kowacz *et al.*, 2012). While this is an example for an IL with both ions positively affecting protein crystallization, the effects are specific to the combination of ions and not to the nature of ILs. As Na^+ and Cl^- ions of the crystallizing agent are also found in the crystal structure, it is feasible that the same results can be obtained with the addition of salts containing the same ions, i.e., choline chloride and sodium acetate.

Concluding remarks

The exact effect of ILs on the protein stability, the enzyme activity, and the protein crystallization has not been resolved yet. However, it seems most likely that the individual ions of the ILs dissociate in low concentrated aqueous solutions, and, consequently, their individual effects are responsible for the observed effects. These effects can be described using previously proposed models for the interactions of salts and proteins. While the anions were proven to be very important, only little is known about the physiochemical properties of the cations of ILs (Weingärtner *et al.*, 2012; Yang, 2009). Future insights in these molecular interactions may enable the targeted optimization of ILs as designer solvents. However, ILs also have a number of downsides, including their high costs and the toxicity of some cations, the latter being especially critical regarding the possible use of ILs for pharmaceutical applications. While the recycling of water-immiscible ILs was recently demonstrated (Dennewald *et al.*, 2011), similar processes for aqueous solutions of ILs containing other substances, e.g., salts and proteins, will be difficult to establish.

4   Material and methods

This chapter describes the experimental methods employed in this work. Section 4.1 focuses on protein analytics. The methods for the preparation of the protein solutions for the crystallization experiments are detailed in section 4.2. Finally, the different crystallization techniques are presented in section 4.3. Materials and abbreviations are listed in the appendix (chapters 0 and 8.1, respectively).

The proteins under study were provided by the cooperation partner (Merck KGaA, Darmstadt, Germany), generated by papain digestion of an antibody or purchased in purified form (Table 4.1).

Table 4.1: Overview of the proteins under study (cooperation partner*: Merck KGaA, Darmstadt, Germany). Cetuximab was only used as source for the generation of the antigen-binding fragment of cetuximab (FAB) by papain digestion.

Abbr.	Protein	Source
(CET)	Cetuximab (used for generation of FAB)	Cooperation partner*
FAB	Antigen-binding fragment of cetuximab	Papain digestion
GLU	Glucose isomerase from *Streptomyces rubiginosus*	Cooperation partner*
LIP	Lipase from *Thermomyces lanuginosus*	Novozymes Lipolase 100L
LYS	Lysozyme from *Gallus gallus*	Sigma-Aldrich (62971)
XYL	Xylanase II from *Trichoderma reesei*	Cooperation partner*

4.1   Protein analytics

The progress of crystallization experiments, the purity of the protein solutions, and the functional activity of LYS and LIP were monitored using the analytical methods described in this subchapter.

4.1.1   Protein concentration determination

As protein solutions with a high purity and free of interfering substances, the protein concentration was determined by UV spectroscopy only (Layne, 1957). The measurement was performed in a 1 mL fused quartz cuvette at 280 nm. The protein concentrations were calculated according to the Lambert-Beer law (Equation 7).

$$E = \varepsilon \cdot c \cdot d \qquad\qquad (Equation\ 7)$$

with	E	extinction	-
	c	concentration	$mol\ L^{-1}$
	d	cuvette width	cm
	ε	extinction coefficient	$mol\ L^{-1}\ cm^{-1}$

For LYS, a standard was used to obtain the extinction coefficient ε. The molecular masses M and the extinction coefficients for the other proteins under study were calculated with ProtParam (Gasteiger *et al.*, 2005) using the protein sequences given in the appendix (chapter 8.6).

4.1.2 Sodium dodecyl sulfate polyacrylamide gel electrophoresis (SDS-PAGE)

The purity of protein solutions and the progress of the papain digestion were analyzed using SDS-PAGE (Fling and Gregerson, 1986; Laemmli, 1970). A 12.5 % separating gel and a 5 % stacking gel were used. The samples were adjusted to 50 μg mL^{-1} protein with ddH$_2$O (equals 1 μg protein per lane), diluted with Laemmli buffer (5x) and then incubated at 95 °C for 5 min. SigmaMarker wide range (6.5 kDa to 200 kDa; S8445; Sigma-Aldrich, Taufkirchen, Germany) was used as molecular weight standard. The electrophoresis was performed at 30 mA and 140 V. After staining (Fairbanks *et al.*, 1971), the gels were digitized. All electrophoresis buffers and staining solutions are detailed in the appendix (Table 8.14, Table 8.15).

4.1.3 Size exclusion chromatography (SEC)

Where quantitative data on the purity of a protein solution was required, a SEC (gel filtration) was performed using a Superdex 300 10/300 GL column (GE Healthcare, Solingen, Germany). 150 mM potassium phosphate buffer pH 6.5 was used as mobile phase with a flow rate of 0.4 mL min^{-1}. 300 μL sample with approx. 0.3 g L^{-1} protein were injected. UV detection was performed at 210 nm. The column was calibrated using purified standards of the proteins under study.

4.1.4 Functional lipase activity assay

A modified 4-nitrophenyl palmitate based assay (Liu *et al.*, 2006) was used for the determination of LIP activity in 300 μL 96-well plates (Nunc, Thermo Electron LED GmbH, Langenselbold, Germany). The reaction mixture with a total volume of 270 μL

consisting of 0.25 g L^{-1} 4-nitrophenyl palmitate, 0.3 g L^{-1} gum Arabic, 2.9 g L^{-1} Triton X-100 and 1.45 M Tris-HCl pH 7.5 was generated by mixing 22.5 µL solution A, 157.5 µL solution B and 90 µL of the LIP sample. Prior to the addition of the sample, the baseline absorbance at 410 nm was measured for 10 min at 37 °C. Subsequently, the kinetics were determined under the same conditions for 20 min. The composition of solutions A and B is detailed in the appendix (Table 8.16).

4.2   Preparation of the protein solutions

Some proteins were provided in solutions containing buffer components unfavorable for protein crystallization. Therefore, buffer changes were performed via dialysis or diafiltration, and the protein solutions were concentrated by ultrafiltration. FAB had to be generated by papain digestion of cetuximab and was subsequently purified by ion exchange chromatography. The specified buffer compositions of the protein stock solutions and the replacement buffers are listed in Table 4.2.

Table 4.2: Buffer composition of the protein stock solutions and the buffers the stock solutions were dialyzed or diafiltrated against. *LYS was provided as crystalline powder and dissolved in ddH$_2$O prior to crystallization.

Protein	c, g L^{-1}	Buffer in the stock solution	Replacement buffer
CET	5	NaCl, glycine, polysorbate 80, citric acid monohydrate, sodium hydroxide	ddH$_2$O
GLU	52	50 % glycerol	0.18 M ammonium sulfate pH 7
LIP	20	25 % (w/w) propylene glycol, 0.5 % (w/w) CaCl$_2$	25 mM Tris-HCl pH 9.0
LYS	-	None*	ddH$_2$O
XYL	34	43 % glycerol, 0.18 M sodium potassium phosphate buffer pH 7.0	(no exchange)

4.2.1 Dialysis

Dialysis was used in order to exchange the buffer of small volumes of protein solutions (up to 50 mL). If a dilution of 1 to 1000 could not be maintained due to the limitation of the dialysis buffer volume, two consecutive dialyses with a dilution of 1 to 100 were performed. The dialysis tubing had a molecular weight cut off of 14 kDa. The dialysis was performed overnight at 4 °C.

4.2.2 Cross-flow dia- and ultrafiltration

Two cross-flow filtration systems were used in order to exchange the buffer or to raise the protein concentration of larger volumes of protein solutions. The filtration equipment was purchased from Sartorius Stedim, Göttingen, Germany. The smaller system had an operating volume of 70 - 500 mL, the larger system had an operating volume of 0.15 L - 25 L. Both systems were operated using the same PESU membrane modules with 5 kDa molecular weight cut off and 0.1 m² filter area (No. 3051462901E--SG) at 4 °C. The transmembrane pressure was kept constant at 1 bar. The components of both cross-flow filtration systems are detailed in the appendix (Table 8.4 and Table 8.5, respectively). The setup of the larger cross-flow filtration system for the diafiltration of 1 L lipase is shown in Figure 4.1.
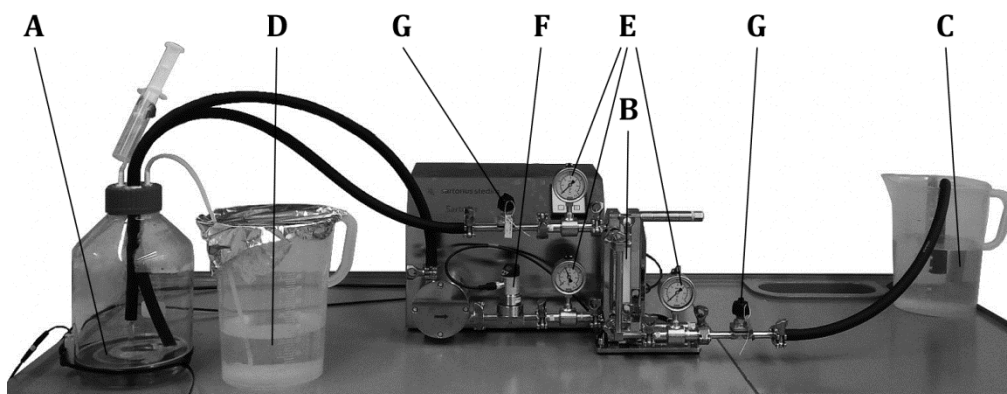
Figure 4.1: Cross-flow diafiltration of 1 L lipase solution using a Sartorius Slice system. The protein solution in the reservoir **(A)** is pumped over the PESU membrane in the filter holder **(B)**. The permeate is collected **(C)** and replaced by fresh buffer **(D)**. Analog and digital pressure gages **(E, F)** enable the calculation of the transmembrane pressure, which can be adjusted using valves **(G)**.

For diafiltration, a reservoir of fresh buffer was attached to the airtight cross-flow filtration circuit. Thereby, the permeate volume was replaced by fresh buffer, effectively removing the components of the initial buffer from the protein solution at a constant protein concentration. 5 diafiltration volumes were used, equaling a theoretical removal

of 99 % of the initial buffer. For the concentration of a protein solution, the buffer reservoir was disconnected and the permeate volume was not replaced by fresh solvent, thus increasing the protein concentration. Samples were taken and analyzed by UV spectroscopy at 280 nm in order to monitor the progress. The filtration was stopped as soon as the desired protein concentration was reached.

4.2.3   Papain digestion

The antigen-binding fragment of cetuximab (FAB) was generated by papain digestion of cetuximab. As the buffer of the cetuximab stock solution contained substances inhibiting proper papain digestion, the buffer was exchanged against ddH$_2$O. For initial screening experiments, 100 mg cetuximab were digested in a 100 mL stirred-tank for 1 h at 37 °C using 1 g L^{-1} cetuximab in a 40 mM phosphate buffer pH 7.0 containing 40 mM L-cysteine, 1 mM EDTA, and 2.5 mg L^{-1} papain from *Carica papaya*. The reaction was stopped by lowering the pH to 5.0 using acetic acid and the digested protein was stored at 4 °C until purification via cation exchange chromatography. The digestion was verified using SDS-PAGE and size exclusion chromatography (SEC). As more FAB was required, the papain digestion was performed with 2 g and finally with 20 g cetuximab under the same reaction conditions in larger-sized stirred-tanks.

4.2.4   Cation exchange chromatography (CEC)

For the crystallization experiments, FAB was separated from undigested cetuximab, the Fc fragment of cetuximab, and papain using cation exchange chromatography (CEC). Fractogel EMD SO3- (M) was kindly provided by Merck KGaA (Darmstadt, Germany) as chromatography medium. Depending on the protein load, different sized chromatography columns with packed bed volumes of 12 mL (12.5 mm ID), 200 mL (25 mm ID) and 900 mL (50 mm ID) were used with a maximum protein load of 25 mg mL^{-1}. The chromatography column was equilibrated with 40 mM sodium acetate buffer pH 5.0. The papain digest was diluted 2.5-fold to reduce the ionic strength and subsequently loaded onto the column. The flow-through was discarded. Using a step gradient, FAB was eluted separately from the other proteins with 150 mM NaCl in 40 mM sodium acetate buffer pH 5.0. The remaining proteins, i.e. papain and the Fc fragment, were eluted using 300 mM NaCl in 40 mM sodium acetate buffer pH 5.0. Finally, the column was cleaned with 1 M NaOH and stored at 4 °C in 20 % (v/v) ethanol. The purity of FAB was verified by SDS-PAGE and size exclusion chromatography (SEC).

4.3   Protein crystallization

A variety of different techniques for protein crystallization was used in this work. First, the initial screening based on crystallization conditions known from previous work or from the literature was carried out in µL-scale vapor diffusion and microbatch experiments. The best crystallization conditions were then transferred into agitated 5 mL-scale crystallizers. Subsequently, selected proteins were crystallized on a 100 mL- and a 1 L-scale, and the obtained crystals were characterized regarding their size. Finally, the removal of impurities, i.e., crystallization agents, from the crystals was studied. The initial crystallization conditions for each protein taken from published previous work and from the literature (see chapter 3.2.6).

4.3.1   Vapor diffusion crystallization

Hanging drop vapor diffusion experiments were performed in 24-well plates (Crystalgen, Commack, USA). Protein and crystallization agent stock solutions were prepared separately and subsequently mixed on siliconized circular cover slides, forming 10 µL drops. The slides were placed above 1 mL reservoir solution with the drop facing downwards (*hanging drop*). The reservoir solution contained twice the crystallization agent concentrations. The plates were sealed using medium viscosity silicon grease (Bayer, Leverkusen, Germany) and stored at 20 °C in a cooling incubator. Microphotographs of the drops for the qualitative evaluation of the crystallization conditions were taken in variable intervals.

4.3.2   Microbatch crystallization

10 µL-scale microbatch crystallization experiments were carried out in 72-well Terasaki plates (Greiner-Bio-One, Frickenhausen, Germany). For each crystallization condition, protein and crystallization agent stock solutions were prepared separately. The drops were prepared by gently mixing both, the protein and crystallization agent stock solutions in the wells. The Terasaki plates were sealed with 8 mL paraffin oil to avoid evaporation. The plates were stored at 20 °C. Microphotographs of the drops for the qualitative evaluation of the crystallization conditions were taken in variable intervals.

4.3.3   Agitated batch crystallization and overview of the crystallization systems

Description of the crystallization systems

Three geometrically similar stirred tanks were used for agitated batch crystallization experiments on a 1 L-, 100 mL- and a 5 mL-scale (Figure 4.2). Pitched-bladed impellers with low shear forces (Mirro and Voll, 2009) were used for gentle mixing of the crystal slurry. A more detailed view of the three-bladed segment-impellers is shown in Figure 4.3.

Figure 4.2: Geometrically similar stirred tanks used for the agitated batch crystallization on a 1 L-, 100 mL-, and 5 mL-scale. The pitched-bladed impellers were driven by stepping motors on top of the reactors. Ports in the tank heads allowed for sampling and feeding of crystallization agent solutions. The 5 mL- and 100 mL-tanks were immersed in a refrigerating circulator for temperature control; the 1 L-tank featured a cooling jacket.

The 1 L stirred tank was built using standard components (Table 8.8). It featured a height to diameter ratio of approximately 1.0 (regarding the fill level) and an agitator diameter to tank inner diameter ratio of 0.5. The glass vessel had a cooling jacket which was connected to a refrigerating circulator for temperature control. Ports in the tank heads allowed for sampling and feeding of crystallization agent solutions. The shaft was agitated by a stepper motor which enabled the use of a wide range of rotational speeds (10 min^{-1} to 2500 min^{-1}).
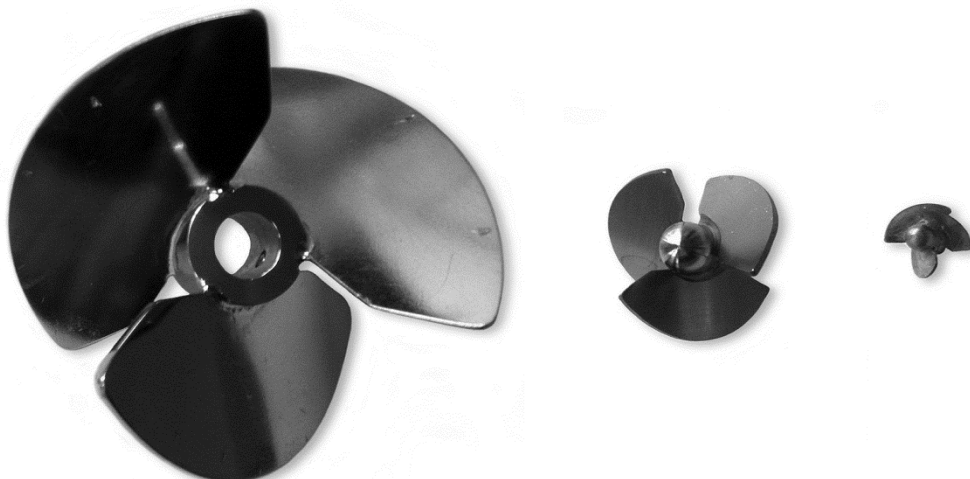
Figure 4.3: The 3 pitched-bladed impellers for the 1 L-, 100 mL-, and 5 mL-scale stirred tanks. The 1 L-scale impeller was attached to the shaft using a setscrew, while the smaller impellers were screwed on a male thread cut on the end of the shaft. The rotational direction was reversed for the 5 mL-scale impeller in order to prevent the screw joint from loosening at higher rotational speeds.

The smaller stirred tanks were custom-built scaled-down versions of the 1 L stirred tank. Standard round-bottom centrifuge tubes were used as glass vessels. Adjustments had to be made during the constructions of the smaller versions of the pitched-bladed impellers. As the diameter of the hub could not be reduced as much as desired, the blades would have had a lower surface compared with a perfectly scaled-down impeller. This was compensated by a slightly increased radius of the blades. For the 5 mL-scale impeller, the blade radius was increased from 12.8 mm to 13.2 mm and from 28.4 mm to 28.5 mm for the 100 mL-scale impeller. The specifications of the three stirred-tank crystallizers are listed in Table 4.3.

For the 5 mL stirred tank, the tank head was made from PTFE. The stainless steel shaft (1.4571) was directly connected to the motor shaft. For the 100 mL stirred tank, all components were made from stainless steel (1.4571). The shaft was mounted using two ball bearings and seals. The motor was connected to the shaft using a coupling on top of the tank head similar to the mechanism used in the 1 L stirred tank, thus reducing the effect of the unbalances of the motor. Other than the 1 L stirred thank, the smaller vessels had no cooling jacket and were therefore immersed in a refrigerating circulator. The experimental setup for the parallel 5 mL-scale crystallization in 12 reactors is shown in Figure 4.4. The design drawings are shown in the appendix (chapters 8.7.1 and 8.7.2).

Table 4.3: Relevant specifications of the three stirred-tank crystallizers. P/V values: personal communication from Benjamin Smejkal, TU München, Garching.

V, mL	5	100	1000
H, mm	20.0	58.9	120
D, mm	22.0	48.8	120
d, mm	11.3	24.8	60
H/D, -	0.9	1.2	1.0
D/d, -	0.51	0.51	0.5
P/V, W m^{-3}	-	-	150 min^{-1}: 19
			250 min^{-1}: 46
Parallel reactors	12	2	1
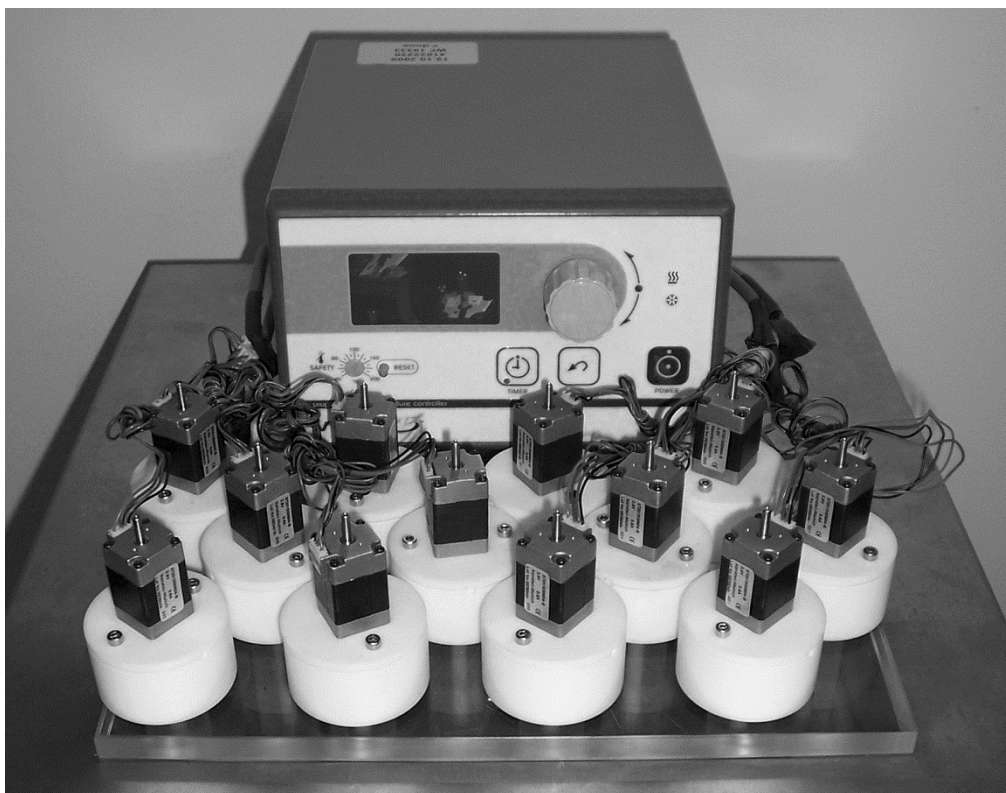
Figure 4.4: Experimental setup for the parallel crystallization using 12 individual 5 mL-scale reactors. The reactors are immersed in a refrigerating circulator for temperature control.

Agitated batch crystallization

Similar to microbatch experiments, the crystallization was started by mixing protein and crystallization agent stock solutions in the stirred tanks. The solutions and the stirred tanks were pre-cooled. In contrast to vapor diffusion and microbatch experiments, the

crystallization conditions could be adjusted during the crystallization process by the addition of crystallization agents. In order to monitor the progress of the crystallization process, samples of approx. 40 μL were taken from the tanks at variable time intervals. Crystals were sedimented for 2 min at 16 200 x g in a refrigerated centrifuge at the same temperature currently employed in the crystallization process. Subsequently, the supernatant was diluted and the protein concentration in solution was determined by UV spectroscopy at 280 nm.

The crystallization yield was determined as the quotient of the crystal mass obtained in the crystallization process and the initial amount of soluble protein. It was assumed, that all protein removed from the solution crystallized, since the formation of precipitate was not observed. Therefore, the crystal mass was estimated by subtraction of the remaining soluble protein at the end of the crystallization process from the protein present at the beginning of the experiment (Equation 8).

$$crystallization\ yield = \frac{protein_{sol.,0} - protein_{sol.,end}}{protein_{sol.,0}} \qquad \textit{(Equation 8)}$$

with $protein_{sol,0.}$ *protein in solution at the beginning*   *g*
                 $protein_{sol,end}$ *protein in solution after crystallization*   *g*

4.3.4 Microscopy and image analysis

Two different microscopes were used in this work. Microphotographs of vapor diffusion experiments were taken with an AxioCam ICc 3 camera attached to an Axioplan microscope (Carl Zeiss Microscopy GmbH, Jena, Germany). Crystals obtained in microbatch experiments or in agitated batch crystallization processes were analyzed using an Eclipse 50i microscope (Nikon Instruments Europe BV, Amsterdam, The Netherlands). The temperature of the microscope was kept constant at 20 °C using a cooled incubator in order to prevent the crystals from melting (Figure 4.5). The components of the two microscopy systems are listed in the appendix (Table 8.6 and Table 8.7, respectively).

Raw measurements were performed using the standard software *NIS Elements AR* (version 3.22). ImageJ (version 1.46r; http://imagej.nih.gov/ij/; Jul 2012) was used for further analysis, e.g., the evaluation of crystal size distributions. Therefore, area density distributions were calculated from measured crystal cross section areas from microphotographs (Hekmat *et al.*, 2007b).

Figure 4.5: Microphotographs of the protein crystals were taken using a DS-2Mv digital camera and a remotely operated OptiScan stage attached to a Nikon Eclipse 50i microscope, which was installed in a cooled incubator (T = 20 °C).

4.3.5 Washing of protein crystals and analysis of the removed substances

Protein crystals were washed in order to deplete unwanted substances from the solvent channels. First, a volume of approximately 150 µL crystals were sedimented by centrifugation for 2 min at 16 200 x g. The supernatant was removed and the crystals were resuspended in 1.5 mL wash solution. After 5 min, the crystals were sedimented again by centrifugation and subsequently dissolved in 1.5 mL ddH$_2$O for analysis. The protein concentration was measured by UV spectroscopy at 280 nm. PEG was determined using a modified Dragendorff reagent method (Jia and Tian, 2009). Acetate, citrate, ethanol, formate, phosphate, and 2-hydroxyethylammonium were quantified using common HPLC methods. The NaCl content was determined using a chloride assay purchased from Merck KGaA, Darmstadt, Germany (No. 1.14897.0001). Ammonium sulfate was determined using an ammonium assay purchased from R-Biopharm, Darmstadt, Germany (No. 11 112 732 035). The analytical methods are detailed in the appendix (chapter 8.5). The level of solvent content in the crystals had to be estimated in order to assess the relative amount of unwanted substances in the crystals.

5   Results and Discussion

5.1   Phase diagrams and protein crystallization on a 5 mL-scale

This chapter details the identification of suitable crystallization conditions for each of the proteins under study based on the literature. Therefore, phase diagrams were recorded to select crystallization conditions for the crystallization of each protein on a 5 mL-scale.

5.1.1   Lysozyme from *Gallus gallus* (LYS)

Phase diagrams for the vapor diffusion crystallization and the microliter-scale batch crystallization of LYS as well as data on the solubility of LYS are described extensively in the literature (see chapter 3.2.6). Consequently, no further screening for LYS phase diagrams was performed.

5.1.1.1   Microbatch-scale validation of crystallization conditions

Prior to the transfer of the LYS crystallization into the 5 mL-scale crystallizers, the crystallization conditions from the literature were validated in 10 µL-scale microbatch experiments. Microphotographs of the crystals obtained using 0.5 M - 1.25 M NaCl are shown in Figure 5.1.
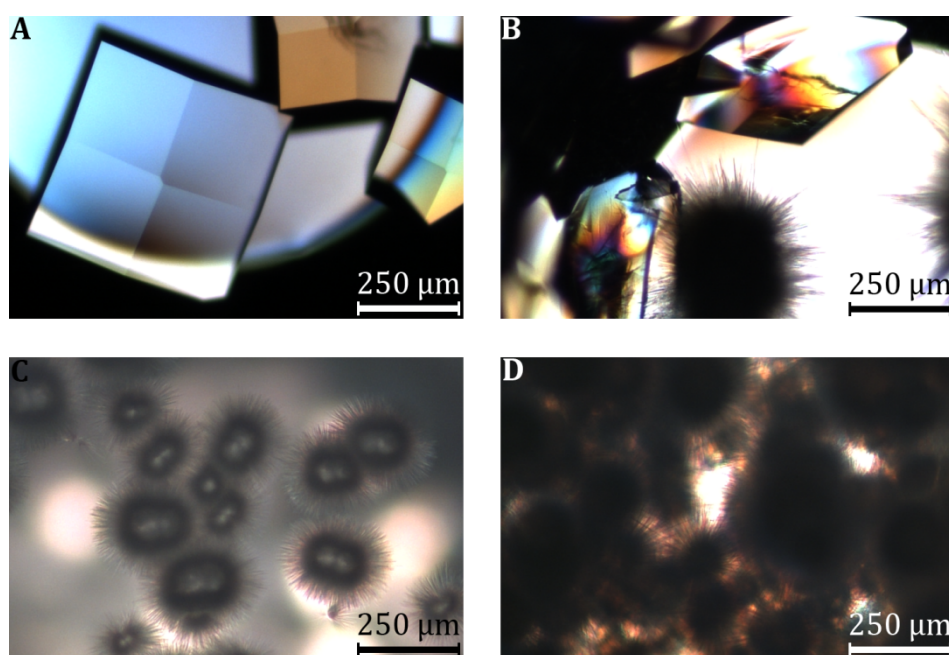
Figure 5.1: Microbatch-scale crystallization of 25 g L^{-1} lysozyme using varying NaCl concentrations, 25 mM sodium acetate buffer pH 4.0 at 20 °C. **A)** 0.5 M ($\approx$ 29 g L^{-1}) NaCl; **B)** 0.65 M ($\approx$ 38 g L^{-1}) NaCl; **C)** 0.95 M ($\approx$ 56 g L^{-1}) NaCl; **D)** 1.25 M ($\approx$ 73 g L^{-1}) NaCl.

The use of 0.5 M NaCl resulted in the formation of large single crystals. With increasing NaCl concentrations, the crystal form changes from large single crystals to sea urchin-like formations consisting of monoclinic crystal needles. At 0.65 M, these two crystal forms coexisted, whereas at 0.95 M and 1.25 M NaCl, only needle-like crystals were observed.

5.1.1.2 Crystallization on a 5 mL-scale

A wide range of crystallization conditions using NaCl as crystallization agent has been identified for LYS. In previous work, 50 g L^{-1} LYS, ≈ 0.68 M (40 g L^{-1}) NaCl and 25 mM sodium acetate buffer pH 4.0 were used for the agitated-batch crystallization at 20 °C in prototypes of the 5 mL-scale crystallizers using paddle impellers (Hekmat *et al.*, 2007b). However, spontaneous precipitation of LYS was sometimes observed upon mixing the LYS solution with the crystallization agent solution. In this work, the concentration of LYS was lowered to 25 g L^{-1} in order to avoid the formation of precipitate. The initial crystallization conditions were: 25 g L^{-1} LYS, ≈ 0.68 M (40 g L^{-1}) NaCl, and 25 mM sodium acetate buffer pH 4.0 at 20 °C.

5 mL-scale batch crystallization without agitation

As a reference, LYS was crystallized in the 5 mL-scale reactors without agitation using the initial crystallization conditions. The results are depicted in Figure 5.2.
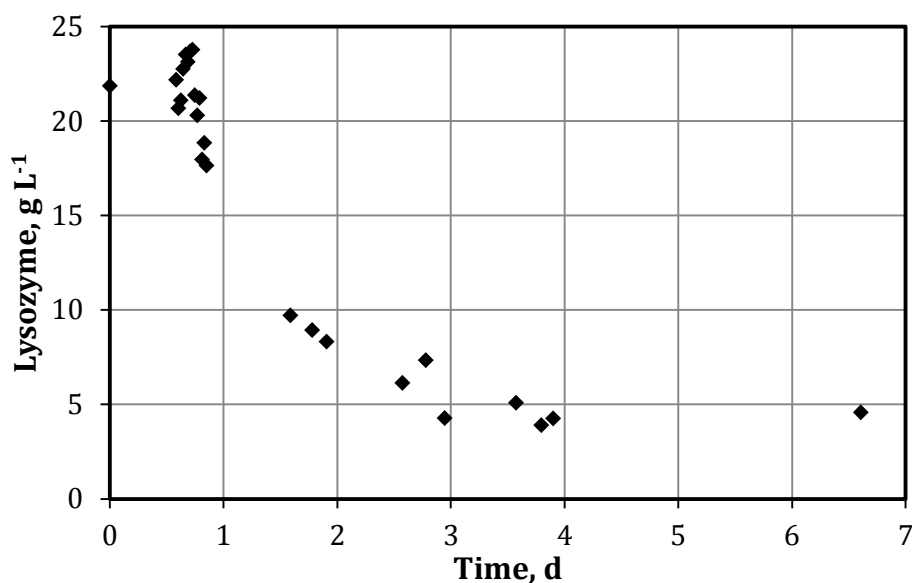
Figure 5.2: Crystallization of 25 g L^{-1} lysozyme on a 5 mL-scale using ≈ 0.68 M (40 g L^{-1}) NaCl, 25 mM sodium acetate buffer pH 4.0 and n = 0 min^{-1} at 20 °C. Depicted is the decrease of the lysozyme concentration in solution.

The crystallization started after 19.5 h due to the low nucleation rate. Crystals grew slowly, until the equilibrium concentration of 4 g L^{-1} was reached after 4 days. The crystals were not in suspension, but attached to the walls of the stirred-tank reactors. Consequently, microphotographs of the crystals could not be taken.

5 mL-scale batch crystallization with agitation

In order to avoid the attachment of crystals to the walls of the stirred-tank reactors and to ensure adequate mixing, the stirred-tank reactors were agitated using pitched-bladed impellers. A stirrer speed of 150 min^{-1}, resulting in a mixing time of 40 s (internal communication from Dr. Dariusch Hekmat, TU München, Garching), was chosen for the crystallization of LYS, as it was sufficient to keep the LYS crystals in suspension (data not shown). The results of the crystallization of LYS using the initial crystallization conditions at n = 150 min^{-1} are shown in Figure 5.3.
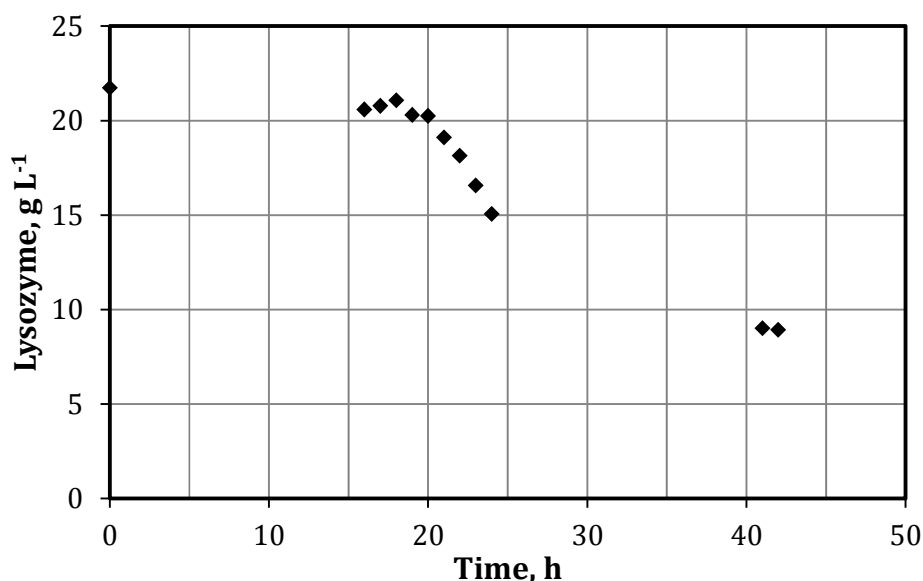
Figure 5.3: Crystallization of 25 g L^{-1} lysozyme on a 5 mL-scale using ≈ 0.68 M (40 g L^{-1}) NaCl, 25 mM sodium acetate buffer pH 4.0 and n = 150 min^{-1} at 20 °C. Depicted is the decrease of the lysozyme concentration in solution.

Similar to the unagitated crystallization of LYS, the crystallization started after 20 h. The equilibrium concentration of 9 g L^{-1} was reached within 40 h. In contrast to the previous unagitated crystallization, the LYS concentration did not decrease any further. The crystallization yield was 60 %. Large tetragonal-like crystals measuring up to 50 μm were observed next to a few needle-like crystals Figure 5.4.
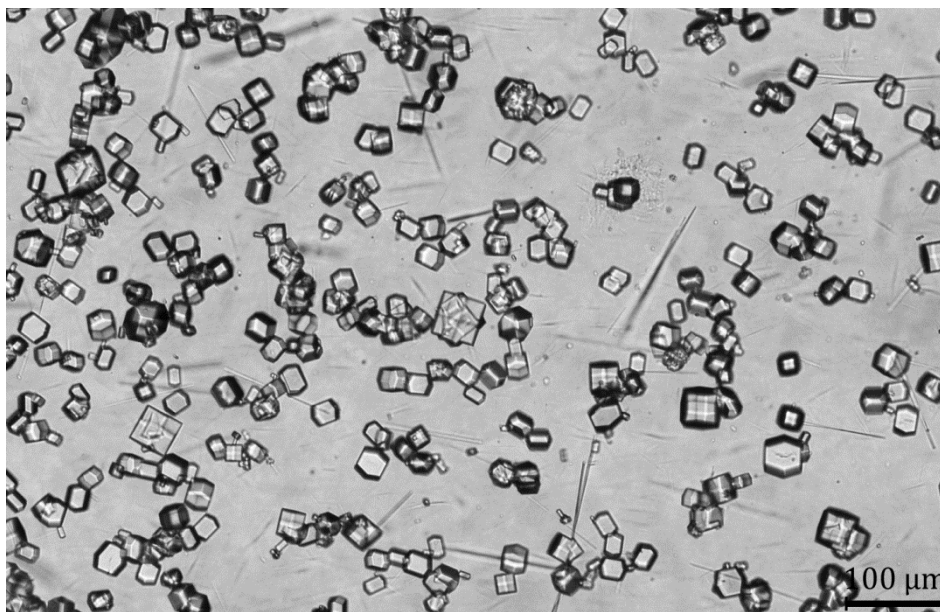
Figure 5.4: Tetragonal-like and a few needle-like lysozyme crystals and crystal clusters grown in the 5 mL-scale reactor using 25 g L^{-1} lysozyme, ≈ 0.68 M (40 g L^{-1}) NaCl, 25 mM sodium acetate buffer pH 4.0 and n = 150 min^{-1}.

5 mL-scale batch crystallization using an increased NaCl concentration

Rather slow crystallization kinetics and an unsatisfactory yield of only 60 % were observed in the previous experiments using the initial LYS crystallization conditions. The supersaturation was consequently raised by an increase of the NaCl concentration to 1.25 M (≈ 73 g L^{-1}). Additionally, a cooling step was introduced, as the solubility of LYS was known to be temperature-dependent (see chapter 3.2.6). When the equilibrium concentration for 20 °C was reached, the temperature was lowered to 10 °C. On the following day, the temperature was lowered to 0 °C. The following crystallization conditions were used: 25 g L^{-1} LYS, 1.25 M (≈ 73 g L^{-1}) NaCl, and 25 mM sodium acetate buffer pH 4.0 at 20 °C (initially). The results of the crystallization experiment implementing these two modifications are depicted in Figure 5.5.

With an increased NaCl concentration of 1.25 M, the crystallization started immediately after the addition of the crystallization agent solution. The LYS concentration in solution rapidly decreased to 7 g L^{-1} within the first hour. When the crystallization process was close to the equilibrium concentration at 20 °C (4 g L^{-1}; taken from Howard *et al.,* 1988), the temperature was reduced to 10 °C, and the LYS concentration continued to decrease. After 23 h, the temperature was lowered to 0 °C. The final equilibrium concentration was 2.7 g L^{-1} after 24 h, equaling a yield of 89 %. An increased formation of needle-like crystals was observed (Figure 5.6).
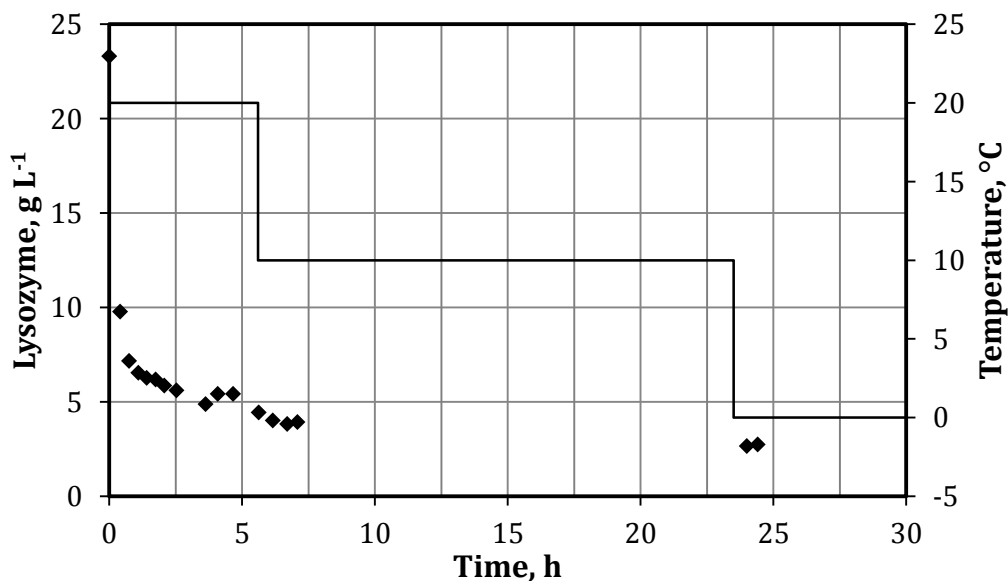
Figure 5.5: Crystallization of $25\,g\,L^{-1}$ lysozyme on a 5 mL-scale using 1.25 M ($\approx 73\,g\,L^{-1}$) NaCl, 25 mM sodium acetate buffer pH 4.0 and n = 150 min^{-1}. Depicted are ◆ the decrease of the lysozyme concentration in solution and the temperature time course (solid line).
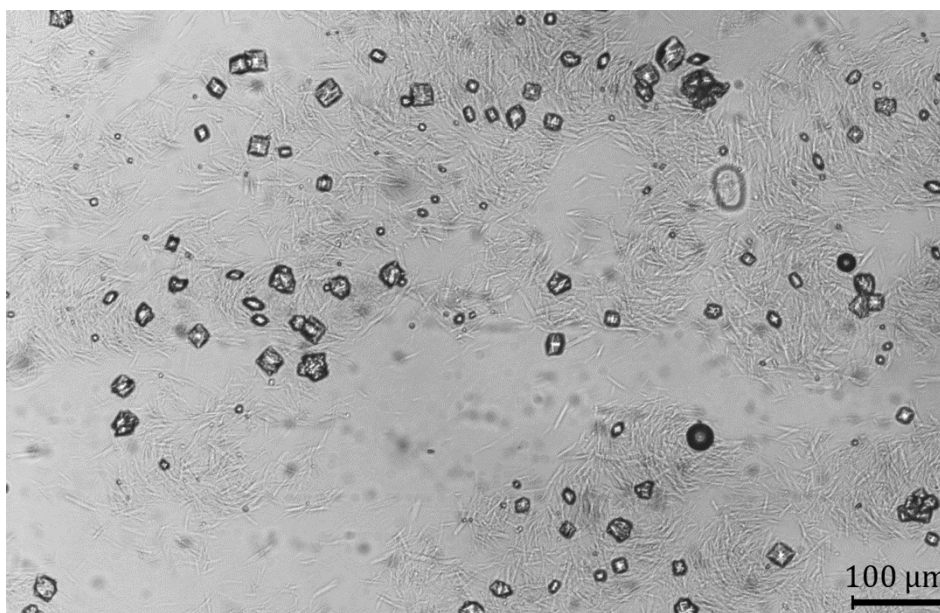
Figure 5.6: Tetragonal-like and needle-like lysozyme crystals and crystal clusters grown in the 5 mL-scale reactor using $25\,g\,L^{-1}$ lysozyme, 1.25 M ($\approx 73\,g\,L^{-1}$) NaCl, 25 mM sodium acetate buffer pH 4.0 and n = 150 min^{-1}.

5.1.1.3 Discussion

The crystallization of LYS was successfully transferred to the 5 mL-scale reactors based on phase diagrams from the literature. A stirrer speed of n = 150 min^{-1} was sufficient for the suspension of the crystals and no crystals were attached to the walls of the glass vessel. No crystal fragments were formed despite the low stability of protein crystals (Chernov, 2003). Nevertheless, an increased formation of needle-like crystals was

observed at 1.25 M NaCl, which would be unfavorable for the further handling (e.g., filtration) in a large-scale production process. This is in accordance to the data from the microbatch-scale validation of crystallization conditions and from the literature (Hekmat *et al.*, 2007a). Similar crystallization kinetics were observed in both, the unagitated and the agitated crystallization, using the initial crystallization conditions. Consequently, the crystallization kinetics were not affected negatively by shear forces due to agitation of the reactor, which is in accordance with the literature (Tait *et al.*, 2009). Also, the crystallization kinetics in the unagitated crystallization experiment were not diffusion limited, as no acceleration of the kinetics was observed in the agitated crystallization experiment using the same crystallization conditions. Compared to previous work, the crystallization yield was improved from 82 % within 8 h to 89 % within 24 h. While the crystallization kinetics were slower and the equilibrium was only reached within 24 h, increased crystallization kinetics should be possible using earlier cooling steps while maintaining the same yield.

5.1.2   Lipase from *Thermomyces lanuginosus* (LIP)

The vapor diffusion sitting drop crystallization of LIP has been described in the literature (see chapter 3.2.6). Prior to the transfer of the LIP crystallization into the 5 mL-scale crystallizers, the crystallization conditions from the literature were validated in 10 µL-scale microbatch experiments. The LIP concentration was raised to 100 g L^{-1} in all experiments. Crystals were obtained using 40 - 100 mM NaCl and 25 mM sodium acetate buffer pH 4.0. Variations of the NaCl concentration within this range did not affect the qualitative results of the microbatch-scale crystallization of LIP. High NaCl concentrations from 0.75 M to 1.0 M resulted in precipitate formation. The crystallization drops remained clear between these two ranges. Due to this very limited nucleation zone, no phase diagram was recorded. A microphotograph of LIP crystals grown using 80 mM NaCl is shown in Figure 5.7.
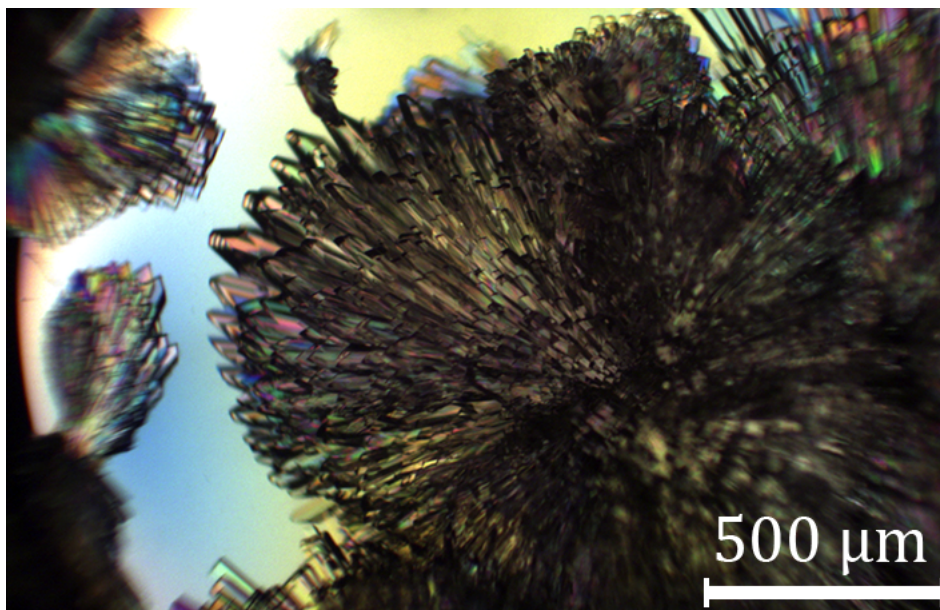
Figure 5.7: Lipase (LIP) crystals obtained in the microbatch-scale crystallization using 100 g L^{-1} LIP, 80 mM NaCl, and 25 mM sodium acetate buffer pH 4.0 at 20 °C.

The following crystallization conditions were chosen for the transfer of the LIP crystallization into the 5 mL-scale stirred-tank reactors: 100 g L^{-1} LIP, 55 mM NaCl, and 25 mM sodium acetate buffer pH 4.0 at 20 °C. The stirrer speed was increased to n = 250 min^{-1}, as a portion of the LIP crystals sedimented at n = 150 min^{-1}. The results of the 5 mL-scale crystallization of LIP are depicted in Figure 5.8.
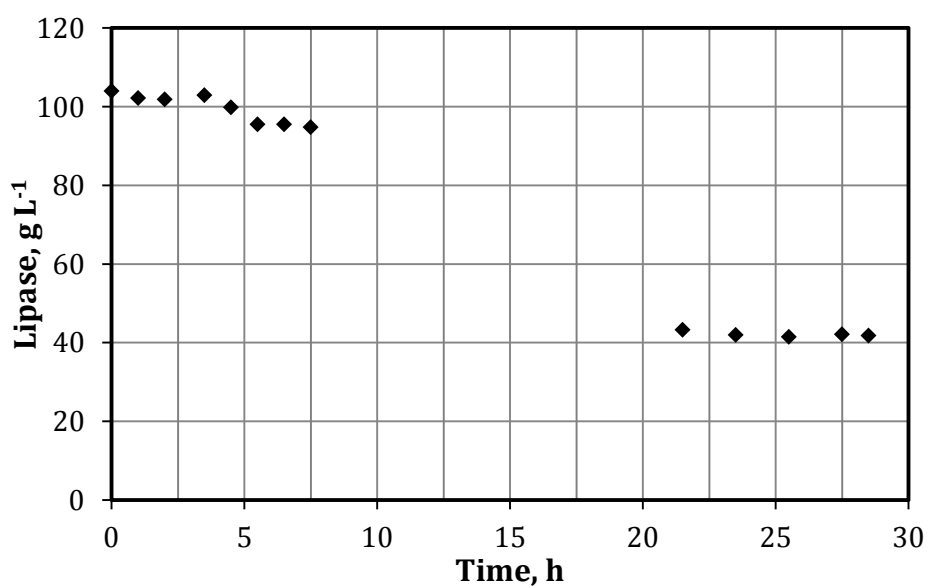
Figure 5.8: Crystallization of 100 g L^{-1} lipase on the 5 mL-scale using 55 mM NaCl, and 25 mM sodium acetate buffer pH 4.0 (T = 20 °C, n = 250 min^{-1}). Depicted is the decrease of the lipase concentration in solution.

The crystallization started after 5 h and the equilibrium was reached within 23.5 h. The equilibrium concentration of LIP was 41.9 g L^{-1}, equaling a crystallization yield of 58 %. Only needle-like crystals up to 120 µm in length were observed (Figure 5.9). The solubility of LIP did not show a temperature-dependency (data not shown).
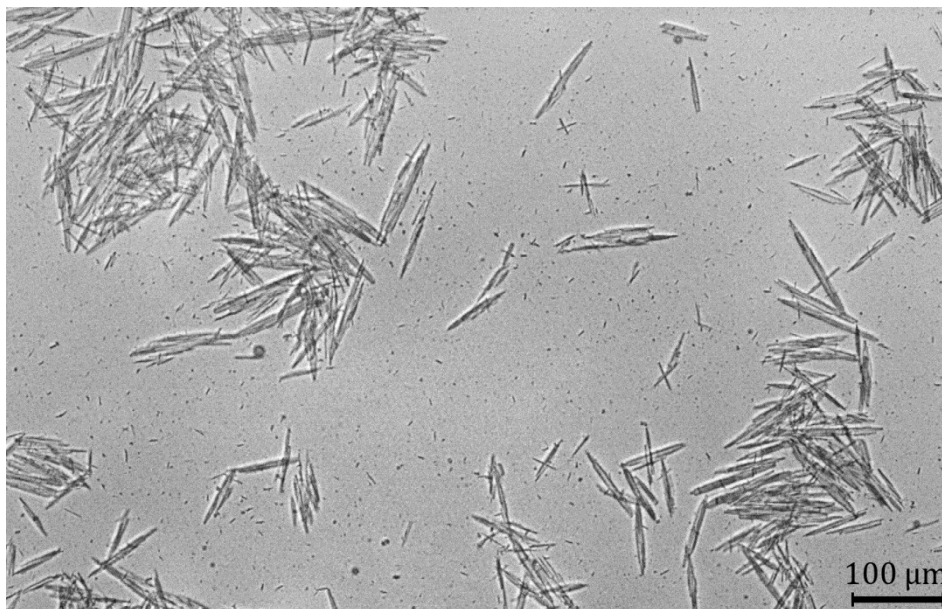
Figure 5.9: Needle-like lipase crystals grown in the 5 mL-scale reactor using 100 g L^{-1} lipase, 55 mM NaCl, and 25 mM sodium acetate buffer pH 4.0 (T = 20 °C, n = 250 min^{-1}).

Discussion

The nucleation zone for the crystallization of LIP using NaCl in sodium acetate buffer pH 4.0 was narrow. Hence, no phase diagram was recorded and the crystallization was directly transferred into the 5 mL-scale reactors. While other lipases were previously crystallized in vessels with volumes up to 500 mL (Jacobsen *et al.*, 1998; Lee *et al.*, 2000), the crystallization of LIP in scalable reactors was reported for the first time. The yield was rather low (58 %). Unlike LYS, LIP did not exhibit a temperature-dependent solubility. Also, a variation of the NaCl concentration was not feasible due to the limited nucleation zone. Needle-like crystals were observed in both the microbatch-scale experiments and the 5 mL-scale reactors. This crystal form is unfavorable for the further processing of the crystals in a large-scale production process. Hekmat *et al.* (2008) reported a shift of the LIP crystal form from needle-like to compact crystals using ionic liquids in vapor diffusion experiments, which shall be investigated in chapter 5.2.2.

5.1.3 Xylanase II from *Trichoderma reesei* (XYL)

5.1.3.1 Microbatch-scale screening of crystallization conditions

Starting point for the microbatch-scale screening of crystallization conditions were the vapor diffusion crystallization conditions described in chapter 3.2.6. The XYL solution used in this work was provided in 43 % glycerol, 0.18 M sodium potassium phosphate buffer pH 7.0. A buffer exchange via dialysis resulted in precipitation of XYL (data not shown). In first experiments, the XYL solution was diluted using bidistilled water for crystallization conditions with a lower XYL concentration. However, an increasing tendency towards precipitation was observed with descreasing XYL concentrations (data not shown). Consequently, XYL solutions were diluted using 43 % glycerol instead of bidistilled water. The qualitative results of microbatch-scale crystallization experiments using the crystallization conditions from the literature and modifications thereof are listed in Table 5.1.

Table 5.1: Qualitative results for the microbatch-scale crystallization of 16 g L^{-1} xylanase. The crystallization conditions were taken from the literature (Hampton, 2010; Törrönen *et al.*, 1993) or modifications thereof.

Crystallization agent	Concentration, M	Result
Sodium potassium phosphate buffer pH 7.0	1.4 - 2.6	Crystals
Sodium potassium phosphate buffer pH 7.4	1.1 - 2.2	Crystals
Sodium potassium phosphate buffer pH 8.2	0.9 - 2.6	Crystals
Ammonium sulfate in sodium acetate buffer pH 4.3	0.8 - 1.4	Precipitate
Ammonium sulfate in sodium citrate buffer pH 4.0 / 4.5	0.8 - 1.4	Precipitate
Ammonium sulfate in Na/K phosphate buffer pH 8.2	1.1 - 2.0	Crystals
Ammonium sulfate in Tris-HCl pH 7.5	1.0 - 2.0	Crystals
Ammonium sulfate in Tris-HCl pH 8.0	1.0 - 1.5	Crystals
Ammonium sulfate in Tris-HCl pH 8.5	1.2 - 1.5	Crystals

No crystals were obtained using the crystallization conditions with ammonium sulfate at pH 4.0 - 4.5. At a neutral to slightly basic pH, both sodium potassium phosphate buffer and ammonium sulfate yielded crystals. Na/K phosphate buffer pH 8.2 was selected for further experiments, since it showed the broadest concentration range for the crystallization of XYL. Microphotographs of crystals grown at different combinations of XYL and crystallization agent concentrations are depicted in Figure 5.10.
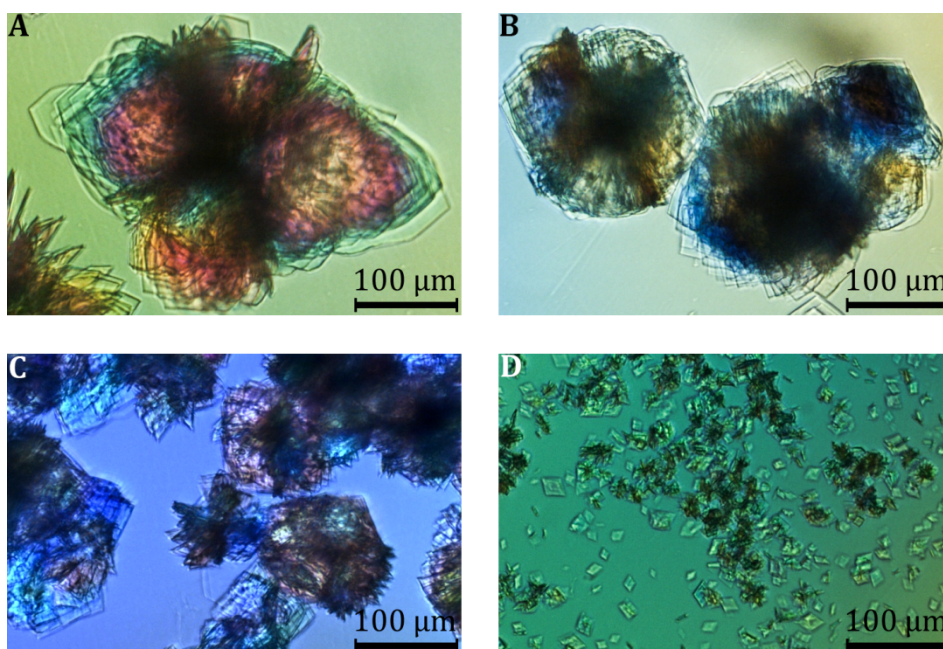
Figure 5.10: Xylanase (XYL) crystals obtained in the microbatch-scale screening using various concentrations of Na/K phosphate buffer pH 8.2 (PB) at 20 °C. **A)** 6.7 g L^{-1} XYL, 0.75 M PB; **B)** 14.7 g L^{-1} XYL, 0.69 M PB; **C)** 22 g L^{-1} XYL, 0.6 M PB; **D)** 29 g L^{-1} XYL, 0.34 M PB.
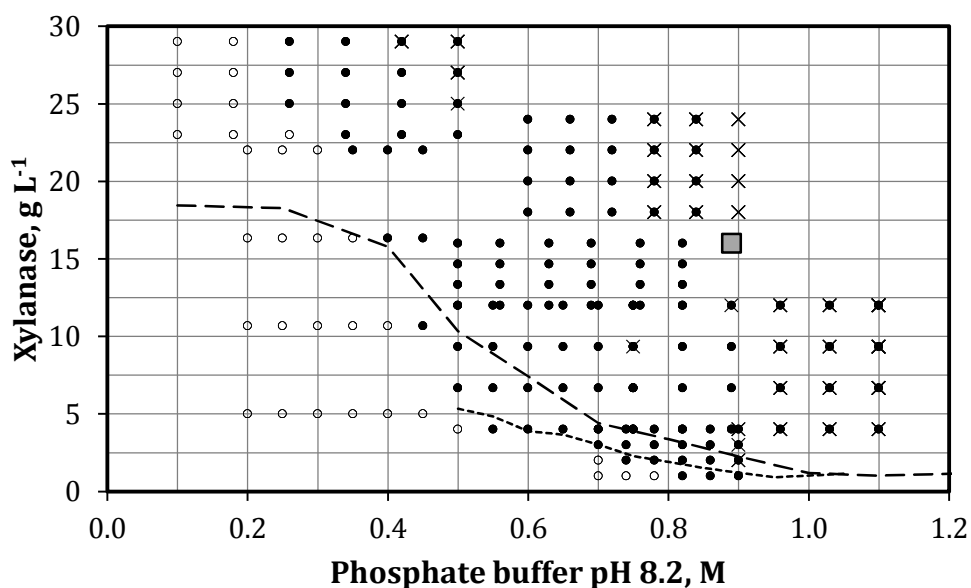
Figure 5.11: Phase diagram for xylanase (XYL) solved in 43 % glycerol obtained from the qualitative evaluation of microbatch-scale crystallization of 1 - 29 g L^{-1} XYL using 0.1 - 1.1 M sodium potassium phosphate buffer pH 8.2 at 20 °C. • crystal growth; × precipitate formation; ○ no crystallization or precipitation. The crystallization condition used for the subsequent 5 mL-scale crystallization is marked with a grey square. The lines denote the XYL solubility (dashed: determined using 29 g L^{-1} XYL; dotted: determined using 10 g L^{-1} XYL). The lines are included for visualization and are not the result of a simulation.

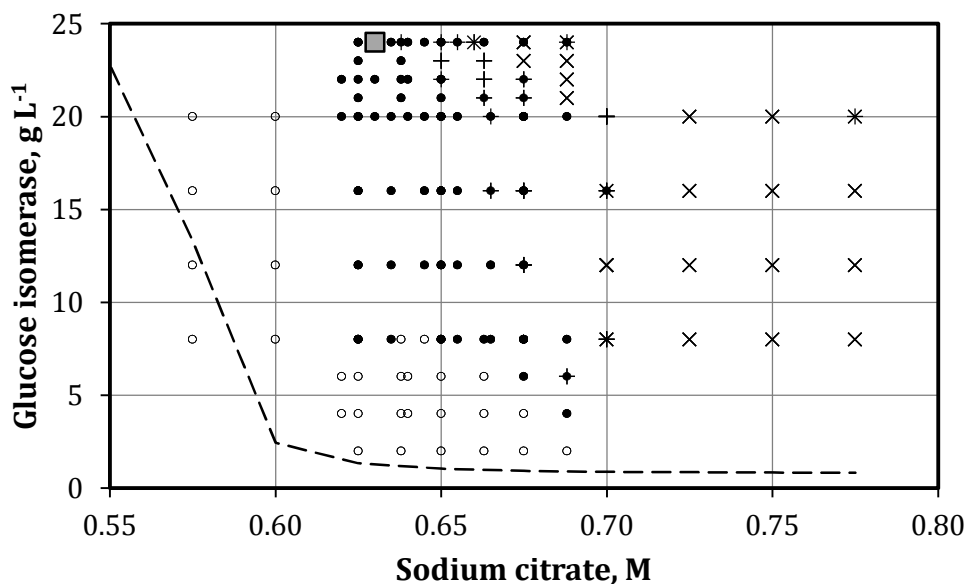The phase diagram derived from the qualitative evaluation of the microbatch-scale crystallization of XYL is depicted in Figure 5.11. Crystallization was observed over a

broad range of XYL and sodium potassium phosphate buffer (PB) concentrations. A distinct metastable zone only existed for PB concentrations below 0.4 M. At PB concentrations over 0.9 M, crystallization was only observed for very low XYL concentrations or with concurrent precipitation. Thus, higher potassium phosphate buffer concentrations were not evaluated for the phase diagram. Different solubility curves were obtained for XYL depending on the initial XYL concentration used in the experiments. A higher solubility was observed in experiments with a higher initial XYL concentration.

5.1.3.2 Crystallization on a 5 mL-scale

During the microbatch-scale screening for crystallization conditions, crystallization was observed for XYL concentrations up to 29 g L^{-1}. Due to the increased XYL solubility at the lower sodium potassium phosphate buffer (PB) concentrations necessary for the crystallization using high XYL concentrations, the supersaturation was only 0.6 and slow nucleation was observed (data not shown). Hence, a lower XYL concentration of 16 g L^{-1} and 0.89 M PB pH 8.2 were used for the crystallization on a 5 mL-scale, resulting in a supersaturation of 2.1. It shall be noted, that the 5 mL-scale crystallization of XYL was performed at an early stage of this work, and the reactors were agitated using prototype marine impellers instead of the pitched-bladed impellers. The marine propellers were operated at 115 min^{-1}. The results of the 5 mL-scale crystallization of XYL are depicted in Figure 5.12.
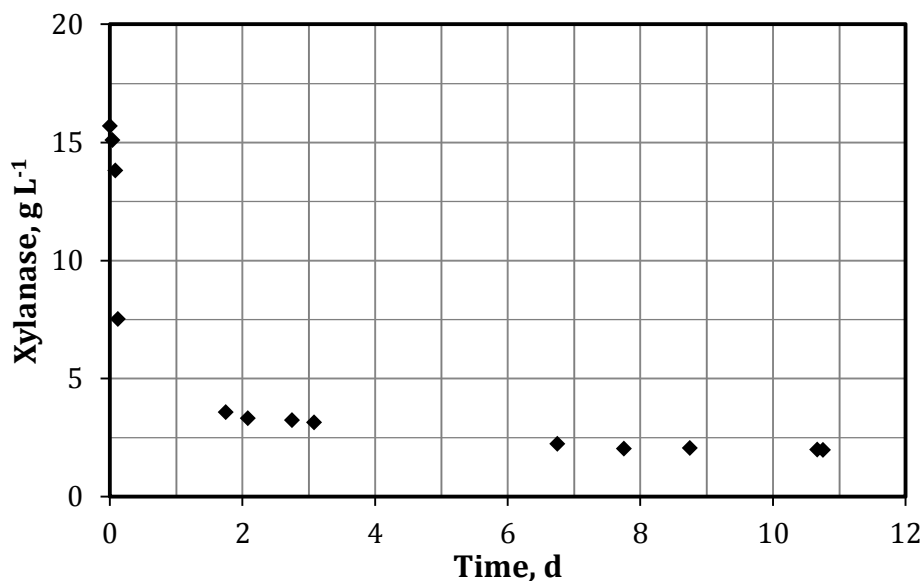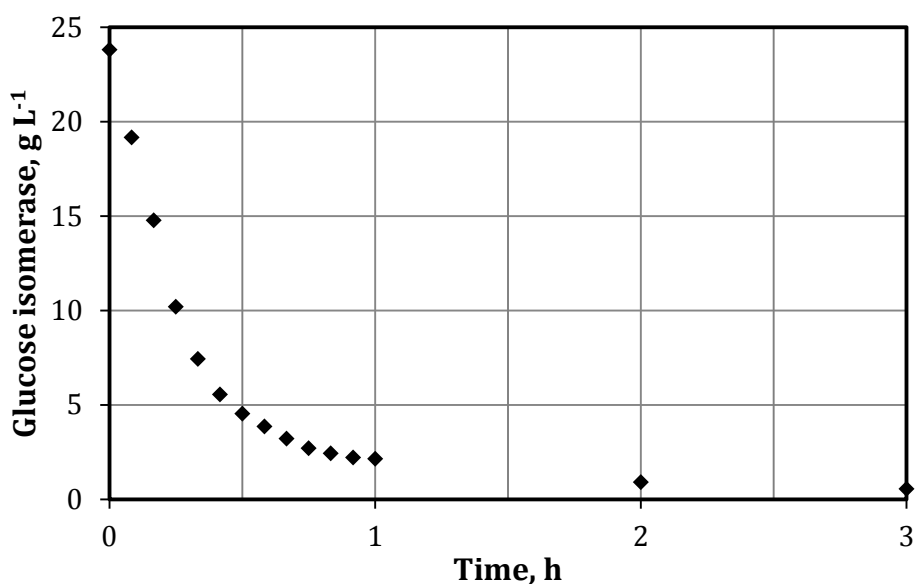
Figure 5.12: Crystallization of 16 g L^{-1} xylanase on a 5 mL-scale using 0.89 M phosphate buffer pH 8.2 at 20 °C and n = 115 min^{-1} (marine propellers). Depicted is the decrease of the xylanase concentration in solution.

The crystallization started immediately after the addition of the crystallization agent solution. Within 3 h, the XYL concentration had decreased to 7.5 g L^{-1} (yield: 53 %) and the crystallization kinetics slowed down. The residual XYL concentration was 3.3 g L^{-1} after 2 d (yield: 79 %) and the equilibrium of 2 g L^{-1} was reached after 7.5 d, equaling a yield of 87 %. The crystals obtained in this experiment initially measured up to 40 μm. Increased secondary nucleation was observed during the long crystallization process (Figure 5.13).
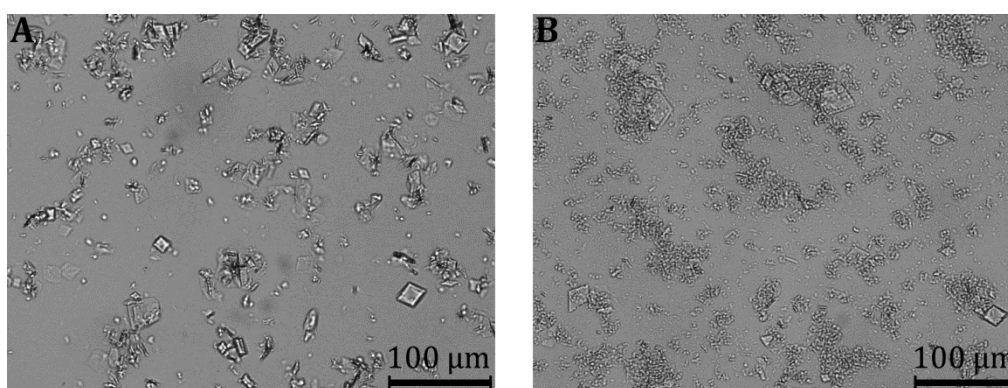
Figure 5.13: Xylanase crystals grown in the 5 mL-scale reactor using 16 g L^{-1} xylanase, and 0.89 M sodium potassium phosphate buffer pH 8.2 (T = 20 °C, marine propellers, n = 115 min^{-1}) after **A)** 2.5 h, and **B)** 10.8 d.

Based on the phase diagram, the XYL solubility was expected to decrease for higher PB concentrations. As higher initial PB concentrations would have caused precipitation, PB was added stepwise up to a final concentration of 1.4 M during the crystallization

process, when the XYL concentration before the crystallization kinetics decreased. It was verified that precipitation occurred at no time. The results of this experiment are depicted in Figure 5.14.
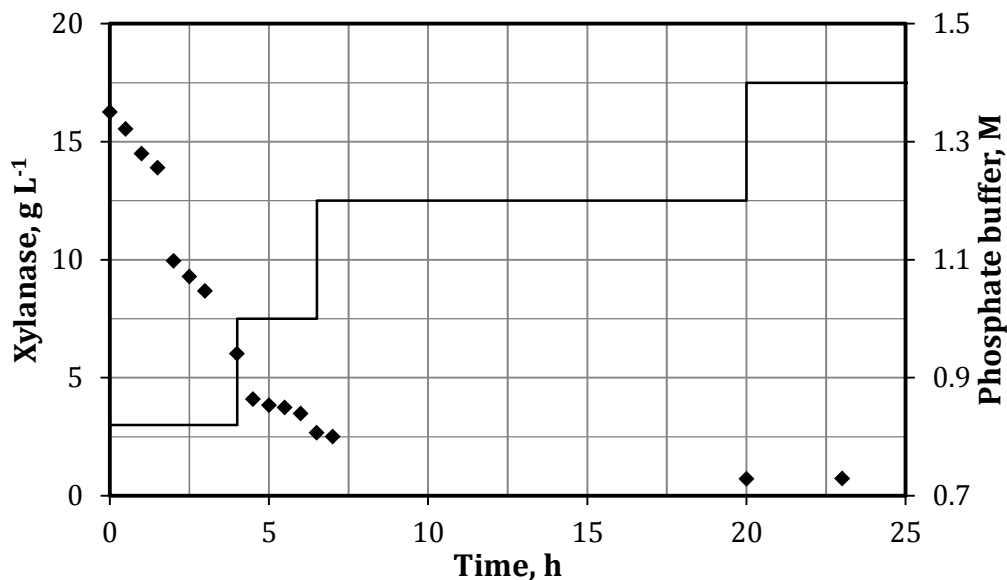
Figure 5.14: Crystallization of 16 g L^{-1} xylanase on a 5 mL-scale at 20 °C and n = 115 min^{-1} (marine propellers). The initial phosphate buffer concentration was 0.82 M. During the crystallization process, phosphate buffer was added in order to increase the crystallization yield. Depicted are ◆ the decrease of the xylanase concentration in solution and the time course of the phosphate buffer concentration (solid line).

Similar to the previous experiment, the crystallization started immediately after the addition of the crystallization agent solution. The PB concentration was increased to 1.0 M when the XYL concentration dropped below 7.5 g L^{-1}. It was further increased to 1.2 M at 3.5 g L^{-1} XYL. Finally, the PB concentration was raised to 1.4 M, resulting in a XYL equilibrium concentration of 0.7 g L^{-1} after 20 h. The crystallization yield was 95 %. Crystals measuring up to 50 μm were observed (Figure 5.15).
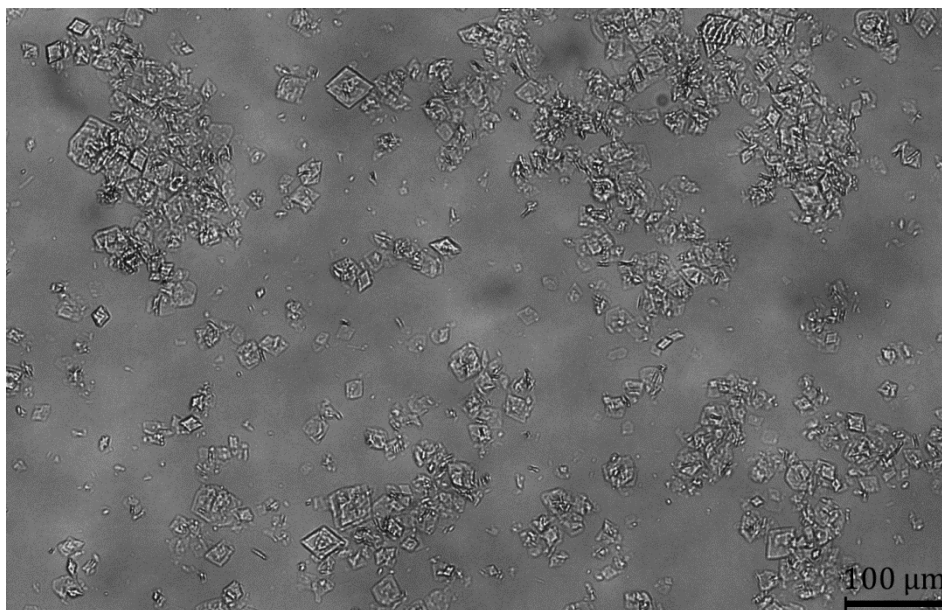
Figure 5.15: Xylanase crystals grown in the 5 mL-scale reactor using 16 g L^{-1} xylanase, and 0.89 M sodium potassium phosphate buffer pH 8.2 (T = 20 °C, marine propellers, n = 115 min^{-1}) after 26 h.

PB concentrations over 1.5 M resulted in a higher solubility of XYL and could consequently not be used to further increase the crystallization yield.

5.1.3.3 Discussion

For XYL, crystallization conditions with a low (4.2) and a high (7.0 - 8.2) pH were reported in the literature (Hampton, 2010; Törrönen *et al.*, 1993). The crystallization conditions with low pH could not be reproduced. The XYL solution used in this work was stabilized using 43 % glycerol and exhibited precipitation upon lowering the glycerol content, whereas Törrönen *et al.* crystallized XYL from a solution never brought in contact with glycerol. Thus, the stabilization of XYL using glycerol might prevent nucleation at low pH. The solubility of XYL was shown to be dependent on the amount of XYL used for the experiment. As the glycerol content was kept constant at 43 %, it is assumed that the XYL stock solution provided from the cooperation partner contained other additional substances which stabilized XYL in solution.

The crystallization of XYL in scalable reactors was reported for the first time. Crystallization conditions with a supersaturation of 2.1 were successfully transferred into the 5 mL-scale reactors. The crystallization yield and the crystallization kinetics were improved from 53 % within 7.5 d to 95 % within 20 h by the addition of crystallization agent during the crystallization process. The shorter process time resulted in less secondary nucleation due to crystal collisions. A similar correlation was

demonstrated for the crystallization of LYS (Tait *et al.*, 2009). The phase diagram suggests a further increase of the crystallization yield to 97 % using a higher initial XYL concentration of 29 g L^{-1} and by increasing the crystallization agent concentration during the crystallization process. However, the crystallization kinetics were very slow due to the low supersaturation of 0.6. Future experiments could investigate crystal seeding as a method to bypass primary nucleation, consequently leading to faster crystallization kinetics.

5.1.4 Glucose isomerase from *Streptomyces rubiginosus* (GLU)

5.1.4.1 Microbatch-scale screening of crystallization conditions

Starting point for the microbatch-scale screening were the following crystallization conditions from the literature: A) 1.5 - 2.5 M ammonium sulfate, pH 7.0; B) 100 - 150 g L^{-1} PEG 4000 - 8000 in 200 mM ammonium sulfate, pH 7.0; C) 0.6 - 1.0 M sodium citrate, pH 8.0 (see chapter 3.2.6). The crystallization conditions with very high precipitant concentrations, e.g., > 1.7 M ammonium sulfate, could not be reproduced due to solubility limitations of the stock solutions. The qualitative results of crystallization experiments using these crystallization conditions and modifications thereof are listed in Table 5.2.

Table 5.2: Qualitative results for the crystallization of 20 g L^{-1} glucose isomerase. The crystallization conditions were taken from the literature (Hampton, 2012) or modifications thereof.

Crystallization agent	Concentration	Result
Ammonium sulfate	0.8 - 1.7 M	Crystals and precipitate
PEG 2000 in 200 mM ammonium sulfate	100 - 150 g L^{-1}	Precipitate
PEG 4000 in 200 mM ammonium sulfate	50 - 70 g L^{-1}	Precipitate
PEG 8000 in 200 mM ammonium sulfate	90 - 110 g L^{-1}	Precipitate
Sodium citrate	0.6 M - 0.8 M	Crystals (compact)
Sodium citrate	0.9 M - 1.1 M	Crystals (rod-shaped)

Precipitation was observed in the experiments with ammonium sulfate and PEG. Compact or rod-shaped GLU crystals were obtained using sodium citrate. Consequently, subsequent experiments were performed with sodium citrate. A number of different buffer systems were used to further characterize the crystallization of GLU using sodium

citrate as crystallization agent. Next to conventional buffers, i.e., sodium citrate itself, HEPES, and Tris-HCl, buffers from the literature were evaluated, i.e., sodium citrate borate and imidazole malate (Stura *et al.*, 1992). All buffer systems performed well. The sodium citrate borate buffer system was chosen for further experiments. A selection of GLU crystals obtained in the microbatch-scale screening is shown in Figure 5.16.
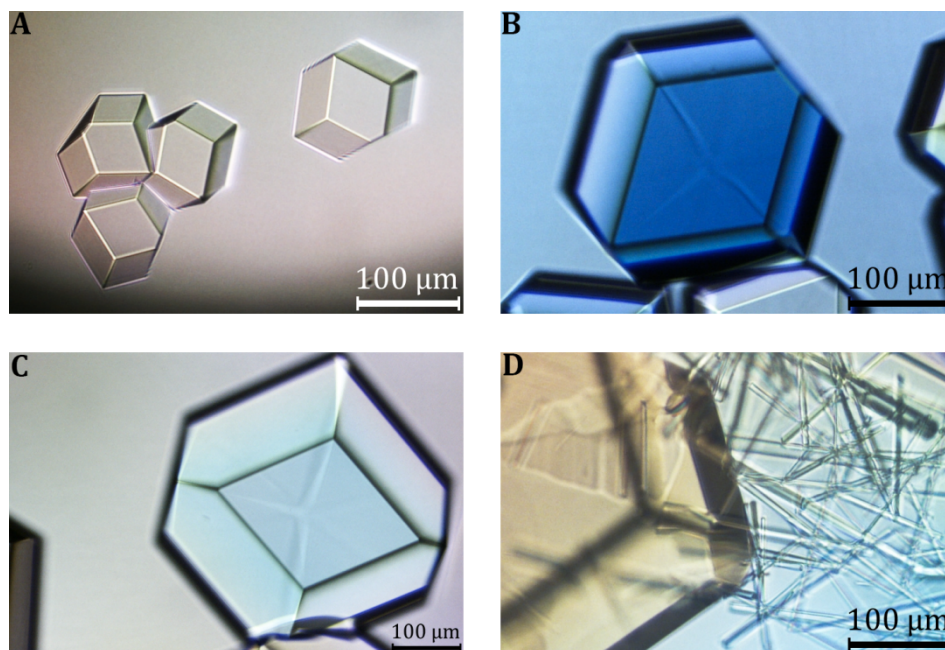
Figure 5.16: Compact and rod-shaped glucose isomerase (GLU) crystals obtained in the microbatch-scale screening using varying concentrations of sodium citrate (SC) in sodium citrate borate buffer pH 8.5 at 20 °C. **A)** 4 g L^{-1} GLU, 0.688 M SC; **B)** 12 g L^{-1} GLU, 0.675 M SC; **C)** 16 g L^{-1} GLU, 0.625 M SC; **D)** 20 g L^{-1} GLU, 0.675 M SC. The scale of figure **C** differs from the other images due to the large size of the crystal.

The phase diagram derived from the qualitative evaluation of the microbatch-scale crystallization of GLU is depicted in Figure 5.17.

Figure 5.17: Phase diagram for glucose isomerase (GLU) obtained from the qualitative evaluation of microbatch-scale crystallization using sodium citrate in 47 mM sodium citrate borate buffer pH 8.5 as crystallization agent. • crystal growth; + rod-shaped crystals; × precipitate formation; ○ no crystallization or precipitation. The crystallization condition used for the subsequent 5 mL-scale crystallization is marked with a grey square. The dashed line denotes the GLU solubility curve. The line is included for visualization and is not the result of a simulation.

The formation of compact single crystals from a broad range of GLU concentrations is observed over a narrow range of sodium citrate concentrations (0.62 M - 0.69 M). At higher concentrations, the formation of rod-shaped crystals and/or precipitation is observed. A distinct metastable zone exists for 0.5 - 0.7 M sodium citrate. Higher GLU concentrations could not be employed due to solubility limits of the protein and crystallization agent stock solutions. For sodium citrate concentrations over 0.65 M, the solubility of GLU is nearly constant.

5.1.4.2 Crystallization on a 5 mL-scale

During the microbatch-scale screening for crystallization conditions, crystallization was observed for 24 g L^{-1} GLU using 0.625 - 0.655 M sodium citrate. As the formation of rod-shaped crystals should be avoided, 0.63 M sodium citrate was chosen for the transfer of the crystallization into the 5 mL-scale stirred-tank reactors. The resulting crystallization conditions were: 24 g L^{-1} GLU, 0.63 M sodium citrate, and 47 mM sodium citrate borate buffer pH 8.5. The supersaturation estimated from the phase diagram was 3.3. It shall be noted, that the 5 mL-scale crystallization of GLU was performed at an early stage of this work, and the reactors were agitated using prototype marine impellers instead of the

pitched-bladed impellers. The marine propellers were operated at 115 min^{-1}. The results of the 5 mL-scale crystallization of GLU are depicted in Figure 5.18.

Figure 5.18: Crystallization of 24 g L^{-1} glucose isomerase on a 5 mL-scale using 0.63 M sodium citrate, and 47 mM sodium citrate borate buffer pH 8.5 at 20 °C and n = 115 min^{-1} (marine propellers). Depicted is the decrease of the glucose isomerase concentration in solution.

The crystallization started immediately after the addition of the crystallization agent solution. Within 1 h, the concentration of GLU decreased to 2.1 g L^{-1} (crystallization yield: 91 %). The final equilibrium concentration of 0.6 g L^{-1} was reached after 3 h, equaling a crystallization yield of 97 %. Compact single crystals measuring up to 25 μm were observed (Figure 5.19).
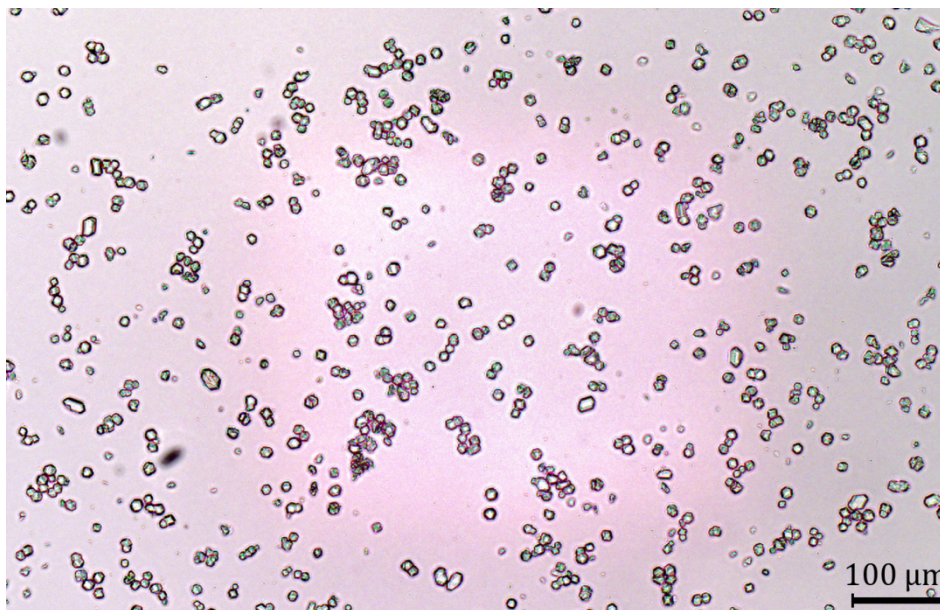
Figure 5.19: Glucose isomerase crystals grown in the 5 mL-scale reactor using 24 g L^{-1} glucose isomerase, 0.63 M sodium citrate, and 47 mM sodium citrate borate buffer pH 8.5 at 20 °C and n = 115 min^{-1} (marine propellers) after 2.5 h.

5.1.4.3 Discussion

Similar to XYL, the stock solution for GLU contained 50 % glycerol for stabilization in contrast to the GLU solutions used for crystallization in the literature. However, the buffer could be exchanged to 0.18 M ammonium sulfate using diafiltration without loss of GLU stability. Using the GLU crystallization conditions detailed in Hampton (2012), GLU crystals were only obtained with sodium as crystallization agent in this work. A possible explanation might be residual glycerol bound to the GLU molecules. GLU crystals were rod-shaped at crystallization conditions close to the precipitation zone. Nevertheless, large and compact crystals were obtained in the majority of the nucleation zone. Crystallization conditions with a very high supersaturation of 3.8 were used for the transfer of the GLU crystallization to the 5 μL-scale reactors. The crystallization of GLU in scalable reactors was reported for the first time. Without further optimization, a yield of 97 % was obtained within 3 h. The phase diagram suggests that neither the yield nor the crystallization kinetics can be further increased, as higher GLU concentrations are not feasible due to solubility limits and the GLU solubility does not continue to decrease at higher crystallization agent concentrations.

5.1.5   Antigen-binding fragment of the antibody cetuximab (FAB)

5.1.5.1 Microbatch-scale screening of crystallization conditions

Starting point for the microbatch-scale screening of crystallization conditions were vapor diffusion crystallization conditions from the literature (see chapter 3.2.6). NaCl and Tris-HCl were present as residuals from the protein A-based purification performed by Li *et al.* (2005). A preliminary screening showed that these two components reduced the nucleation rate of FAB and, consequently, slowed the crystallization kinetics down (Figure 5.20).
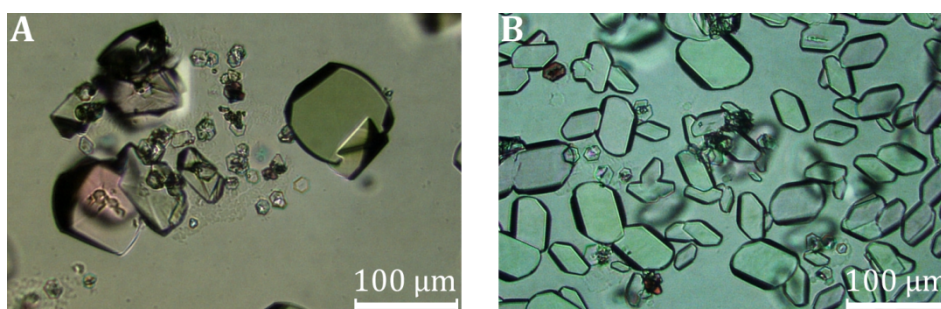
Figure 5.20: Crystallization of 15 g L^{-1} Fab fragment of cetuximab using 1.8 M ammonium sulfate, 100 mM sodium citrate buffer pH 6.25, and **A)** 100 mM NaCl and 10 mM Tris-HCl pH 8.5; **B)** no NaCl and/or Tris-HCl.

A screening for crystallization conditions using other crystallization agents, e.g., sodium sulfate, sodium chloride, or different PEGs, did not yield any crystals (data not shown). Hence, the screening was focused on variations of the aforementioned crystallization conditions. The FAB stock solution was stable up to 250 g L^{-1}. Consequently, high FAB concentrations up to 128.5 g L^{-1} could be used during screening. Combinations of high FAB and ammonium sulfate concentrations, however, could not be examined due to solubility limits. A selection of FAB crystals obtained during the microbatch-scale screening is depicted in Figure 5.21.
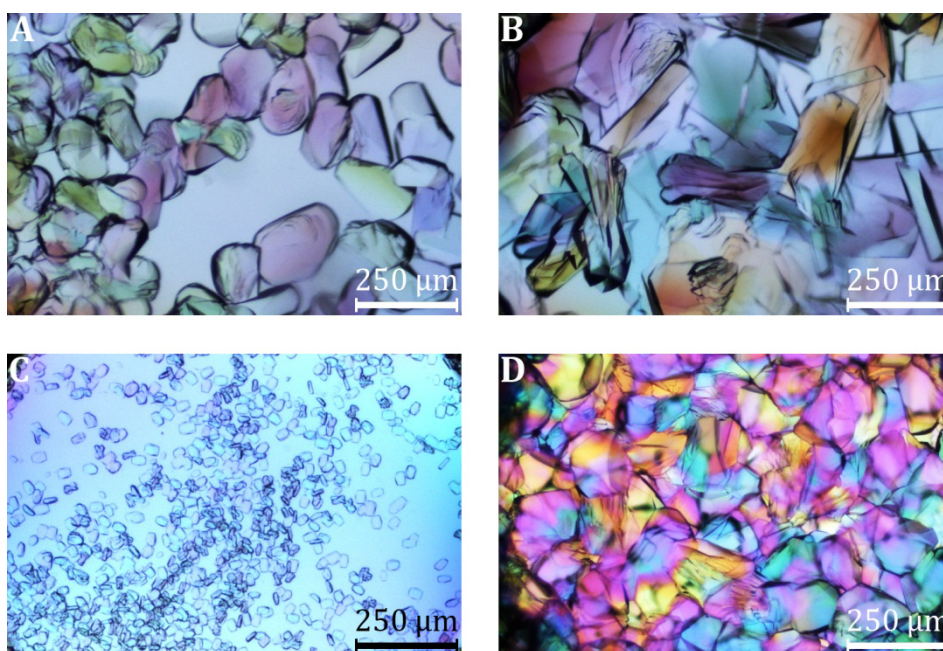
Figure 5.21: Compact crystals of the Fab fragment of cetuximab (FAB) obtained in the microbatch-scale screening using varying concentrations of FAB and ammonium sulfate (AS) at 20 °C. **A)** 18.3 g L^{-1} FAB, 1.4 M AS; **B)** 27.5 g L^{-1} FAB, 1.2 M AS; **C)** 73.4 g L^{-1} FAB, 0.8 M AS; **D)** 73.4 g L^{-1} FAB, 1.3 M AS.

The phase diagram derived from the qualitative evaluation of the microbatch-scale crystallization of FAB is depicted in Figure 5.22.
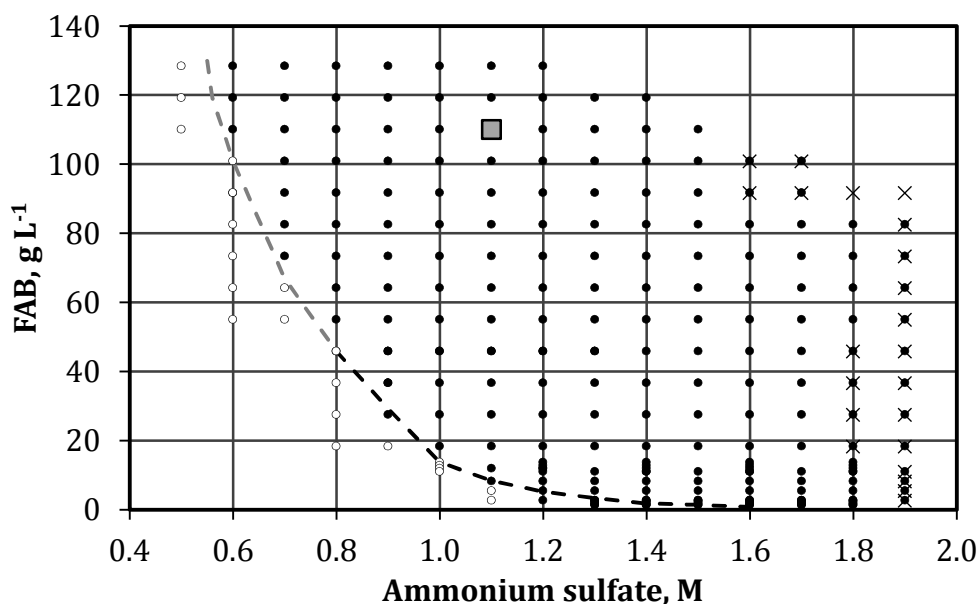
Figure 5.22: Phase diagram for the Fab fragment of cetuximab (FAB) obtained from the qualitative evaluation of microbatch-scale crystallization using varying ammonium sulfate concentrations in 40 mM sodium citrate buffer pH 6.25 at 20 °C. • crystal growth; × precipitate formation; ○ no crystallization or precipitation. The crystallization condition used for the subsequent 5 mL-scale crystallization is marked with a grey square. The dashed line denotes the FAB solubility curve for ammonium sulfate concentrations over 0.8 M. The line is included for visualization and is not the result of a simulation.

Crystallization was observed over a wide range of FAB and ammonium sulfate concentrations. Precipitation occurred only at very high ammonium sulfate concentrations over 1.8 M for all FAB concentrations and over 1.6 M for FAB concentrations above 90 g L^{-1}. The FAB solubility für ammonium sulfate concentrations below 0.8 M could not be determined. No metastable zone exists for ammonium sulfate concentrations above 0.8 M.

5.1.5.2 Crystallization on a 5 mL-scale

For the 5 mL-scale crystallization of FAB, crystallization conditions with FAB and ammonium sulfate concentrations well below the maximum concentrations were chosen in order to avoid problems due to solubility limitations of the stock solutions. The crystallization conditions were: 110 g L^{-1} FAB, 1.1 M ammonium sulfate, and 40 mM sodium citrate buffer pH 6.25. Based on the phase diagram, the supersaturation was estimated to be 2.4. The results of the 5 mL-scale crystallization of FAB are depicted in Figure 5.23.
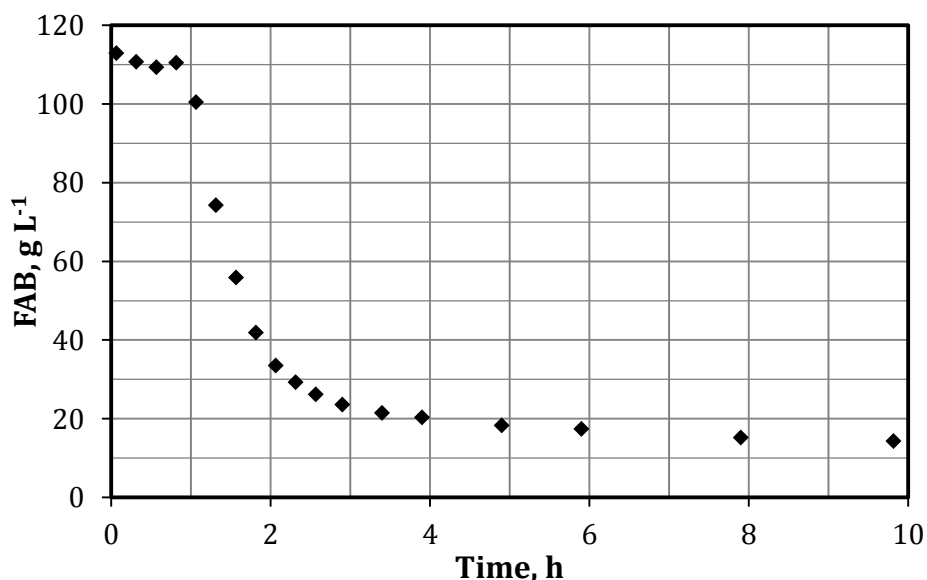
Figure 5.23: Crystallization of 110 g L^{-1} Fab fragment of cetuximab on a 5 mL-scale using 1.1 M ammonium sulfate, and 40 mM sodium citrate buffer pH 6.25 at 20 °C and n = 150 min^{-1}. Depicted is the decrease of the glucose isomerase concentration in solution.

The crystallization started after 1 h. Fast crystallization kinetics were observed. After 4 h, the residual FAB concentration was 20.3 g L^{-1} (crystallization yield: 82 %), and after 10 h, 14.3 g L^{-1} FAB were still in solution (crystallization yield: 87 %). The equilibrium concentration of 11.5 g L^{-1} FAB was reached after 33 h, equaling a crystallization yield of

89 %. The phase diagram suggested that a lower equilibrium concentration could be obtained using a higher ammonium sulfate concentration of 1.6 M. Hence, the ammonium sulfate concentration was increased to 1.2 M and subsequently to 1.6 M before the crystallization kinetics slowed down in the previous experiment. The results of this follow-up experiment are depicted in Figure 5.24.
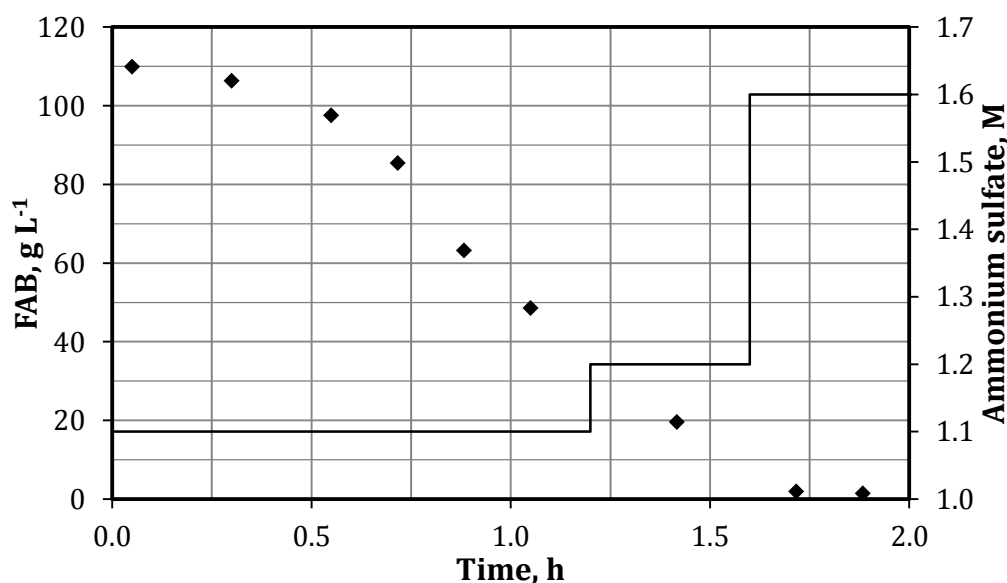
Figure 5.24: Crystallization of 110 g L^{-1} Fab fragment of cetuximab (FAB) on a 5 mL-scale using 1.1 M ammonium sulfate, and 40 mM sodium citrate buffer pH 6.25 at 20 °C and n = 150 min^{-1}. The ammonium sulfate concentration was raised to 1.2 M and 1.6 M after 1 h and 1.5 h, respectively. Depicted are ◆ the decrease of the FAB concentration in solution and the time-course of the ammonium sulfate concentration (solid line).

Before the increase of the ammonium sulfate concentrations, the crystallization kinetics were similar to those obtained in the previous experiment. However, the nucleation occurred more quickly and the crystallization started after 0.5 h. Fast crystallization kinetics were maintained by the increase of the ammonium sulfate concentration to 1.2 M and 1.6 M after 1 h and 1.5 h, respectively. The equilibrium was reached within 2 h with a residual FAB concentration of 0.9 g L^{-1}, equaling a crystallization yield of 99 %. Large crystals measuring up to 70 μm were observed next to a few smaller crystals measuring less than 10 μm (Figure 5.25).
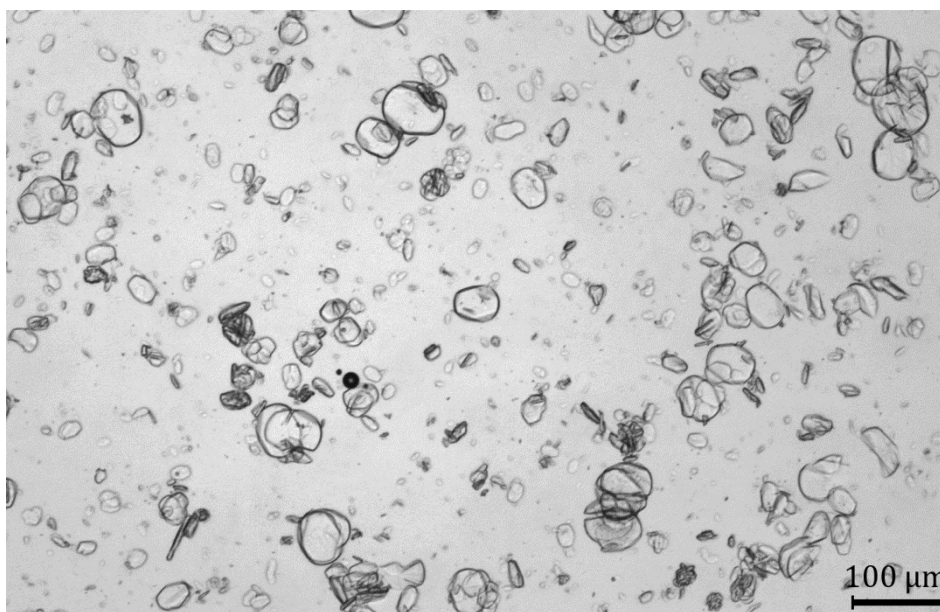
Figure 5.25: Crystals of the Fab fragment of cetuximab (FAB) grown in the 5 mL-scale reactor using 110 g L^{-1} FAB, 1.1 M ammonium sulfate (initially), and 40 mM sodium citrate buffer pH 6.25 at 20 °C and n = 150 min^{-1}. The ammonium sulfate concentration was raised to 1.2 M and 1.6 M after 1 h and 1.5 h, respectively.

5.1.5.3 Crystallization in the presence of protein contaminants

Very high purities are vital for therapeutic proteins. Hence, the crystallization process for the Fab fragment of cetuximab (FAB) was investigated in the presence of protein contaminants. As FAB was not generated by protein expression in bacterial cultivation, experiments regarding the crystallization from crude material could not be performed. Instead, the crystallization of FAB from FAB solutions spiked with protein contaminants was studied as well as from a pretreated papain digest.

Crystallization of FAB from solutions spiked with protein contaminants

The crystallization of FAB from impure solutions spiked with protein contaminants was investigated in microbatch experiments. The crystallization conditions were 20 g L^{-1} FAB, 1.2 M ammonium sulfate, 40 mM sodium citrate pH 6.25 and 0.1 - 1.5 g L^{-1} protein contaminant. The FAB and protein contaminant stock solutions were mixed prior to the addition of the crystallization agent stock solution. The protein contaminants used and the qualitative results are detailed in Table 5.3. A selection of FAB crystals grown in the presence of 1.5 g L^{-1} protein contaminant is shown in Figure 5.26.

Table 5.3: Qualitative evaluation of the microbatch-scale crystallization of the Fab fragment of cetuximab (FAB) from solutions spiked with 0.1 - 1.5 g L^{-1} protein contaminant using 20 g L^{-1} FAB, 1.2 M ammonium sulfate, and 40 mM sodium citrate pH 6.25 at 20 °C. **C:** crystal growth; **P:** precipitation; **C/P**: crystal growth with concurrent precipitation. Gamma-Norm*: commercially available mixture of human immunoglobulins.

Protein contaminant	Protein contaminant concentration, g L^{-1}					
	0.1	**0.25**	**0.5**	**0.75**	**1.0**	**1.5**
Albumin	C	C	C/P	C	C	C
Endonuclease	C	C	C	C/P	C/P	C/P
Gamma-Norm*	C/P	C/P	C/P	C/P	C/P	C/P
Lipase (LIP)	C	C	C	C/P	C/P	C/P
Lysozyme (LYS)	C	C	C	C	C	C
Xylanase (XYL)	C	C/P	C/P	C/P	C/P	C/P
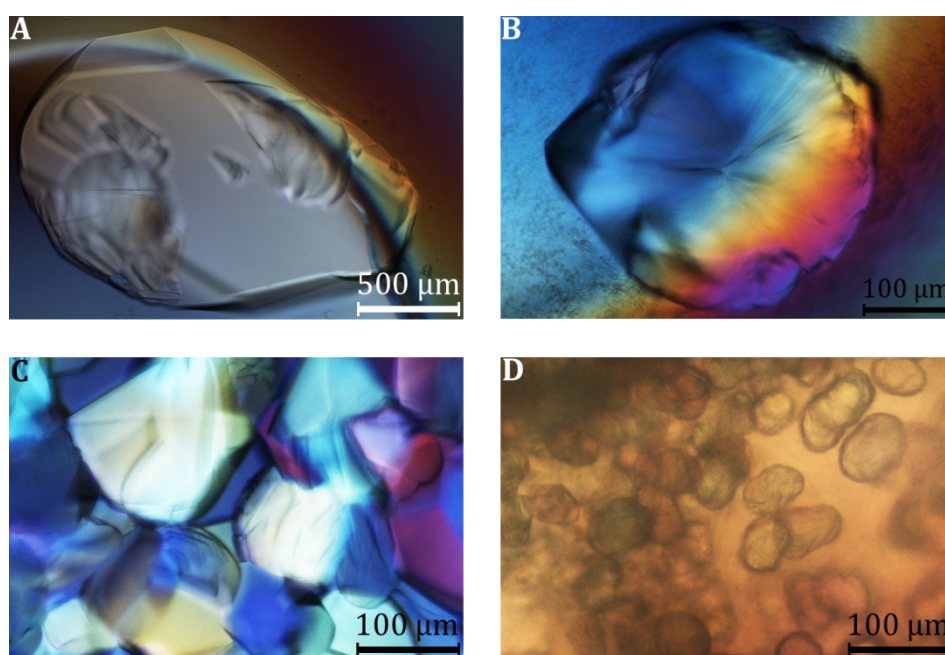
Figure 5.26: Crystals of the Fab fragment of cetuximab (FAB) grown in presence of protein contaminants using 20 g L^{-1} FAB, 1.2 M ammonium sulfate, 40 mM sodium citrate pH 6.25, and 1.5 g L^{-1} protein contaminant at 20 °C. **A:** albumin; **B:** endonuclease; **C:** lysozyme; **D:** xylanase. The scales of figures **A** and **B** differ from the other images due to the large size of the crystals.

FAB crystals were obtained in the presence of all protein contaminants under study. For all concentrations of Gamma-Norm, concurrent precipitation was observed, whereas concurrent precipitation occurred only at higher concentrations for the other protein contaminants. At 1.5 g L^{-1}, precipitation was observed in the presence of all protein contaminants except albumin and LYS. FAB crystals grown in the presence of 1.5 g L^{-1}

albumin measured up to 1.5 mm and were larger compared to crystals from the other experiments.

Crystallization of FAB from a pretreated papain digest

FAB was generated by papain digestion from cetuximab. In one case, the antibody was overdigested and the digest was contaminated with small peptides, which were not further characterized. Papain and the Fc fragment were removed from the digest using cation exchange chromatography as usual, but the peptides remained in the FAB solution. FAB was purified from this solution by crystallization on a 5 mL-scale. The concentrations of FAB and the peptides could not be determined separately using UV spectroscopy. The crystallization conditions were: $\approx$ 11 g L^{-1} FAB and peptides, 1.6 M ammonium sulfate, and 40 mM sodium citrate buffer pH 6.25. The results of the crystallization are depicted in Figure 5.27.
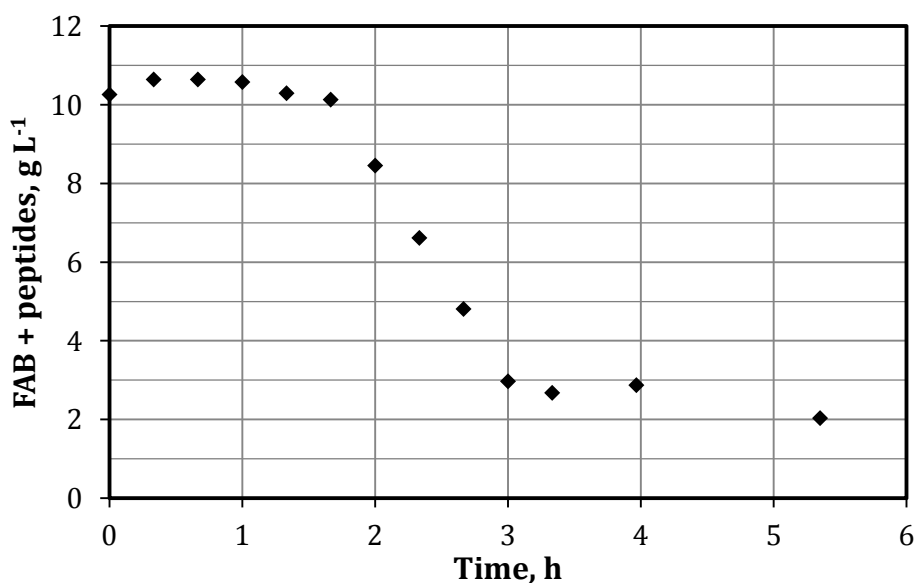
Figure 5.27: 5 mL-scale crystallization of FAB from a pretreated papain digest containing small peptides from an overdigestion using 1.6 M ammonium sulfate and 40 mM sodium citrate buffer pH 6.25 at 20 °C (n = 150 min^{-1}). The total concentration of FAB and peptides at the beginning was approximately 11 g L^{-1}.

The crystallization started after 1.7 h. The concentration of FAB and peptides decreased quickly and the equilibrium was reached after 5 h. The equilibrium concentration was higher than in previous crystallization experiments using purified FAB solutions. Both, the crystals and the supernatant were analyzed using size exclusion chromatography (SEC). The chromatograms are depicted in Figure 5.28.
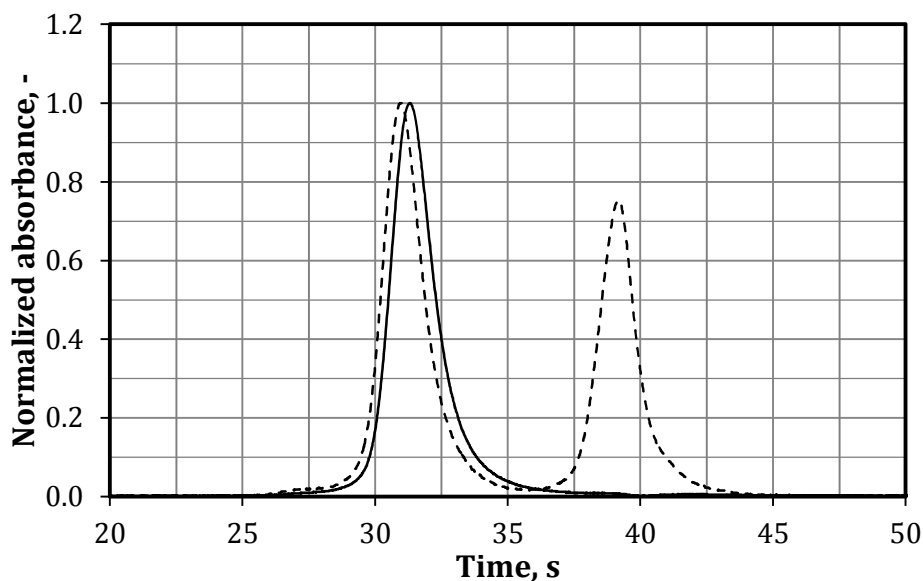
Figure 5.28: Chromatograms obtained by size exclusion chromatography (SEC) of crystals (solid line) and the supernatant (dotted line) from the 5 mL-scale crystallization of FAB from a pretreated papain digest containing small peptides from an overdigestion using the crystallization conditions detailed in Figure 5.27.

FAB was eluted in the first peak with a retention time of 31 min, whereas the smaller peptides were eluted in the second peak with a retention time of 39 min. The chromatograms show that small peptides are only present in the supernatant.

5.1.5.4 Discussion

A screening was performed based on the crystallization conditions reported by Li *et al.* (2005) and a phase diagram for the microbatch crystallization of FAB was reported for the first time. The crystallization conditions of Li *et al.* were outside the nucleation zone. However, Li *et al.* used vapor diffusion crystallization with increasing concentrations of protein and crystallization agent over time. Hence, the nucleation zone is gradually reached in vapor diffusion crystallization and the results are consistent. Compact crystals of FAB were obtained throughout the large nucleation zone. Since Li *et al.* did not describe the morphology of their FAB crystals, no comparison could be made.

Subsequently, FAB was crystallized in scalable reactors for the first time using crystallization conditions with a supersaturation of 2.4. Similar to the crystallization of XYL, the crystallization yield and the crystallization kinetics for FAB were improved by the addition of crystallization agent, resulting in an excellent yield of 99 % within 2 h. Due to the fast crystallization kinetics, the crystals grew irregularly and no definite

crystal morphology could be assigned. However, the crystals looked fairly similar to those obtained in the initial microbatch-scale screening.

For protein crystallization to be an alternative to current purification techniques, the target protein has to be crystallized selectively from an impure solution. Crystals of FAB were obtained in the presence of 1.5 g L^{-1} protein contaminant. However, concurring precipitation was observed for a number of protein contaminants. While crystals can be recovered from clear solutions by filtration, the separation of crystals from solutions with concurrent precipitation is difficult in a hypothetical large-scale process. It is unclear whether the FAB, the protein contaminant or both form the precipitate. If the precipitate contains the protein contaminant, it might be separated from the solution prior to the crystallization by adjusting the buffer to conditions close to, but outside of the nucleation zone for FAB. In a second experiment, FAB was successfully separated from small peptides resulting from a papain overdigestion. Using SEC, it was confirmed that the crystals contained only FAB and that the peptides remained in the supernatant. These preliminary results demonstrate the feasibility of protein crystallization in the presence of protein contaminants and may serve as proof-of-principle and starting point for future work.

5.1.6   Concluding remarks

The crystallization of five functionally and structurally different proteins on a 5 mL-scale based on phase diagrams generated from microbatch-scale screening experiments was successful. Crystallization yields of 58 - 99 % were obtained within 2 - 24 h using crystallization conditions from the preliminary microbatch-scale screening (Table 5.4).

Table 5.4: Overview of the 5 mL-scale crystallization processes derived from the preliminary microbatch-scale screening for the five proteins under study. Given are the crystallization yields, the process durations, and the method(s) employed in order to increase the crystallization yield and to accelerate the crystallization kinetics.

Protein	Yield, %	Time, h	Method(s) employed	Outcome
LYS	89	24	Temperature shift	Yield increased
LIP	58	23.5	-	1st 5 mL-scale cryst.
XYL	95	20	Feeding of crystallization agent	1st 5 mL-scale cryst.
GLU	97	3	-	1st 5 mL-scale cryst.
FAB	99	2	Feeding of crystallization agent	1st 5 mL-scale cryst.

Four of the five proteins were crystallized in 5 mL-scale stirred-tanks for the first time. For LYS, the yield was increased compared to previously reported crystallization processes. Phase diagrams have proven useful for the crystallization of proteins in the 5 mL-batch reactors. They provide qualitative information on the crystallization yield and the supersaturation. Crystallization conditions with a higher supersaturation usually exhibit an increased nucleation rate. Consequently, phase diagrams can be used to improve the 5 mL-batch crystallization processes, as shown for LYS, XYL and FAB. However, the application of phase diagrams is limited by the diversity of available crystallization conditions. Thus, phase diagrams are less useful for improving the crystallization of proteins that are sensitive even to slight changes of the crystallization conditions, e.g., LIP. Consequently, an empiric screening for complementary crystallization agents and/or additives becomes necessary.

5.2   Protein crystallization using additives

This chapter focuses on the crystallization using different additives, e.g., ionic liquids (ILs) and complementary crystallization agents. ILs were reported to positively influence protein crystallization, resulting in faster kinetics, a more compact crystal morphology, and an increased protein stability in small-scale vapor-diffusion and microbatch experiments (see chapter 3.3). For xylanase (XYL), no changes were observed in preliminary vapor diffusion crystallization experiments with ionic liquids as additives (data not shown). Hence, no further experiments were performed using XYL. The results of the crystallization of the four other proteins using additives are described in the following subchapters.

5.2.1   Lysozyme from *Gallus gallus* (LYS)

5.2.1.1   Identification of crystallization conditions on a microbatch-scale

Vapor diffusion crystallization conditions for LYS with the addition of the ionic liquid 2-hydroxyethylammonium formate (2-HEAF) served as starting point for the crystallization of LYS using additives. 2-HEAF was previously reported to increase the crystallization kinetics vapor diffusion experiments up to 5.5-fold and outperformed other ionic liquids under study (see chapter 3.2.6). The crystallization conditions from the literature featured a high LYS concentration of $50 \, \text{g} \, \text{L}^{-1}$. As this was shown to be unfavorable due to the occasional spontaneous precipitation of LYS, the crystallization conditions were adjusted to a lower LYS concentration and a higher NaCl concentration as described before for the crystallization of LYS without additives (see chapter 5.1.1.2). The crystallization conditions were: $25 \, \text{g} \, \text{L}^{-1}$ LYS, 1.25 M NaCl, 0.5 M 2-HEAF, and 25 mM sodium acetate buffer pH 4.0.

Identification of the relevant ion of the ionic liquid

As the literature suggested that the effects of water-miscible ionic liquids were caused by the individual characteristics of the anion and the cation of the ionic liquid (see chapter 3.3), the crystallization of LYS using salts containing one of the two ions was investigated. The influence of the formate anion was characterized by replacing 2-HEAF with an equimolar amount of A) sodium formate and B) magnesium formate, respectively. However, no crystallization experiments using just the cation of 2-HEAF

were carried out due to the toxic nature of its deprotonated form (ethanolamine). Microphotographs taken from this experiment are shown in Figure 5.29.
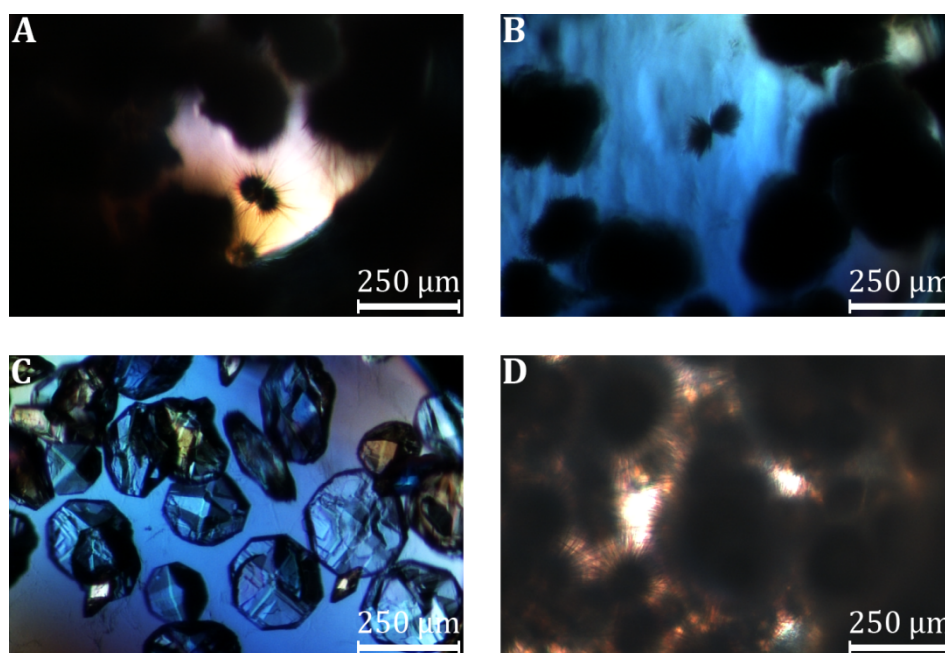
Figure 5.29: Microphotographs of the microbatch-crystallization of 25 g L^{-1} LYS using 1.25 M NaCl, 25 mM sodium acetate buffer pH 4.0, and **A)** 0.5 M sodium formate, **B)** 0.5 M magnesium formate, **C)** 0.5 M 2-hydroxyethylammonium formate, **D)** no additive at 20 °C.

As previously described, sea urchin-like formations of monoclinic crystal needles were observed without an additive (see chapter 5.1.1.1). With the addition of the two formate salts, similar sea urchin-like formations were obtained. However, the formations were denser and, in case of magnesium formate, concurrent gel-like precipitation occurred. In contrast, compact crystals were observed with the addition of 2-HEAF.

5.2.1.2 Crystallization using the ionic liquid 2-HEAF on a 5 mL-scale

The ionic liquid 2-HEAF exhibited positive effects on the crystal form of LYS in microbatch crystallization experiments. Hence, the crystallization conditions with the addition of 2-HEAF were transferred into the 5 mL-scale reactors in order to quantify the influence of 2-HEAF on the crystallization yield and the crystallization kinetics. The crystallization conditions were: 25 g L^{-1} LYS, 1.25 M NaCl, 0.5 M 2-HEAF, and 25 mM sodium acetate buffer pH 4.0. The temperature was lowered during the crystallization process as previously described for the crystallization of LYS without additives. The results of the 5 mL-scale crystallization of LYS with the addition of 2-HEAF and the previous crystallization without the addition of 2-HEAF (see chapter 5.1.1.2) are depicted in Figure 5.30.
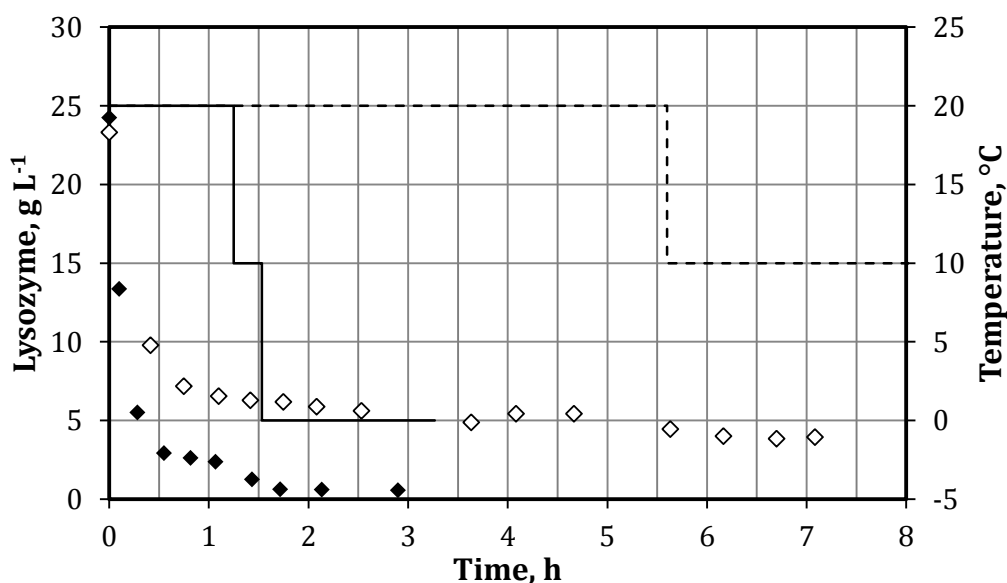
Figure 5.30: Crystallization of 25 g L^{-1} lysozyme on a 5 mL-scale using 1.25 M NaCl, 0.5 M 2-hydroxyethylammonium formate and 25 mM sodium acetate buffer pH 4.0 (n = 150 min^{-1}). Depicted are the decrease of the lysozyme concentration in solution ◆ with and ◇ without the addition of 2-HEAF and the time course of the temperature (with 2-HEAF: solid line; without 2-HEAF: dashed line) which was lowered during the crystallization process in order to increase the crystallization yield.

The crystallization started immediately after the addition of the crystallization agent solution. The crystallization kinetics were faster than previously described for the experiment without 2-HEAF. A residual LYS concentration of 5 g L^{-1} was observed after 0.3 h compared to 3 h. The equilibrium at 20 °C was reached within 1 h instead of 4 h. The final equilibrium was reached within 2 h after the temperature was lowered to 0 °C. The residual LYS concentration at the equilibrium was 0.6 g L^{-1}, equaling a crystallization yield of 97 %. Compared to the 5 mL-scale crystallization without additives, the equilibrium concentration was lowered by 77 %, and the crystallization yield was increased by 8 %. No needle-like crystals were observed. A microphotograph of the compact crystals obtained in this experiment is shown in Figure 5.31.
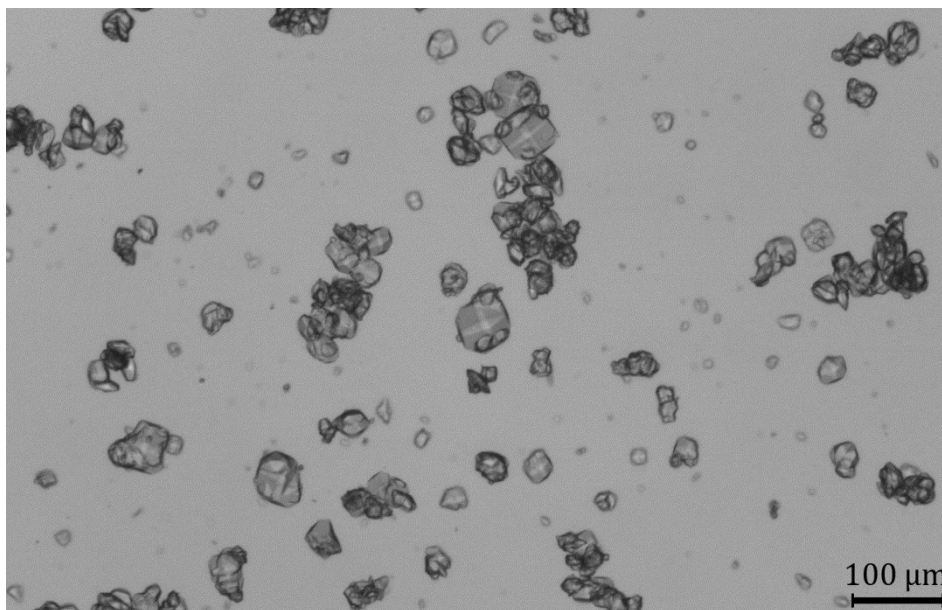
Figure 5.31: Lysozyme crystals and crystal clusters grown in the 5 mL-scale reactor using 25 g L^{-1} lysozyme, 1.25 M NaCl, 0.5 M 2-hydroxyethylammonium formate, and 25 mM sodium acetate buffer pH 4.0 (n = 150 min^{-1}).

5.2.2   Lipase from *Thermomyces lanuginosus* (LIP)

5.2.2.1 Identification of crystallization conditions on a microbatch-scale

Vapor diffusion crystallization conditions for LIP with the addition of the ionic liquid choline dihydrogenphosphate (CDHP) were previously reported and served as starting point for the crystallization of LIP using additives (see chapter 3.2.6). The addition of other ionic liquids (Table 8.13) was evaluated in vapor diffusion experiments, but yielded unfavorable needle-like crystals, exhibited slow crystallization kinetics or led to precipitation (data not shown). The LIP concentration was raised to 100 g L^{-1} as previously described for the crystallization of LIP without additives (see chapter 5.1.2). The crystallization conditions were: 100 g L^{-1} LIP, 55 mM NaCl, 0.275 M CDHP, and 25 mM sodium acetate buffer pH 4.

Identification of the relevant ion of the ionic liquid

As mentioned before, the effects of water-miscible ionic liquids are suggested to be caused by the individual characteristics of the anion and the cation of the ionic liquid (see chapter 3.3). Hence, the microbatch-scale crystallization of LIP was investigated with the aforementioned crystallization conditions and alterations thereof, where CDHP was replaced with an equimolar amount of A) choline chloride and B) sodium dihydrogenphosphate, respectively. For this experiment, the sodium acetate buffer

concentration was increased to 50 mM. Microphotographs taken from this experiment are shown in Figure 5.32.
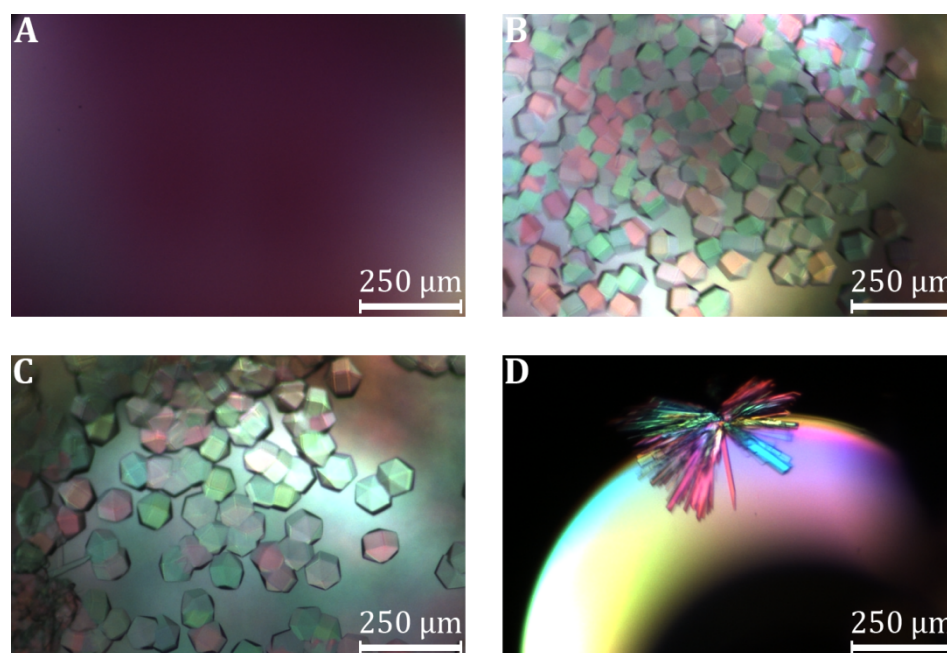
Figure 5.32: Microphotographs of the microbatch-crystallization of 100 g L^{-1} LIP using 55 mM NaCl, 50 mM sodium acetate buffer pH 4.0, and **A)** 0.275 M choline chloride, **B)** 0.275 M sodium dihydrogenphosphate, **C)** 0.275 M choline dihydrogenphosphate, **D)** no additive at 20 °C taken after 1 d.

Similar sturdy crystals and crystal clusters were obtained using both, CDHP and sodium dihydrogenphosphate. No crystal growth was observed in the wells containing choline chloride. Without any additives, the previously described needle-like crystal clusters were observed.

5.2.2.2 Crystallization using phosphate and choline salts on a 5 mL-scale

Qualitatively, the same results were obtained using choline dihydrogenphosphate (CDHP) and sodium dihydrogenphosphate. Hence, sodium dihydrogenphosphate was used for subsequent experiments in order to reduce the costs of the crystallization agents. The results 5 mL-scale crystallization using 100 g L^{-1} LIP, 75 mM NaCl, 0.275 M sodium dihydrogenphosphate, and 25 mM sodium acetate buffer pH 4.0 are depicted in Figure 5.33.
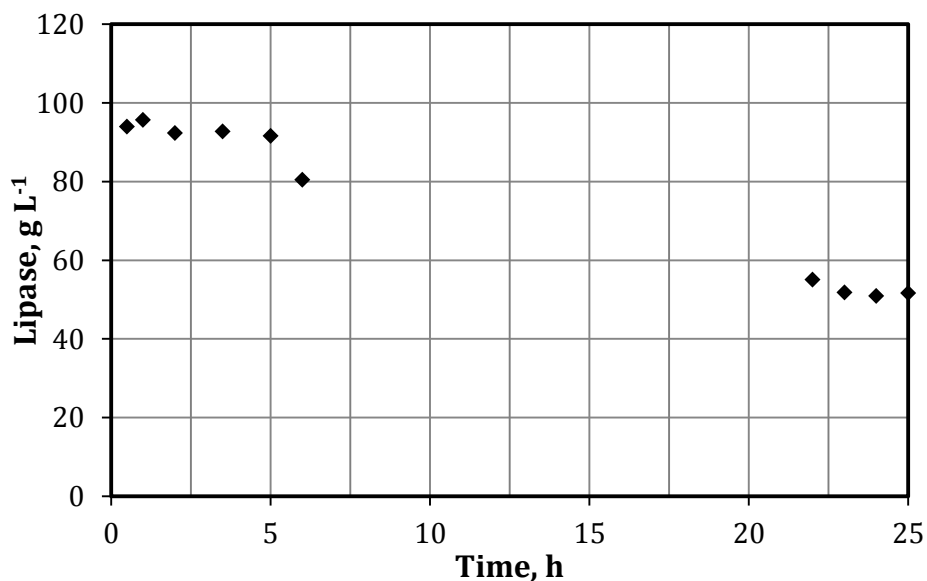
Figure 5.33: Crystallization of 100 g L^{-1} lipase on the 5 mL-scale using 75 mM NaCl, 0.275 M sodium dihydrogenphosphate, and 25 mM sodium acetate buffer pH 4.0 at 20 °C (n = 250 min^{-1}). Depicted is the decrease of the lipase concentration in solution.

Similar to the previous 5 mL-scale crystallization of LIP without additives, the crystallization started after 5 h and the equilibrium was reached after 23 h. The crystallization yield was 50 % and thus 8 % lower than without the addition of sodium dihydrogenphosphate. However, favorable compact crystals were obtained in contrast to needle-like crystals (Figure 5.34).
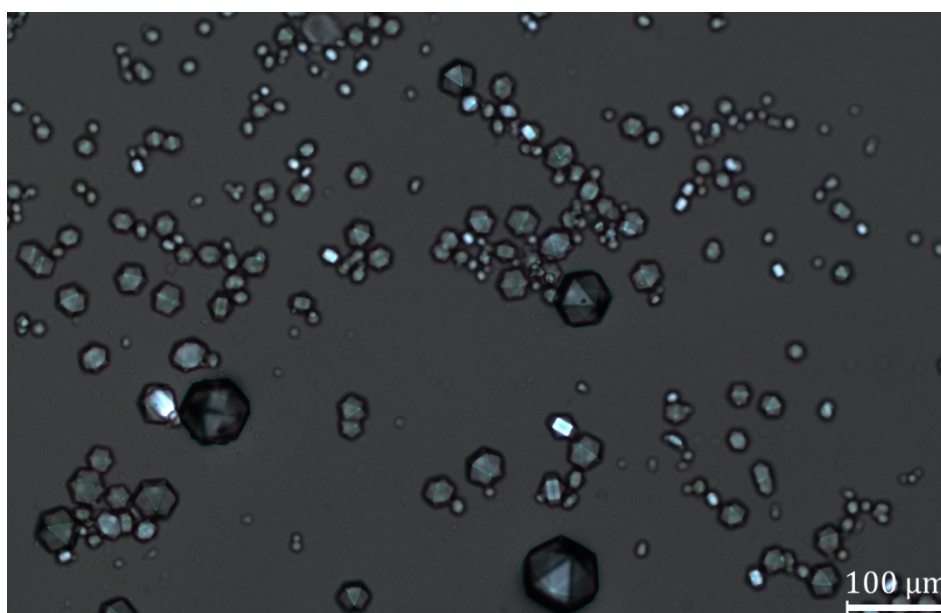
Figure 5.34: Lipase crystals grown in the 5 mL-scale reactor using 100 g L^{-1} lipase, 75 mM NaCl, 0.275 M sodium dihydrogenphosphate, and 25 mM sodium acetate buffer pH 4.0 at 20 °C (n = 250 min^{-1}).

5.2.2.3 Identification of a suitable complementary crystallization agent

Since both, crystallization conditions with and without sodium dihydrogenphosphate, exhibited an unsatisfactory yield of 50 % and 58 %, respectively, a microbatch-scale screening for a suitable complementary crystallization agent was carried out. The addition of various salts did not qualitatively improve the crystallization or resulted in precipitation (data not shown). In contrast, the addition of different-sized polyethylenglycols (PEGs) resulted in an increased formation of smaller crystals. Subsequently, the impact of the PEGs on the equilibrium concentration of LIP (and thus on the crystallization yield) was quantified in the 5 mL-scale reactors by adding a concentrated PEG solution to a crystal slurry at equilibrium (Table 5.5).

Table 5.5. Equilibrium concentration and crystallization yield of lipase (LIP) upon the addition of a complementary crystallization agent to a crystal slurry obtained in a 5 mL-scale LIP crystallization using the following conditions: 100 g L^{-1} LIP, 75 mM NaCl, 0.275 M sodium dihydrogenphosphate, and 25 mM sodium acetate buffer pH 4 (T = 20 °C, n = 250 min^{-1}).

Complementary crystallization agent	Equilibrium concentration, g L^{-1}	Yield, %
None	50.1	50
25 g L^{-1} PEG 200	50.2	50
25 g L^{-1} PEG 3000	47.2	52
25 g L^{-1} PEG 10000	35.5	64
25 g L^{-1} PEG 20000	32.3	67
25 g L^{-1} PEG 35000	39.8	60
50 g L^{-1} PEG 10000	5.0	95
60 g L^{-1} PEG 10000	4.9	95

The addition of 25 g L^{-1} PEG 200 or PEG 3000 did not lower the equilibrium concentration. In contrast, an average reduction of the equilibrium concentration by 35.5 g L^{-1} was observed upon the addition of 25 g L^{-1} PEG 10000, PEG 20000, and PEG 35000. Furthermore, the equilibrium concentration was distinctly lowered to 5.0 g L^{-1} at an increased PEG 10000 concentration of 50 g L^{-1}, equaling a crystallization yield of 95 %. An increase of the PEG 10000 concentration to 60 g L^{-1} did not result in a further reduction of the equilibrium concentration. Precipitation was observed when 50 g L^{-1} PEG 10000 was added at the beginning of the crystallization process (data not shown).

5.2.2.4 Crystallization using phosphate and PEG 10 000 on a 5 mL-scale

PEG 10000 was added over a time period of 2 h to a final concentration of 50 g L^{-1} in order to avoid the formation of precipitate at the beginning of the crystallization process.
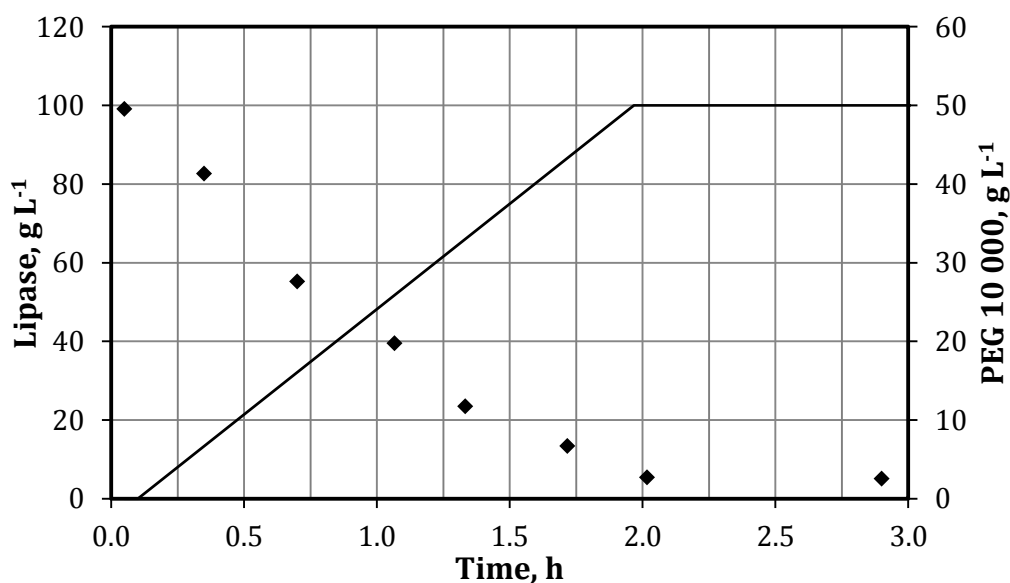
Figure 5.35: Crystallization of 100 g L^{-1} lipase on a 5 mL-scale using 75 mM NaCl, 0.275 M sodium dihydrogenphosphate, and 25 mM sodium acetate buffer pH 4.0 (T = 20 °C, n = 250 min^{-1}). PEG 10000 was gradually added over 2 h to a final concentration of 50 g L^{-1}. Depicted are ◆ the decrease of the lipase concentration in solution and the concentration of PEG 10000 (solid line).

The crystallization was started by the addition of PEG 10000. The residual concentration of LIP decreased steadily until the equilibrium concentration of 5.0 g L^{-1} was reached after 2 h (crystallization yield: 95 %). In comparison to the 5 mL-scale crystallization of LIP without the addition of phosphate buffer and PEG 10000, the equilibrium concentration of LIP was lowered by 88 % and the crystallization yield increased by 37 %. However, reversible precipitation sometimes occurred due to dropwise addition of concentrated PEG 10000 solution. The precipitate dissolved quickly. The irregular crystals grown in this experiment are shown in Figure 5.36.
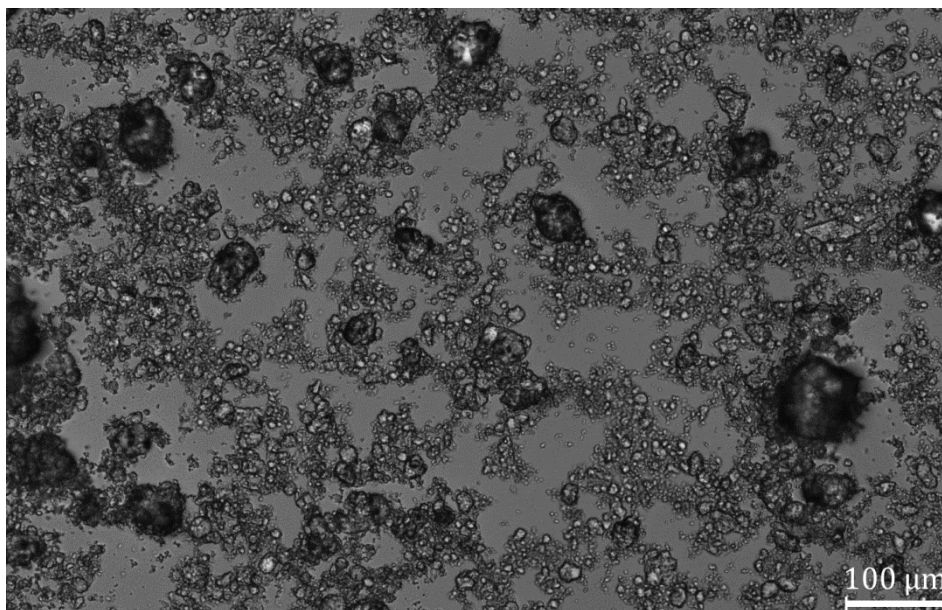
Figure 5.36: Lipase crystals grown in the 5 mL-scale reactor using 100 g L^{-1} lipase, 75 mM NaCl, 0.275 M sodium dihydrogenphosphate, and 25 mM sodium acetate buffer pH 4.0 at 20 °C (n = 250 min^{-1}). PEG 10000 was gradually added over 2 h to a final concentration of 50 g L^{-1}.

5.2.3   Glucose isomerase from *Streptomyces rubiginosus* (GLU)

Starting point for the screening of crystallization conditions with additives for GLU were the following crystallization conditions without additives from the previously described phase diagram (see chapter 5.1.4.1): 15 g L^{-1} GLU, 0.65 M sodium citrate, 45 mM sodium citrate borate buffer pH 8.5. Since no crystallization conditions using additives were reported for GLU, the influence of 40 g L^{-1} of all ILs available in this work (see Table 8.13) was investigated in vapor diffusion crystallization experiments one at a time. No crystal growth was achieved using 1-butyl-4-(dimethylamino)-pyridinium chloride and 1-ethyl-4-(dimethylamino)-pyridinium chloride. For all other ILs, large, rod-shaped crystals were observed (Figure 5.37).
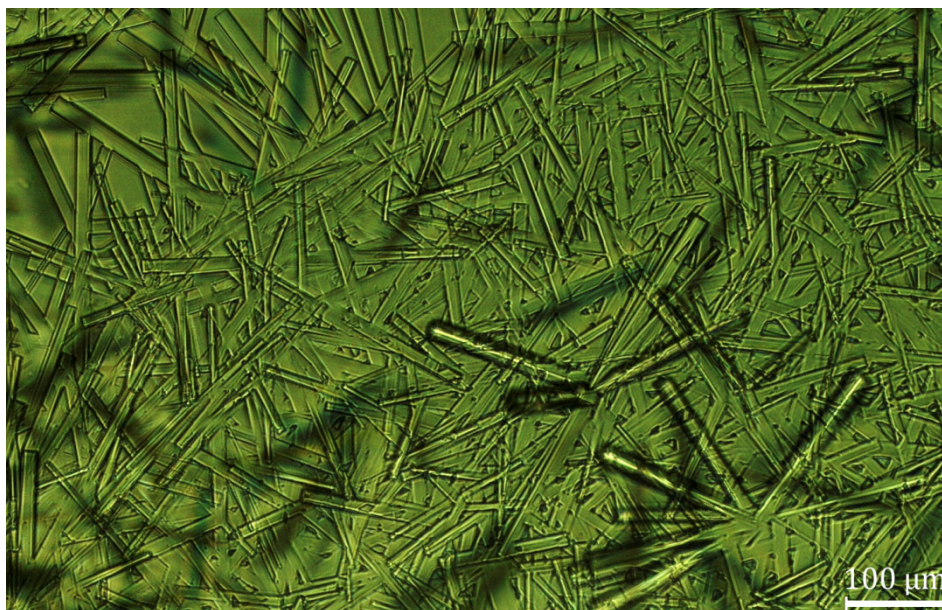
Figure 5.37: Microphotographs of the microbatch-crystallization of 15 g L^{-1} GLU using 0.65 M sodium citrate, 45 mM sodium citrate borate buffer pH 8.5, and 40 g L^{-1} bis-(2-methoxyethyl)-ammonium acetate (IL2) at 20 °C.

Similar rod-shaped crystals were observed for crystallization conditions close to the precipitation zone during the initial screening (see chapter 5.1.4.1). As this crystal form is unfavorable for the large-scale crystallization of proteins, no further experiments were performed for GLU.

5.2.4 Antigen-binding fragment of the antibody cetuximab (FAB)

The starting point for the screening of crystallization conditions with additives for FAB was taken from the previously described phase diagram (see chapter 5.1.5.1). As no differences could be determined for the crystallization of 3.6 g L^{-1} FAB with and without additives (data not shown), a higher FAB concentration was employed for the screening. The usability of all ILs available in this work (see Table 8.13) for the crystallization of FAB was investigated. The crystallization conditions were: 50 g L^{-1} FAB, 1.2 M ammonium sulfate, 200 mM IL, and 40 mM sodium citrate buffer pH 6.25. Selected microphotographs taken from crystals grown in this experiment are shown in Figure 5.38.
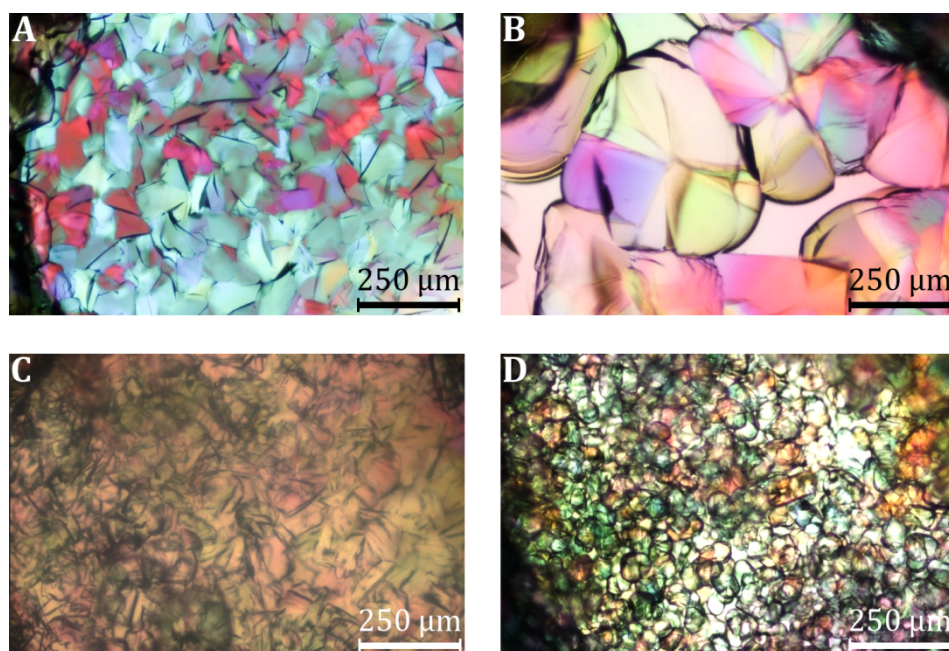
Figure 5.38: Microphotographs of the microbatch-crystallization of 50 g L^{-1} FAB using 1.2 M ammonium sulfate, 40 mM sodium citrate buffer pH 6.25, and 200 mM **A)** 2-hydroxyethylammonium formate (2-HEAF), **B)** ethylammonium nitrate, **C)** bis-(2-methoxyethyl)-ammonium acetate, **D)** 4-cyanomethylmorpholinium chloride at 20 °C taken after 1 d.

A qualitative evaluation of the microbatch-scale crystallization using ionic liquids as additives and the crystallization yields achieved with the addition of ILs are listed in Table 5.6.

Table 5.6: Qualitative evaluation of microbatch-scale crystallization experiments using different ILs as additives for the crystallization of 50 g L^{-1} FAB using 1.2 M ammonium sulfate, 200 mM IL, and 40 mM sodium citrate buffer pH 6.25. The yields were calculated from the FAB solubility at the equilibrium. A value for 1-methyl-4-(dimethylamino)-pyrodinium chloride could not be determined due to a hardware failure.

Ionic liquid	Qualitative effect	Yield, %
No ionic liquid	(Reference)	99
2-Hydroxyethylammonium formate	Unchanged	53
N,N-Dimethylethanolammonium glycolate		65
N,N-Dimethylethanolammonium acetate		59
Ethylammonium nitrate	Larger crystals	71
4-Cyanomethylmorpholinium chloride	Smaller crystals	54
1-Methyl-4-(dimethylamino)-pyridinium chloride		-
Bis-(2-methoxyethyl)-ammonium acetate	Precipitation and	-
Choline dihydrogenphosphat	crystals	-
4-(2-Hydroxyethyl)-morpholinium chloride	Precipitation	-
1-Ethyl-4-(dimethylamino)-pyridinium chloride	Drop stayed clear	-
1-Butyl-4-(dimethylamino)-pyridinium chloride		-

For the crystallization of FAB using six of the ILs under study, qualitatively similar results were obtained. For some ILs, the crystals were larger or smaller, but all crystals exhibited the same crystal form. However, measurements of the equilibrium concentration of FAB showed that the yields were lowered by 28 - 46 % due to the presence of the ILs. For the other five of the ILs, no crystallization or concurrent precipitation were observed.

5.2.5 Summary and discussion

The use of additives, primarily ionic liquids (ILs), for the stirred-batch crystallization of proteins has been investigated. Hence, the objectives were an increase of the crystallization yield, an acceleration of the crystallization kinetics, and/or the shift to a more favorable crystal form. First, suitable crystallization conditions were identified by the qualitative evaluation of vapor diffusion and/or microbatch crystallization experiments. For LYS and LIP, crystallization conditions from the literature were used as starting point, whereas a screening was performed for GLU, XYL and FAB.

The ionic liquids had no effect on the crystallization of XYL. The addition of ionic liquids led to a shift from the previously observed needle-like crystal form to compact crystals for LYS and LIP. However, for GLU, the crystal form was shifted from compact crystals to unfavorable rod-shaped crystals upon the addition of ILs. For FAB, the addition of some ILs influenced the crystal size, but not the crystal form. For example, larger crystals of the same crystal form were observed upon the addition of ethylammonium nitrate. However, all ILs under study were shown to distinctively lower the crystallization yield of FAB. It was assumed that the ILs stabilized the FAB in solution and thus raised the solubility of FAB.

As recent reports in the literature suggested, that water-immiscible ILs in low concentrations are similar to regular salts and the characteristics of the individual ions of an IL are responsible for its effects, the ions of the favorable ILs were studied separately. For the crystallization of LYS with the addition of 2-HEAF, the positive effects are either caused by the 2-hydroxyethylammonium cation or by synergistic effects of both, the cation and the formate anion. The addition of different salts containing just the formate anion did not result in positive effects. In contrast, the dihydrogenphosphate anion (DHP) was shown to be responsible for the positive effects of the IL choline dihydrogenphosphate (CDHP) on the crystallization of LIP. Water-immiscible ILs, which basically are salts with a relatively low melting point, dissociate upon mixing with water just as any other salt. Hence, the effects due to ion-protein interactions dominate the nature of the influence of the IL on protein crystallization (compare chapters 3.2.2 and 3.3).

While the crystallization yield for LYS was successfully increased to 97 % within 2 h by the addition of 2-HEAF, the crystallization yield for LIP was still unsatisfactory low after

the addition of sodium dihydrogenphosphate. Consequently, a screening for a complementary crystallization agent was carried out. The screening was augmented by quantitative data generated in the 5 mL-scale stirred-tank reactors in contrast to a conventional screening for crystallization conditions based only on qualitative data from vapor diffusion or microbatch experiments. PEG 10000 was identified as a suitable complementary crystallization agent, leading to an increase of the crystallization yield to 95 % within 2 h.

An overview of the five 5 mL-scale crystallization processes after the evaluation of additives is given in Table 5.7. The crystallization processes featured a crystallization yield of 95 % or above and, with the exception of XYL, process times of 3 h or below.

Table 5.7: Overview of the 5 mL-scale crystallization processes derived from the preliminary microbatch-scale screening for the five proteins under study. Given are the crystallization yields, the process durations, and the method(s) employed in order to increase the crystallization yield and to accelerate the crystallization kinetics.

Protein	Yield, %	Time, h	Method(s) employed	Additive(s) used
LYS	97	2	Temperature shift, addition of 2nd crystallization agent (IL)	2-HEAF
LIP	95	2	Feeding of a complementary crystallization agent	PEG 10000, sodium dihydrogenphosphate
XYL	95	20	Feeding of crystallization agent	-
GLU	97	3	-	-
FAB	99	2	Feeding of crystallization agent	-

5.3   Protein crystallization on a 100 mL- and a L-scale

This chapter details the crystallization of LYS, LIP and FAB on a 100 mL- and a 1 L-scale using the previously optimized crystallization conditions. The L-scale stirred tanks were agitated at the same stirrer speeds used in the 5 mL-crystallizers, as crystallization kinetics in stirred tanks were found to be nearly independent of the stirrer speed and a reduced formation of crystal clusters was expected at higher stirrer speeds (see chapter 3.2.4).

5.3.1   Lysozyme from *Gallus gallus* (LYS)

For LYS, crystallization conditions with the ionic liquid 2-hydroxyethylammonium formate (2-HEAF) were used (see chapter 5.2.1.2). As in the 5 mL-scale crystallization, the temperature was stepwise decreased to 0 °C during the crystallization process. The results of two crystallization processes on a 100 mL- and on a 1 L-scale are depicted in Figure 5.39.
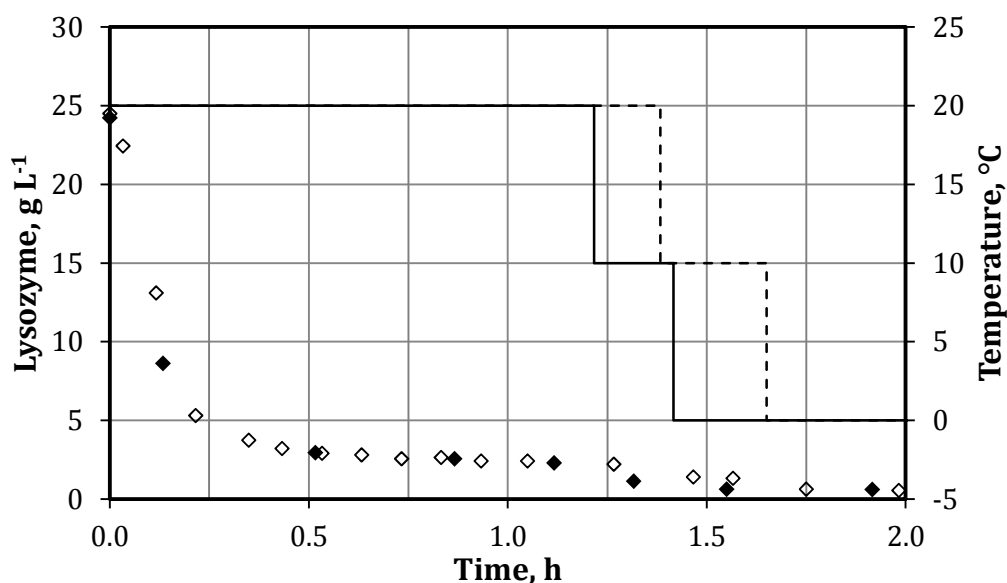
Figure 5.39: Crystallization of 25 g L^{-1} lysozyme on a ◆ 100 mL- and a ◇ 1 L-scale using 1.25 M NaCl, 0.5 M 2-hydroxyethylammonium formate and 25 mM sodium acetate buffer pH 4.0 (n = 150 min^{-1}). Depicted are the decrease of the lysozyme concentration in solutionand the temperature time course (100 mL: solid line; 1 L: dashed line). The temperature was lowered during the crystallization process in order to increase the crystallization yield.

The crystallization kinetics were similar to those obtained in the 5 mL-scale crystallization of LYS using 2-HEAF as additive. The crystallization started immediately after the addition of the crystallization agent solution and the LYS concentration decreased quickly. After the LYS equilibrium concentration for 20 °C was reached after approximately 1 h, the temperature was decreased to 10 °C and subsequently to 0 °C. In both reactors, the LYS equilibrium concentration of 0.6 g L^{-1} was reached within 2 h (crystallization yield: 97 %). Compact irregular tetragonal-like crystals measuring up to 70 μm and crystal clusters of up to 120 μm were observed (Figure 5.40).
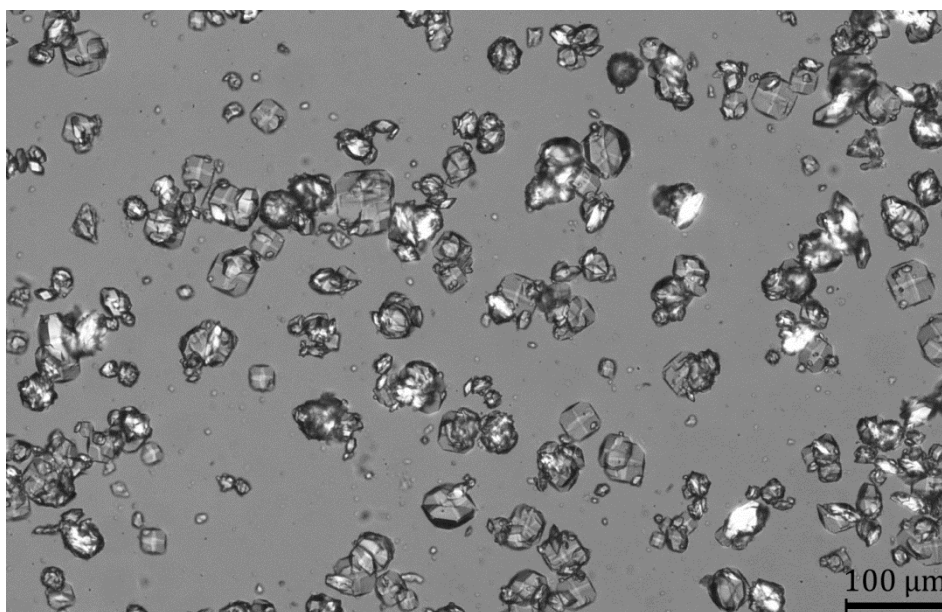
Figure 5.40: Lysozyme crystals and crystal clusters grown in the 1 L-scale reactor using 25 g L^{-1} lysozyme, 1.25 M NaCl, 0.5 M 2-hydroxyethylammonium formate, and 25 mM sodium acetate buffer pH 4.0 (n = 150 min^{-1}).

An area density distribution was calculated from the microphotograph in order to characterize the crystal size distribution in the 1 L-scale reactor (Figure 5.41). 97 % of the crystals and crystal clusters measured between 20 and 120 μm. 63 % thereof were single crystals measuring between 40 and 60 μm. No crystal or crystal cluster was larger than 120 μm. 3 % of the crystals were smaller than 20 μm.
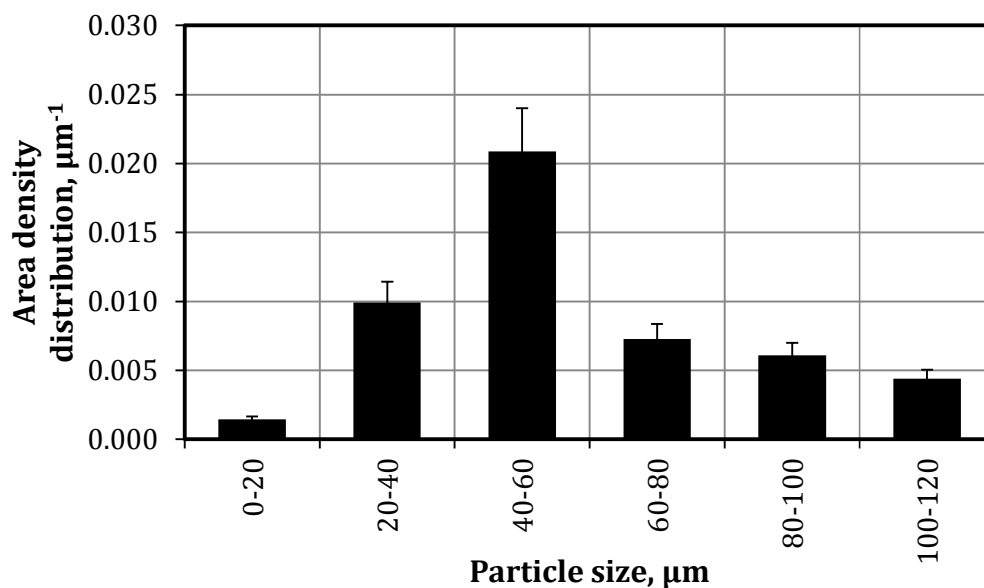
Figure 5.41: Area density distribution of lysozyme crystals and crystal clusters grown in the 1 L-scale reactor using 25 g L^{-1} lysozyme, 1.25 M NaCl, 0.5 M 2-hydroxyethylammonium formate, and 25 mM sodium acetate buffer pH 4.0 (n = 150 min^{-1}). The error bars are equivalent to a measurement error of approximately 15 %.

5.3.2   Lipase from *Thermomyces lanuginosus* (LIP)

For LIP, crystallization conditions with sodium dihydrogenphosphate and the addition of PEG 10000 to a final concentration of 50 g L^{-1} during the crystallization process were used (see chapter 5.2.2.4). The results of two crystallization processes on a 100 mL- and on a 1 L-scale are depicted in Figure 5.42.
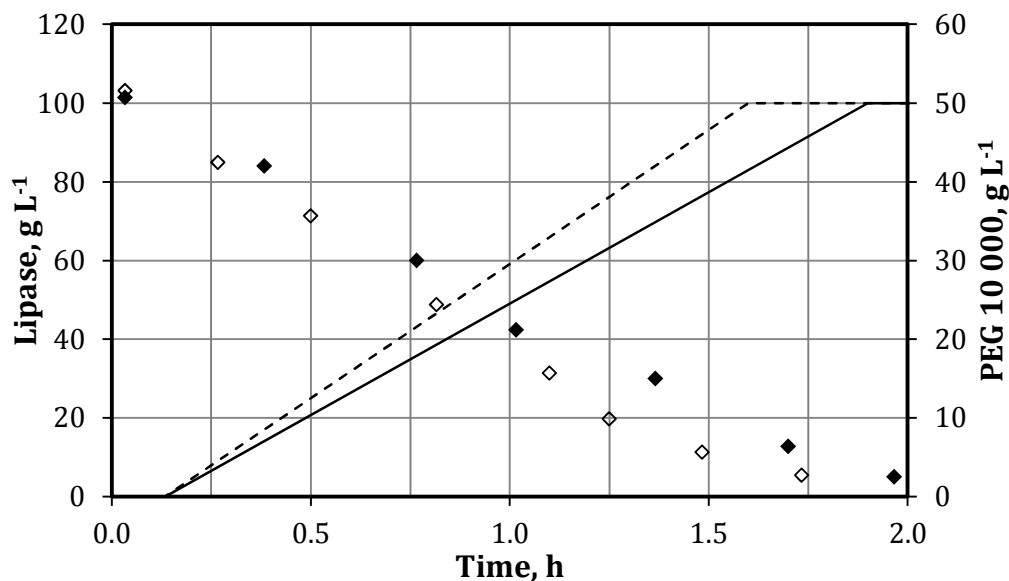
Figure 5.42: Crystallization of 100 g L^{-1} lipase on a ◆ 100 mL- and a ◇ 1 L-scale using 75 mM NaCl, 0.275 M sodium dihydrogenphosphate, and 25 mM sodium acetate buffer pH 4.0 (T = 20 °C, n = 250 min^{-1}). PEG 10000 was gradually added over 2 h to a final concentration of 50 g L^{-1}. Depicted are the decrease of the lipase concentration in solution and the concentration of PEG 10000 (100 mL: solid line; 1 L: dashed line).

The crystallization kinetics were similar to those obtained in the 5 mL-scale crystallization of LIP using the same crystallization conditions. PEG 10000 was added slightly faster in the 1 L-scale reactor and the equilibrium concentration was reached within 1.75 h. The 100 mL-scale crystallization was at equilibrium after 2 h. The equilibrium concentration on both scales was 5.0 g L^{-1}, equaling a crystallization yield of 95 %. Microphotographs of the LIP crystals obtained in the 100 mL- and 1 L-crystallization processes are shown in Figure 5.43.
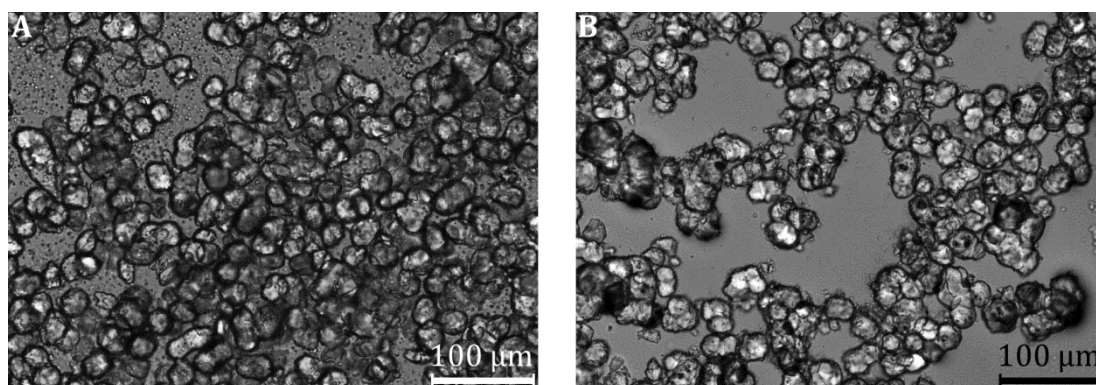
Figure 5.43: Crystals of lipase (LIP) grown on **A)** the 100 mL-scale and **B)** the 1 L-scale using 100 g L^{-1} LIP, 75 mM NaCl, 0.275 M sodium dihydrogenphosphate, and 25 mM sodium acetate buffer pH 4.0 (T = 20 °C, n = 250 min^{-1}) with gradual addition of PEG 10000 to a final concentration of 50 g L^{-1}.

Crystals with an irregular morphology were observed in both reactors. The crystals obtained in the 1 L-scale reactor were slightly larger than the crystals in the 100 mL-scale reactor. Next to the large crystals, crystals smaller than 10 µm were observed on the 100 mL-scale. An area density distribution was calculated from Figure 5.43B in order to characterize the crystal size distribution in the 1 L-scale reactor (Figure 5.44).
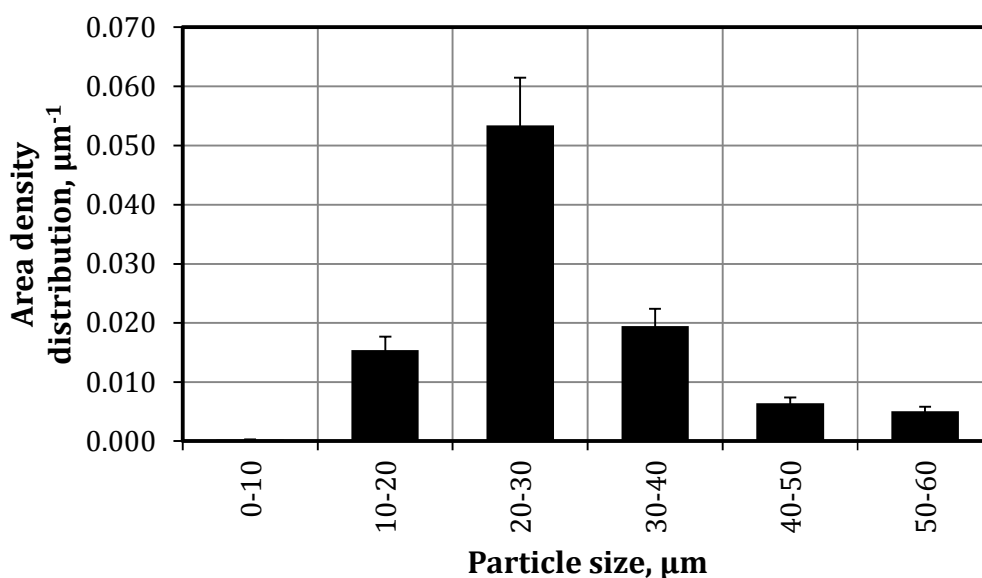
Figure 5.44: Area density distribution of lipase crystals grown using 100 g L^{-1} lipase, 75 mM NaCl, 0.275 M sodium dihydrogenphosphate, 50 g L^{-1} PEG 10000, and 25 mM sodium acetate buffer pH 4.0 (T = 20 °C, n = 250 min^{-1}). The error bars are equivalent to a measurement error of approximately 15 %.

The area density distribution showed a clear maximum for crystals measuring 20 - 30 µm with 69 % of the crystal area. 88 % of the crystal area was within 10 - 40 µm. Less than 1 % of the crystals were smaller than 10 µm. The largest crystal clusters measured up to 60 µm. The average crystal size was 25 µm.

In order to assess how crystallization affects LIP activity, the specific activity of LIP was determined for:

A: LIP stock solution as provided by the manufacturer

B: Stock solution of LIP prepared from A by exchange of the buffer to 25 mM
    Tris-HCl pH 9 via UF/DF (removal of stabilizing substances)

C: Resolubilized LIP crystals from a 100 mL-scale crystallization from solution B

D: Stock solution of LIP prepared from C by exchange of the buffer to 25 mM
    Tris-HCl pH 9 via UF/DF (removal of crystallization agents)

E: Resolubilized LIP crystals from a 100 mL-scale crystallization from solution D

The results of the activity measurements are depicted in Figure 5.45.
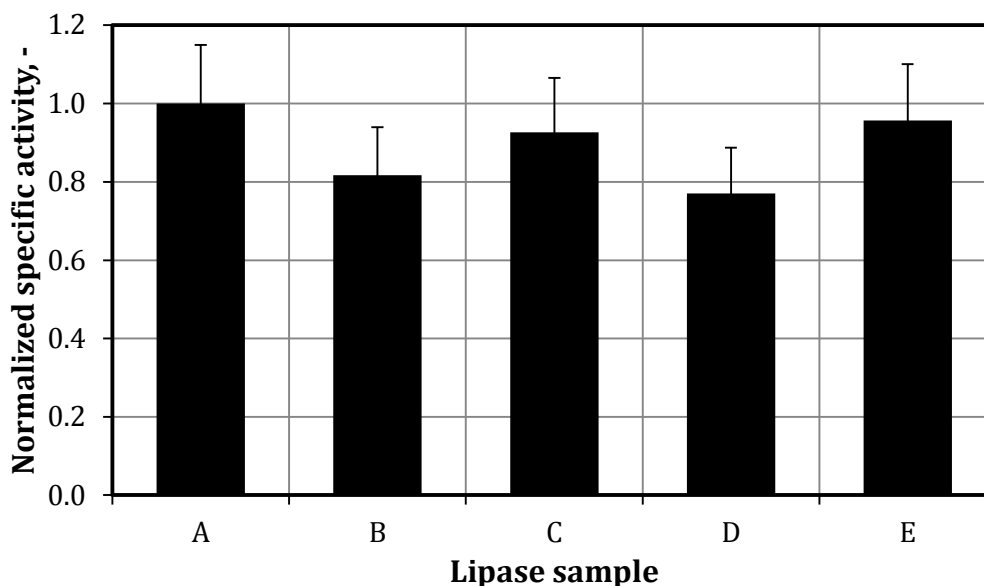
Figure 5.45: Normalized specific activity of lipase (LIP) solutions. **A)** stock solution provided by the manufacturer; **B)** stock solution after ultrafiltration/diafiltration (buffer 25 mM Tris-HCl pH 9); **C)** resolubilized LIP crystals from first 100 mL-scale crystallization; **D)** resolubilized LIP crystals from first 100 mL-scale crystallization after ultrafiltration/diafiltration for removal of the crystallization agents (buffer: 25 mM Tris-HCl pH 9); **E)** resolubilized LIP crystals from second 100 mL-scale crystallization. The crystallization conditions were: 100 g L^{-1} LIP, 75 mM NaCl, 0.275 M sodium dihydrogenphosphate, and addition of PEG 10000 to a final concentration of 50 g L^{-1} at 20 °C (n = 250 min^{-1}).

During the UF/DF, the specific activity of LIP is lowered by approximately 20 % (solutions B and D). The specific activity of LIP increases during the crystallization of LIP from these solutions. The specific activity of the resolubilized LIP crystals exhibited a specific activity of 93 % and 96 % of the specific activity of the stock solution provided by the manufacturer.

5.3.3 Antigen-binding fragment of the antibody cetuximab (FAB)

Since none of the additives positively influenced the crystallization of FAB (see chapter 5.2.4), crystallization conditions without additives and with addition of ammonium sulfate during the crystallization process were used (see chapter 5.1.5.2). Due to the limited availability of FAB and the high FAB concentrations used in the crystallization processes, the FAB crystallization was not performed in the 1 L-scale stirred tanks. The results of the FAB crystallization on the 100 mL-scale are depicted in Figure 5.46.
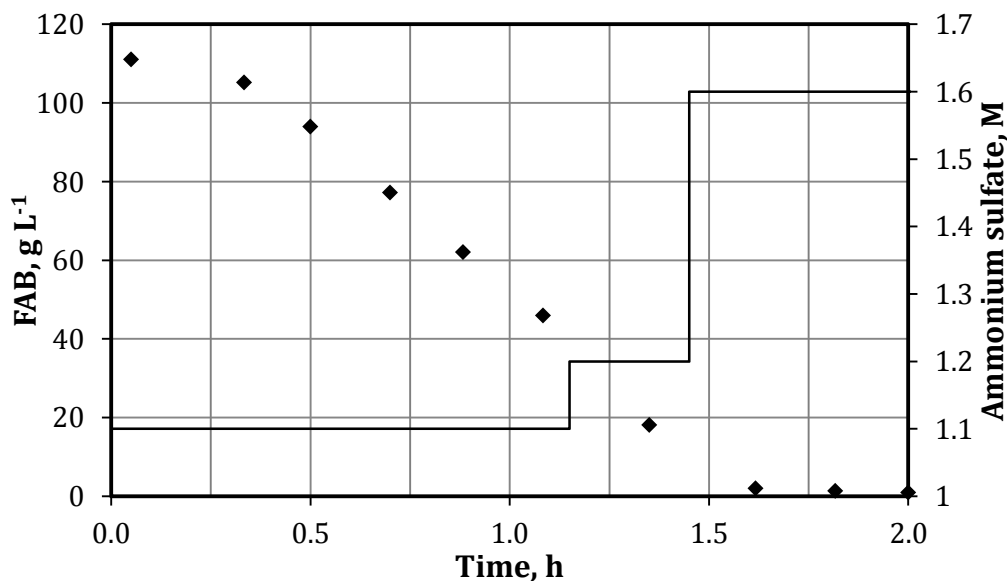
Figure 5.46: Crystallization of 110 g L^{-1} Fab fragment of cetuximab (FAB) on a 100 mL-scale using 1.1 M ammonium sulfate, and 40 mM sodium citrate buffer pH 6.25 at 20 °C (n = 150 min^{-1}). The ammonium sulfate concentration was raised to 1.2 M and 1.6 M after 1.1 h and 1.5 h, respectively. Depicted are ◆ the decrease of the FAB concentration in solution and the time-course of the ammonium sulfate concentration (solid line).

The crystallization started immediately after the addition of the crystallization agent solution. Fast crystallization kinetics were maintained by the increase of the ammonium sulfate concentration to 1.2 M and 1.6 M after 1.1 h and 1.45 h, respectively. The equilibrium was reached within 2 h with a residual FAB concentration of 0.9 g L^{-1}, equaling a crystallization yield of 99 %. A microphotograph of the crystals grown in the 100 mL-scale crystallization of FAB is shown in Figure 5.47. The morphology of the crystals was similar to that observed in the 5 mL-scale crystallization. An area density distribution was calculated from the microphotograph in order to characterize the crystal size distribution in the 100 mL-scale reactor (Figure 5.48).
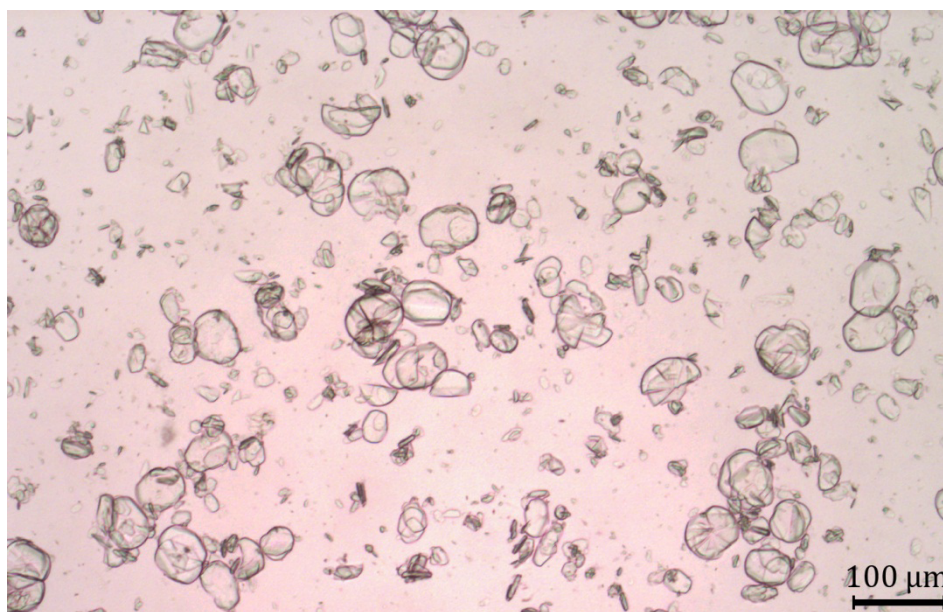
Figure 5.47: Crystals of the Fab fragment of cetuximab (FAB) grown in the 100 mL-scale reactor using 110 g L^{-1} FAB, 1.1 M ammonium sulfate (initially), and 40 mM sodium citrate buffer pH 6.25 at 20 °C and n = 150 min^{-1}. The ammonium sulfate concentration was raised to 1.2 M and 1.6 M after 1.1 h and 1.5 h, respectively.
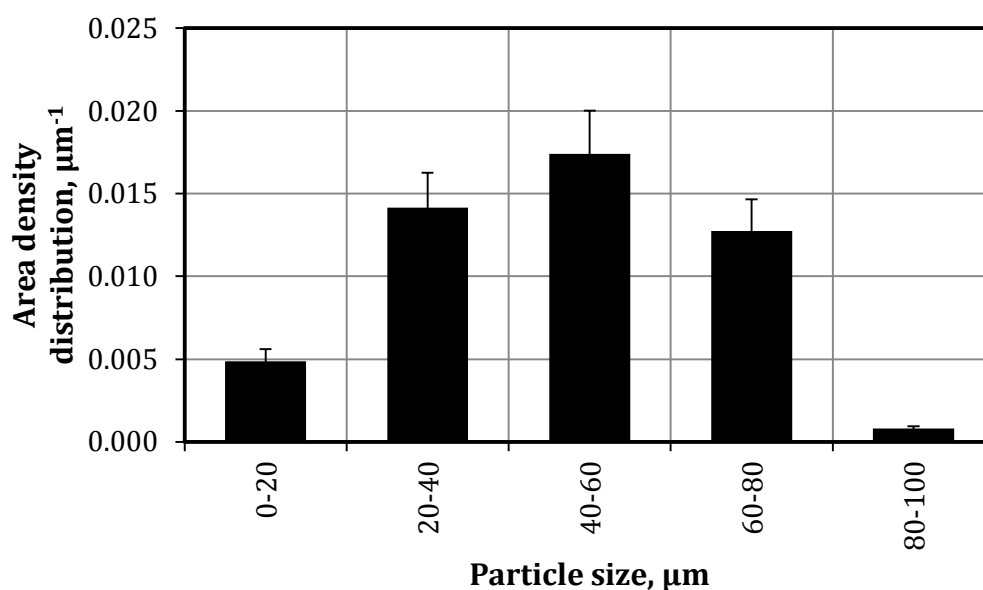
Figure 5.48: Area density distribution of FAB crystals grown in the 100 mL-scale crystallizer using 110 g L^{-1} FAB, 1.1 M ammonium sulfate (initially), and 40 mM sodium citrate buffer pH 6.25 at the equilibrium after the increase of the ammonium sulfate concentration to 1.6 M (T = 20 °C, n = 150 min^{-1}). The error bars are equivalent to a measurement error of approximately 15 %.

A broad maximum from 20 - 80 μm was observed. 88 % of the crystal area was within this range, whereas 2 % were in large crystal clusters measuring 80 - 100 μm and 10 % were in crystals smaller than 20 μm. The mid infrared spectroscopy (MIR) of FAB from

solution and resolubilized FAB crystals showed no conformational changes (internal communication from Dr. Bernd Stanislawski, Merck KGaA, Darmstadt, Germany).

5.3.4   Summary and discussion

The crystallization processes for LYS, LIP and FAB were successfully transferred into L-scale stirred-tanks. Due to its limited availability, FAB was only crystallized on a 100 mL-scale, whereas the other two proteins were crystallized on a 100 mL- and a 1 L-scale. The crystallization conditions for the three proteins were previously characterized and improved in scaled-down 5 mL-scale versions of the 1 L-scale reactors. The fast crystallization kinetics and the high crystallization yields observed on a L-scale were similar to those observed in the 5 mL-scale reactors. For all proteins, crystallization yields over 95 % were obtained within 2 h. The 5 mL-scale and the 100 mL-scale reactor were scaled-down from the 1 L-scale reactor based on geometric similarity. Hence, all length dimensions were adjusted by a single ratio and the stirrer speed remained as the only variable. In this work, the same stirrer speeds were used for all scales, as the crystallization kinetics were reported to be nearly independent of the stirrer speed (Schmidt *et al.*, 2005), and a reduced formation of crystal clusters was expected. Nevertheless, the same stirrer speed results in a higher power per volume in larger reactors. While this did not pose a problem in this work, stirrer speeds will probably need to be adjusted for a further scale-up of the crystallization processes.

Using crystals from 100 mL-scale crystallization experiments, the effects of protein crystallization on the enzyme activity of LIP and the conformation of FAB molecules were investigated. For LIP, crystallization was shown to increase the specific activity of a LIP solution that has been exposed to extensive shear stress during UF/DF back up to 94.5 % of its native activity. The comparison of crystalline FAB and FAB in solution via mid infrared spectroscopy (MIR) showed no conformational changes. Hence, protein crystallization has no negative, if not positive effects on protein stability.

For therapeutic proteins, Shukla and Thömmes (2010) estimated the production of 50 kg drug substance per production run to be realized in the near future. Derived from the crystallization conditions for FAB using 110 g L^{-1} protein, the large-scale purification by crystallization could be performed in a volume of 455 L. Even if lower protein concentrations have to be used, e.g. 25 g L^{-1} protein as for LYS, the volume necessary for the crystallization of 50 kg would be only 2000 L.

5.4 Removal of impurities from protein crystals

This chapter deals with the removal of undesirable impurities from the solvent channels of protein crystals (see chapter 3.2.5). These undesirable impurities include potentially toxic crystallization additives, i.e., ionic liquids, and crystallization agents which should not be included in formulation buffers, i.e., sulfate (see chapter 3.1.3). The removability of impurities by washing the protein crystals was investigated. First, wash solutions exhibiting a low solubility for each protein were identified empirically. The wash solutions and the losses of protein during the wash step are listed in Table 5.8.

Table 5.8: Wash solutions used for the depletion of impurities from protein crystals and the losses of protein observed.

Protein	Wash solution	Protein solubility, g L^{-1}	Loss of protein, %
LYS	60 % (v/v) ethanol	0.6	9
LIP	4 M NaCl	1.9	3
FAB	4 M NaCl in 0.2 M sodium citrate buffer pH 4.2	0.4	2

The specific content of unwanted impurities of the protein crystals prior to and after washing is listed in Table 5.9.

Table 5.9: Specific content of unwanted impurities of lysozyme, lipase and Fab fragment crystals prior to and after washing with the wash solutions listed in Table 5.8. **2-HEAF:** 2-hydroxyethylammonium formate.

Protein	Substance	Specific content before wash, g g^{-1}	Specific content after wash, g g^{-1}	Decrease, %
LYS	NaCl	2.92	0.08	98
	Sodium acetate	0.08	≈ 0.00	-
	2-HEAF	2.14	0.04	98
LIP	NaCl	0.10	0.57	(+ 470)
	PEG 10000	0.50	0.13	72
	Phosphate	0.26	0.01	95
FAB	Ammonium sulfate	1.70	0.14	92

For LIP, the specific content of NaCl and 2-hydroxyethylammonium formate was lowered by 98 %. For LIP, the specific content of phosphate and PEG 10000 was depleted by 95 % and 72 %, respectively. For FAB, the ammonium sulfate content was lowered by 92 %. Nevertheless, the NaCl content of the LIP crystals was increased 5.7-fold due to the high NaCl concentration in the wash solution. The same tendency is expected for the FAB crystals. However, the NaCl content of the FAB crystals was not experimentally determined.

Discussion

The specific content of the impurities, i.e., crystallization agents and/or additives, was successfully reduced by the introduction of a wash step. The impurities were not completely depleted from the crystals. Multiple subsequent wash steps could be used to further remove the impurities from the crystals in future work. However, an increased loss of protein would occur, effectively decreasing the overall yield of the crystallization processes. Hence, it is imperative to find crystallization conditions with non-toxic crystallization agents. For example, the crystallization agents used for the crystallization of LIP, i.e., NaCl, PEG 10000, and phosphate, are considered non-toxic and would not need to be removed. Ammonium sulfate is non-toxic, but it is unfavored for current protein formulations, e.g., aqueous solutions and amorphous precipitated lyophilisates, as it may lead to increased aggregation (Lewus *et al.*, 2010). Since the protein molecules are stabilized by the crystal lattice in crystalline proteins, ammonium sulfate might be tolerated in crystalline formulations. Future research could focus on the addition of stabilizing components, e.g., sugars, in the wash solutions, to further enhance the stability of protein crystals as formulation.

6 Conclusions and Outlook

Recent developments have led to increasing concentrations of target protein in state-of-the-art large-scale production processes, especially for therapeutic proteins. With 50 kg protein per production batch (Shukla and Thömmes, 2010), the limitations of established purification techniques are expected to soon create a bottleneck in downstream processing.

In this work, the feasibility of protein crystallization as novel protein purification technique for the downstream processing of proteins was investigated on the example of five different proteins (Table 6.1).

Table 6.1: Proteins under study, their molecular weight, their isoelectric point pI and their oligomerization.

Abbr.	Protein	Organism	Size, kDa	pI, -	Oligomerization
LYS	Lysozyme	*Gallus gallus*	14	11	monomer
LIP	Lipase	*Thermomyces lanuginosus*	29	5	monomer
XYL	Xylanase	*Trichoderma reesei*	21	9	monomer
GLU	Glucose isomerase	*Streptomyces rubiginosus*	173	3	homotetramer
FAB	Fab fragment of cetuximab	Chimeric (mouse/human)	47	-	heterodimer

First, scaled-down 5 mL- and 100 mL-scale versions of an existing 1 L-scale stirred-tank reactor were designed based on geometric similarity. The availability of small-scale reactors was imperative for the subsequent characterization of protein crystallization processes using low amounts of protein prior to the transfer of the refined crystallization processes into the L-scale reactors. On the 5 mL-scale, up to 12 reactors could be operated in parallel in order to simultaneously characterize different crystallization conditions.

For protein crystallization, suitable crystallization conditions have to be identified. Ideally, preliminary crystallization conditions for the proteins under study were reported in the literature, e.g., from structure determination, and could be used as starting point for screening. For all five proteins, suitable crystallization conditions were

identified and improved in microbatch-scale experiments. Using the qualitative data from the screening, phase diagrams were generated for the five proteins.

Subsequently, the batch crystallization processes for the proteins under study were successfully transferred into the same 5 mL-scale stirred-tank reactors. As agitated batch crystallization and microbatch crystallization share the same functional principle, the aforementioned phase diagrams were a valuable tool for the subsequent refinement of the crystallization conditions. These initial 5 mL-scale crystallization processes featured crystallization yields of 58 - 99 % within 2 - 24 h. Stirred-tank batch crystallization processes of LIP, XYL, GLU and FAB were reported for the first time. The yield of the LYS crystallization process was raised from 82 % to 89 % compared to the crystallization process reported by Hekmat *et al.* (2007b).

Next, the addition of additives, i.e., water-immiscible protic ionic liquids (ILs), was investigated in order to further increase the crystallization yields and to accelerate the crystallization kinetics. For XYL, GLU and FAB, the addition of ILs resulted in an unfavorable crystal form, no noticeable changes, and a decrease of the crystallization yield, respectively. In contrast, both, crystal form and the crystallization kinetics were improved upon the addition of the ionic liquid 2-hydroxyethylammonium formate (2-HEAF) to the crystallization of LYS. Compact crystals were observed instead of unfavorable needle-like crystals, and the crystallization yield was increased from 89 % to 97 % compared to the crystallization process without additive. For LIP, the addition of the ionic liquid choline dihydrogenphosphate (CDHP) resulted also in a favorable shift of the crystal form from needle-like to compact crystals. But it was also demonstrated that this positive effect was caused solely by the dihydrogenphosphate anion of the IL. Hence, CDHP could be replaced with sodium dihydrogenphosphate while maintaining the positive effects. This confirms the reports in the literature stating that individual ions of low-concentrated water-immiscible ILs are solely responsible for the effects observed, as they dissociate in aqueous solution and function just as ions of regular salts.

Despite the addition of sodium dihydrogenphosphate to the LIP crystallization process, the crystallization yield remained unsatisfactory low (50 %). Hence, a microbatch-scale screening for a complementary crystallization agent was carried out augmented by quantitative data from 5 mL-scale stirred-batch experiments. PEG 10000 was deemed suitable and consequently added during the LIP crystallization process to a final

concentration of 50 g L^{-1}. The crystallization yield was thereby increased to 95 % within 2 h. An overview of the refined crystallization processes for all five proteins, their crystallization yields and the process durations is given in Table 6.2.

Table 6.2: Overview of the refined crystallization processes for the five proteins under study. Given are the crystallization yields, the process durations, and the method(s) employed in order to increase the crystallization yield and to accelerate the crystallization kinetics.

Protein	Yield, %	Time, h	Method(s) employed
LYS	97	2	Temperature shift, addition of 2nd crystallization agent (ionic liquid)
LIP	95	2	Feeding of a complementary crystallization agent
XYL	95	20	Feeding of crystallization agent
GLU	97	3	-
FAB	99	2	Feeding of crystallization agent

Next, the refined 5 mL-scale crystallization processes for LYS, LIP and FAB were transferred into the 100 mL-scale reactors based on geometric similarity and using constant stirrer speeds. The results of the 5 mL- and 100 mL-scale FAB crystallization processes and crystals obtained from these processes are shown in Figure 6.1. The crystallization processes for LYS and LIP were subsequently transferred into the 1 L-scale reactor. Comparable results regarding the fast crystallization kinetics, the excellent crystallization yields, and the compact crystal morphologies were obtained. The general proof-of-principle for the crystallization of different proteins in scalable stirred-tanks was demonstrated on the example of LYS, LIP and FAB. Since GLU and XYL were not available in the quantities needed for the transfer, the crystallization of these two proteins was not investigated on the larger scale.

The removability of impurities, i.e., residual crystallization agents, from the solvent channels of the protein crystals was demonstrated by the introduction of a wash step. Nevertheless, the impurities could not be completely depleted from the protein crystals with a single wash step. Hence, repeated wash steps would be necessary, resulting in a considerable loss of protein. Consequently, unfavorable crystallization agents, e.g., toxic compounds, should be completely avoided during the crystallization process.
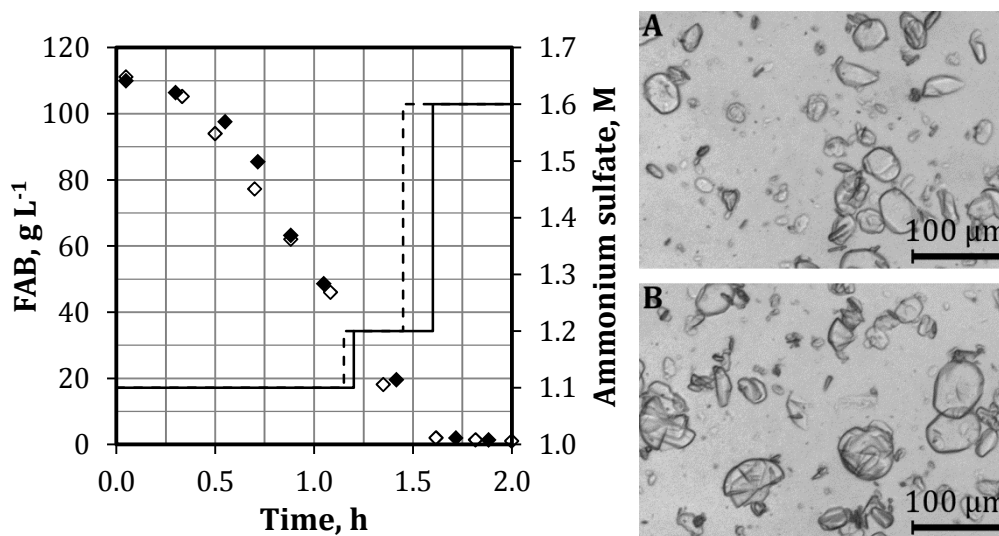
Figure 6.1: Crystallization of 110 g L^{-1} Fab fragment of cetuximab (FAB) on a ◆ 5 mL- and a ◇ 100 mL-scale using 1.1 M ammonium sulfate, and 40 mM sodium citrate buffer pH 6.25 at 20 °C (n = 150 min^{-1}). The ammonium sulfate concentration was raised to 1.2 M and 1.6 M after 1.1 h and 1.5 h, respectively. Depicted are the decrease of the FAB concentration in solution, the time-course of the ammonium sulfate concentration (5 mL: solid line; 100 mL: dashed line), and FAB crystals obtained in the **A)** 5 mL-scale and the **B)** 100 mL-scale crystallization process.

Finally, feasibility of protein crystallization from impure solutions was demonstrated by the crystallization of FAB from artificial solutions containing protein contaminants. For example, FAB was crystallized from solutions spiked with different proteins, or was successfully separated from small peptides originating from the papain overdigestion of an antibody.

To summarize, the feasibility of technical-scale protein crystallization for polishing and/or formulation steps at the end of the downstream processing pipeline was demonstrated. Stirred-tanks for the crystallization of 50 kg protein (Shukla and Thömmes, 2010) would need a capacity of 500 L or 2000 L for crystallization conditions with 100 g L^{-1} or 25 g L^{-1} protein, respectively. Compared to current purification techniques, i.e., preparative chromatography, the reusability of existing stirred-tank reactors and the low-cost crystallization agents used for protein crystallization should allow a significant cost-reduction.

The process integration of protein crystallization has to be investigated in future work. Since the feasibility of protein crystallization from impure solutions was demonstrated, protein crystallization directly from pretreated crude solutions could be investigated as an alternative to combinations of different conventional purification technologies.

Seeding with protein crystals from previous crystallization processes could be used if nucleation from impure solutions proves difficult.

Alternatively, a two-step process is proposed for the purification of proteins. In the first step, protein capture from crude material could be performed using another emerging technology, e.g., expanded bed chromatography (EBA) or aqueous two-phase separation (ATPS). Subsequently, high-purity protein crystals could be grown from the rudimentarily purified protein solution using protein crystallization. These crystals could then be used as formulation. Stabilizing agents, e.g., sugars, might be added to crystallization processes in order to further enhance protein crystals as formulation.

7 References

Albertsson PÅ (1961): Fractionation of particles and macromolecules in aqueous two-phase systems. *Biochemical Pharmacology*, *5*(4), 351-358.

Andya JD, Hsu CC, and Shire SJ (2003): Mechanisms of aggregate formation and carbohydrate excipient stabilization of lyophilized humanized monoclonal antibody formulations. *AAPS pharmSci*, *5*(2), E10.

Arnold JN, Wormald MR, Sim RB, Rudd PM, and Dwek R a (2007): The impact of glycosylation on the biological function and structure of human immunoglobulins. *Annual review of immunology*, *25*, 21-50.

Arteaga CL (2001): The epidermal growth factor receptor: from mutant oncogene in nonhuman cancers to therapeutic target in human neoplasia. *Journal of clinical oncology*, *19*(18 Suppl), 32S-40S.

Asenjo JA, and Andrews BA (2011): Aqueous two-phase systems for protein separation: a perspective. *Journal of chromatography. A*, *1218*(49), 8826-8835.

Asenjo JA, and Andrews BA (2012): Aqueous two-phase systems for protein separation: Phase separation and applications. *Journal of chromatography. A*, *1238*, 1-10.

Astier J-P, and Veesler S (2008): Using Temperature To Crystallize Proteins: A Mini-Review. *Crystal Growth & Design*, *8*(12), 4215-4219.

Atha DH, and Ingham KC (1981): Mechanism of Precipitation of Proteins by Polyethylene Glycols. *The Journal of biological chemistry*, *256*(23), 12108-12117.

Baldwin RL (1996): How Hofmeister ion interactions affect protein stability. *Biophysical journal*, *71*(4), 2056-63.

Bang M-L, Centner T, Fornoff F, Geach a. J, Gotthardt M, McNabb M, Witt CC, Labeit D, Gregorio CC, Granzier H, and Labeit S (2001): The Complete Gene Sequence of Titin, Expression of an Unusual 700-kDa Titin Isoform, and Its Interaction With Obscurin Identify a Novel Z-Line to I-Band Linking System. *Circulation Research*, *89*(11), 1065-1072.

Basu SK, Govardhan CP, Jung CW, and Margolin AL (2004): Protein crystals for the delivery of biopharmaceuticals. *Expert opinion on biological therapy*, *4*(3), 301-17.

Beg QK, Kapoor M, Mahajan L, and Hoondal GS (2001): Microbial xylanases and their industrial applications: a review. *Applied Microbiology and Biotechnology*, *56*(3-4), 326-338.

Behlke J, and Knespel A (1997): Crystallisation of proteins using ultracentrifugation to induce nucleation.

Bergfors T (1999): *Protein Crystallization. Techniques, Strategies, and Tips*. La Jolla, CA, USA: International University Line.

Berman HM, Westbrook J, Feng Z, Gilliland G, Bhat TN, Weissig H, Shindyalov IN, and Bourne PE (2000): The Protein Data Bank. *Nucleic acids research*, *28*(1), 235-42.

Bermejo R, and Ramos A (2012): Pilot Scale Recovery of Phycocyanin from Spirulina platensis Using Expanded Bed Adsorption Chromatography. *Chromatographia*, *75*(5-6), 195-204.

Bhamidi V, Skrzypczak-Jankun E, and Schall C a. (2001): Dependence of nucleation kinetics and crystal morphology of a model protein system on ionic strength. *Journal of Crystal Growth*, *232*(1-4), 77-85.

Bhamidi V, Varanasi S, and Schall CA (2002): Measurement and Modeling of Protein Crystal Nucleation Kinetics. *Crystal Growth & Design*, *2*(5), 395-400.

Bhamidi V, Varanasi S, and Schall CA (2005): Protein crystal nucleation: is the pair interaction potential the primary determinant of kinetics? *Langmuir : the ACS journal of surfaces and colloids*, *21*(20), 9044-50.

Bhosale SH, Rao MB, and Deshpande VV (1996): Molecular and industrial aspects of glucose isomerase. *Microbiological reviews*, *60*(2), 280-300.

Bolton G, Cabatingan M, Rubino M, Lute S, Brorson K, and Bailey M (2005): Normal-flow virus filtration: detection and assessment of the endpoint in bio-processing. *Biotechnology and applied biochemistry*, *42*(Pt 2), 133-42.

Brandt S, Goffe RA, Kessler SB, O'Connor JL, and Zale SE (1988): Membrane-Based Affinity Technology for Commercial Scale Purifications. *Bio/Technology*, *6*(7), 779-782.

Brocchieri L, and Karlin S (2005): Protein length in eukaryotic and prokaryotic proteomes. *Nucleic acids research*, *33*(10), 3390-400.

Brorson K, Brown J, Hamilton E, and Stein KE (2003): Identification of protein A media performance attributes that can be monitored as surrogates for retrovirus clearance during extended re-use. *Journal of chromatography. A*, *989*(1), 155-63.

Brzozowski AM, Savage H, Verma CS, Turkenburg JP, Lawson DM, Svendsen A, and Patkar S (2000): Structural origins of the interfacial activation in Thermomyces (Humicola) lanuginosa lipase. *Biochemistry*, *39*(49), 15071-82.

Bräutigam S, Dennewald D, Schürmann M, Lutje-Spelberg J, Pitner W-R, and Weuster-Botz D (2009): Whole-cell biocatalysis: Evaluation of new hydrophobic ionic liquids for efficient asymmetric reduction of prochiral ketones. *Enzyme and Microbial Technology*, *45*(4), 310-316.

Buchfink R, Tischer A, Patil G, Rudolph R, and Lange C (2010): Ionic liquids as refolding additives: variation of the anion. *Journal of biotechnology*, *150*(1), 64-72.

Carrell HL, Hoier H, and Glusker JP (1994): Modes of binding substrates and their analogues to the enzyme D-xylose isomerase. *Acta crystallographica. Section D, Biological crystallography*, *50*(Pt 2), 113-23.

Chayen NE (2004): Turning protein crystallisation from an art into a science. *Current opinion in structural biology*, *14*(5), 577-83.

Chayen NE (2005): Methods for separating nucleation and growth in protein crystallisation. *Progress in biophysics and molecular biology*, *88*(3), 329-37.

Chebotareva N a. (2007): Effect of molecular crowding on the enzymes of glycogenolysis. *Biochemistry (Moscow)*, *72*(13), 1478-1490.

Chen X, Ji Y, and Wang J (2010): Improvement on the crystallization of lysozyme in the presence of hydrophilic ionic liquid. *The Analyst*, *135*(9), 2241-8.

Chernov A (2003): Protein crystals and their growth. *Journal of Structural Biology*, *142*(1), 3-21.

Chi EY, Krishnan S, Randolph TW, and Carpenter JF (2003): Physical stability of proteins in aqueous solution: mechanism and driving forces in nonnative protein aggregation. *Pharmaceutical research*, *20*(9), 1325-36.

Chowdhury PS, and Wu H (2005): Tailor-made antibody therapeutics. *Methods*, *36*(1), 11-24.

Christopher GK, Phipps AG, and Gray RJ (1998): Temperature-dependent solubility of selected proteins. *Journal of Crystal Growth*, *191*(4), 820-826.

Collins KD (2004): Ions from the Hofmeister series and osmolytes: effects on proteins in solution and in the crystallization process. *Methods (San Diego, Calif.)*, *34*(3), 300-11.

Collins KD, and Washabaugh MW (1985): The Hofmeister effect and the behaviour of water at interfaces. *Quarterly Reviews of Biophysics*, *18*(04), 323.

Curbelo DR, Garke G, Guilarte RC, Anspach FB, and Deckwer W-D (2003): Cost Comparison of Protein Capture from Cultivation Broths by Expanded and Packed Bed Adsorption. *Engineering in Life Sciences*, *3*(10), 406-415.

Cvetkovic A, Picioreanu C, Straathof AJJ, Krishna R, and van Der Wielen LAM (2005): Quantification of binary diffusion in protein crystals. *The journal of physical chemistry. B*, *109*(21), 10561-6.

Dennewald D, Pitner W-R, and Weuster-Botz D (2011): Recycling of the ionic liquid phase in process integrated biphasic whole-cell biocatalysis. *Process Biochemistry*, *46*(5), 1132-1137.

Derewenda U, Swenson L, Wei Y, Green R, Kobos PM, Joerger R, Haas MJ, and Derewenda ZS (1994): Conformational lability of lipases observed in the absence of an oil-water interface: crystallographic studies of enzymes from the fungi Humicola lanuginosa and Rhizopus delemar. *Journal of lipid research*, *35*(3), 524-34.

Derewenda ZS, and Vekilov PG (2006): Entropy and surface engineering in protein crystallization. *Acta crystallographica. Section D, Biological crystallography*, *62*(Pt 1), 116-24.

Diamond R (1974): Real-space refinement of the structure of hen egg-white lysozyme. *Journal of Molecular Biology*, *82*(3), 371-391.

Dimitrov I, and Nanev CN (2006): Sedimentation as a tool for crystallization from protein mixtures. *Crystal Research and Technology*, *41*(11), 1063-1066.

Durbin SD, and Feher G (1986): Crystal growth studies of lysozyme as a model for protein crystallization. *Journal of Crystal Growth*, *76*(3), 583-592.

Dutta PR, and Maity A (2007): Cellular responses to EGFR inhibitors and their relevance to cancer therapy. *Cancer letters*, *254*(2), 165-77.

Earle MJ, and Seddon KR (2000): Ionic liquids. Green solvents for the future. *Pure and Applied Chemistry*, *72*(7), 1391-1398.

Elkordy AA, Forbes RT, and Barry BW (2002): Integrity of crystalline lysozyme exceeds that of a spray dried form. *Int. J. Pharm.*, *247*, 79-90.

Elkordy AA, Forbes RT, and Barry BW (2004): Stability of crystallised and spray-dried lysozyme. *International journal of pharmaceutics*, *278*(2), 209-19.

Endres F (2010): Physical chemistry of ionic liquids. *Physical chemistry chemical physics : PCCP*, *12*(8), 1648.

Englard S, and Seifter S (1990): Precipitation techniques. *Methods in enzymology*, *182*, 285-300.

Erdemir D, Lee AY, and Myerson AS (2009): Nucleation of Crystals from Solution: Classical and Two-Step Models. *Accounts of chemical research*, (April).

Eyal E, Gerzon S, Potapov V, Edelman M, and Sobolev V (2005): The limit of accuracy of protein modeling: influence of crystal packing on protein structure. *Journal of molecular biology*, *351*(2), 431-42.

Fairbanks G, Steck TL, and Wallach DFH (1971): Electrophoretic analysis of the major polypeptides of the human erythrocyte membrane. *Biochemistry*, *10*(13), 2606-2617.

Farid SS (2007): Process economics of industrial monoclonal antibody manufacture. *Journal of chromatography. B, Analytical technologies in the biomedical and life sciences*, *848*(1), 8-18.

Fischer I, and Franzreb M (2011a): Direct determination of the composition of aqueous micellar two-phase systems (AMTPS) using potentiometric titration—A rapid tool for detergent-based bioseparation. *Colloids and Surfaces A: Physicochemical and Engineering Aspects*, *377*(1-3), 97-102.

Fischer I, and Franzreb M (2011b): Magnetic Extraction – Magnetic Particle Mediated Protein Separation in Aqueous Micellar Two-Phase Systems. *BPP 2011. Puerto Vallarta, Mexico, 18. - 22.09.2011*.

Fischer I, and Franzreb M (2012): Continous magnetic Extraction – a novel method for the large-scale separation of functional magnetic sorbents. *GVC/Dechema Vortrags- und Diskussionstagung Biopharmazeutische Produktion. Freiburg, Germany, 14. - 16.05.2012*.

Fleischman JB, Porter RR, and Press EM (1963): the Arrangement of the Peptide Chains in Gamma-Globulin. *The Biochemical journal*, *88*(1960), 220-8.

Fleming A (1922): On a Remarkable Bacteriolytic Element Found in Tissues and Secretions. *Proceedings of the Royal Society B: Biological Sciences*, *93*(653), 306-317.

Fling SP, and Gregerson DS (1986): Peptide and protein molecular weight determination by electrophoresis using a high-molarity tris buffer system without urea. *Analytical biochemistry*, *155*(1), 83-8.

Franzreb M, Siemann-Herzberg M, Hobley TJ, and Thomas ORT (2006): Protein purification using magnetic adsorbent particles. *Applied microbiology and biotechnology*, *70*(5), 505-16.

Fujita K, MacFarlane DR, and Forsyth M (2005): Protein solubilising and stabilising ionic liquids. *Chemical communications (Cambridge, England)*, *70*(38), 4804-6.

Fujita K, MacFarlane DR, Forsyth M, Yoshizawa-Fujita M, Murata K, Nakamura N, and Ohno H (2007): Solubility and stability of cytochrome c in hydrated ionic liquids: effect of oxo acid residues and kosmotropicity. *Biomacromolecules*, *8*(7), 2080-6.

Gagnon P (2012): Technology trends in antibody purification. *Journal of chromatography. A*, *1221*, 57-70.

Galkin O, and Vekilov PG (2001): Nucleation of protein crystals : critical nuclei , phase behavior , and control pathways. *Journal of Crystal Growth*, *232*, 63-76.

García-Ruiz MJ (2003): Nucleation of protein crystals. *Journal of structural biology*, *142*(1), 22-31.

Garlitz JA, Summers CA, Flowers RA, and Borgstahl GE (1999): Ethylammonium nitrate: a protein crystallization reagent. *Acta crystallographica. Section D, Biological crystallography*, *55*, 2037-8.

Gasteiger E, Hoogland C, Gattiker A, Duvaud S, Wilkins MR, Appel RD, and Bairoch A (2005): Protein Identification and Analysis Tools on the ExPASy Server. In J. M. Walker (Ed.), *The Proteomics Protocols Handbook* (pp. 571-607). Humana Press.

George A, Chian Y, Guo B, Arabshahi A, Cai Z, and Wilson WW (1997): Second Virial Coefficient as Predictor in Protein Crystal Growth. *Methods in enzymology*, *276*, 100-110.

Gottschalk U (2005): Downstream processing of monoclonal antibodies: From high dilution to high purity. *BioPharm International*, *18*(6), 42.

Hallas-Moller K, Petersen K, and Schlichtkrull J (1952): Crystalline and amorphous insulin-zinc compounds with prolonged action. *Science*, *116*(3015), 394-398.

Hampton (2001): Microdialysis Crystallization. Retrieved August 30, 2012, from http://hamptonresearch.com/documents/growth_101/7.pdf

Hampton (2010): Xylanase User Guide. Retrieved August 7, 2012, from http://hamptonresearch.com/documents/product/hr001193_7-104_user_guide.pdf

Hampton (2012): Glucose Isomerase User Guide. Retrieved August 7, 2012, from http://hamptonresearch.com/documents/product/hr002558_web_100,102.pdf

Hansen CL, Skordalakes E, Berger JM, and Quake SR (2002): A robust and scalable microfluidic metering method that allows protein crystal growth by free interface diffusion. *Proceedings of the National Academy of Sciences of the United States of America*, *99*(26), 16531-6.

Harrison R, Todd P, Rudge S, and Petrides D (2003): *Bioseparations science and engineering. Bioseparations science and engineering* (pp. 355-356). New York: Oxford University Press.

Hart RA, Lester PM, Reifsnyder DH, Ogez JR, and Builder SE (1994): Large Scale, In Situ Isolation of Periplasmic IGF–I from E. coli. *Bio/Technology*, *12*(11), 1113-1117.

Hekmat D, Hebel D, Joswig S, Schmidt M, and Weuster-Botz D (2007a): Advanced protein crystallization using water-soluble ionic liquids as crystallization additives. *Biotechnology letters*, *29*(11), 1703-11.

Hekmat D, Hebel D, Schmid H, and Weuster-Botz D (2007b): Crystallization of lysozyme: From vapor diffusion experiments to batch crystallization in agitated ml-scale vessels. *Process Biochemistry*, *42*(12), 1649-1654.

Hekmat D, Hebel D, and Weuster-Botz D (2008): Crystalline Proteins as an Alternative to Standard Formulations. *Chemical Engineering & Technology*, *31*(6), 911-916.

Hekmat D, Mornhinweg R, Bloch G, Sun Y, Jeanty P, Neubert M, and Weuster-Botz D (2011): Macroscopic investigation of the transient hydrodynamic memory behavior of preparative packed chromatography beds. *Journal of chromatography. A*, *1218*(7), 944-50.

Hofmeister F (1888): Zur Lehre von der Wirkung der Salze. *Arch. Exp. Pathol. Pharmacol.*, *24*, 247-260.

Holschuh K, and Schwämmle A (2005): Preparative purification of antibodies with protein A—an alternative to conventional chromatography. *Journal of Magnetism and Magnetic Materials*, *293*(1), 345-348.

Howard SB, Twigg PJ, Baird JK, and Meehan EJ (1988): The Solubility of Henn Egg-White Lysozyme. *Journal of Crystal Growth*, *90*, 94-104.

Hubbuch J, and Kula M-R (2007): Isolation and Purification of Biotechnological Products. *Journal of Non-Equilibrium Thermodynamics*, *32*(2), 99-127.

Hubbuch JJ, Matthiesen DB, Hobley TJ, and Thomas OR (2001): High gradient magnetic separation versus expanded bed adsorption: a first principle comparison. *Bioseparation*, *10*(1-3), 99-112.

Jacobsen C, Garside J, and Hoare M (1998): Nucleation and growth of microbial lipase crystals from clarified concentrated fermentation broths. *Biotechnology and bioengineering*, *57*(6), 666-75.

Jaeger KE, and Reetz MT (1998): Microbial lipases form versatile tools for biotechnology. *Trends in biotechnology*, *16*(9), 396-403.

Jazwinska EC, Dunckley H, Propert DN, Gatenby P a, and Serjeantson SW (1988): Gm typing by immunoglobulin heavy-chain gene RFLP analysis. *American journal of human genetics*, *43*(2), 175-81.

Jia Z, and Tian C (2009): Quantitative determination of polyethylene glycol with modified Dragendorff reagent method. *Desalination*, *250*, 87-93.

Jiang C, Liu J, Rubacha M, and Shukla A a (2009): A mechanistic study of Protein A chromatography resin lifetime. *Journal of chromatography. A*, *1216*(31), 5849-55.

Jion AI, Goh L, and Oh SKW (2006): Crystallization of IgG1 by mapping its liquid-liquid phase separation curves. *Biotechnology and bioengineering*, *95*(5), 911-8.

Judge RA, Johns MR, and White ET (1995): Protein purification by bulk crystallization: the recovery of ovalbumin. *Biotechnology and bioengineering*, *48*(4), 316-23.

Judge RA, Takahashi S, Longenecker KL, Fry EH, Abad-Zapatero C, and Chiu ML (2009): The Effect of Ionic Liquids on Protein Crystallization and X-ray Diffraction Resolution. *Crystal Growth & Design*, *9*(8), 3463-3469.

Kamm B, and Kamm M (2007): Biorefineries--multi product processes. *Advances in biochemical engineering/biotechnology*, *105*(January), 175-204.

Kantardjieff KA, Jamshidian M, and Rupp B (2004): Distributions of pI versus pH provide prior information for the design of crystallization screening experiments: response to comment on "Protein isoelectric point as a predictor for increased crystallization screening efficiency." *Bioinformatics*, *20*(14), 2171-2174.

Kantardjieff KA, and Rupp B (2004): Protein isoelectric point as a predictor for increased crystallization screening efficiency. *Bioinformatics*, *20*(14), 2162-8.

Kasche V, and De Boer M (2000): Aufarbeitung von Bioprodukten. *Chemie Ingenieur Technik*, *72*(12), 1448.

Kelley B (2007): Very large scale monoclonal antibody purification: the case for conventional unit operations. *Biotechnology progress*, *23*(5), 995-1008.

Kelley B (2009): Industrialization of mAb production technology: the bioprocessing industry at a crossroads. *mAbs*, *1*(5), 443-52.

Kennedy DF, Drummond CJ, Peat TS, and Newman J (2011): Evaluating Protic Ionic Liquids as Protein Crystallization Additives. *Crystal Growth & Design*, *11*(5), 1777-1785.

Knudsen HL, Fahrner RL, Xu Y, Norling L a, and Blank GS (2001): Membrane ion-exchange chromatography for process-scale antibody purification. *Journal of chromatography. A*, *907*(1-2), 145-54.

Kowacz M, Mukhopadhyay A, Carvalho AL, Esperança JMSS, Romão MJ, and Rebelo LPN (2012): Hofmeister effects of ionic liquids in protein crystallization: Direct and water-mediated interactions. *CrystEngComm*, *14*(15), 4912.

Laemmli UK (1970): Cleavage of Structural Proteins during the Assembly of the Head of Bacteriophage T4. *Nature*, *227*, 680-685.

Lange C, Patil G, and Rudolph R (2005): Ionic liquids as refolding additives: N'-alkyl and N'-(omega-hydroxyalkyl) N-methylimidazolium chlorides. *Protein science : a publication of the Protein Society*, *14*(10), 2693-701.

Layne E (1957): Spectrophotometric and Turbidimetric Methods for Measuring Proteins. *Methods in enzymology*, *3*, 447-454.

Lee SHS, Hatton TA, and Khan S a. (2011): Microfluidic continuous magnetophoretic protein separation using nanoparticle aggregates. *Microfluidics and Nanofluidics*, *11*(4), 429-438.

Lee T, Vaghjiani J, Lye G, and Turner M (2000): A systematic approach to the large-scale production of protein crystals. *Enzyme and Microbial Technology*, *26*(8), 582-592.

Lenhoff AM, Pjura PE, Dilmore JG, and Godlewski TS (1997): Ultracentrifugal crystallization of proteins: transport-kinetic modelling, and experimental behavior of catalase. *Journal of Crystal Growth*, *180*(1), 113-126.

Lewandowski A, and Świderska-Mocek A (2009): Ionic liquids as electrolytes for Li-ion batteries—An overview of electrochemical studies. *Journal of Power Sources*, *194*(2), 601-609.

Lewus R a, Darcy P a, Lenhoff AM, and Sandler SI (2010): Interactions and phase behavior of a monoclonal antibody. *Biotechnology progress*.

Li S, Schmitz KR, Jeffrey PD, Wiltzius JJW, Kussie P, and Ferguson KM (2005): Structural basis for inhibition of the epidermal growth factor receptor by cetuximab. *Cancer cell*, *7*(4), 301-11.

Linke D, Zorn H, Gerken B, Parlar H, and Berger RG (2005): Foam fractionation of exo-lipases from a growing fungus (Pleurotus sapidus). *Lipids*, *40*(3), 323-7.

Liu D, Schmid RD, and Rusnak M (2006): Functional expression of Candida antarctica lipase B in the Escherichia coli cytoplasm--a screening system for a frequently used biocatalyst. *Applied microbiology and biotechnology*, *72*(5), 1024-32.

Liu J, Yin D-C, Guo Y-Z, Wang X-K, Xie S-X, Lu Q-Q, and Liu Y-M (2011): Selecting temperature for protein crystallization screens using the temperature dependence of the second virial coefficient. *PloS one*, *6*(3), e17950.

Lorber B (2008): Virus and Protein Crystallization under Hypergravity. *Crystal Growth & Design*, *8*(8), 2964-2969.

Low D, O'Leary R, and Pujar NS (2007): Future of antibody purification. *Journal of chromatography. B, Analytical technologies in the biomedical and life sciences*, *848*(1), 48-63.

Mage MG (1980): Preparation of Fab fragments from IgGs of different animal species. *Methods in enzymology*, *70*(A), 142-50.

Manning MC, Chou DK, Murphy BM, Payne RW, and Katayama DS (2010): Stability of Protein Pharmaceuticals: An Update. *Pharmaceutical research*, *27*(4), 544-75.

Margolin AL, and Navia MA (2001): Protein Crystals as Novel Catalytic Materials. *Angewandte Chemie (International ed. in English)*, *40*(12), 2204-2222.

Maruyama H, Seki H, Suzuki A, and Inoue N (2007): Batch foam separation of a soluble protein. *Water research*, *41*(3), 710-8.

Matthews T, and Bean B (2006): Development of a Scaleable Protein Purification Process Using Crystallization. *Bioprocess International Conference & Exhibition San Francisco, CA.*

McDonald P, Victa C, Carter-Franklin JN, and Fahrner R (2009): Selective antibody precipitation using polyelectrolytes: a novel approach to the purification of monoclonal antibodies. *Biotechnology and bioengineering*, *102*(4), 1141-51.

McPherson A (2004): Introduction to protein crystallization. *Methods*, *34*(3), 254-65.

Merz J, Burghoff B, Zorn H, and Schembecker G (2011): Continuous foam fractionation: Performance as a function of operating variables. *Separation and Purification Technology*, *82*, 10-18.

Mirro R, and Voll K (2009): Which Impeller Is Right for Your Cell Line? *BioProcess International*, *7*(1), 52-57.

Moreno M, Castiglione F, Mele A, Pasqui C, and Raos G (2008): Interaction of water with the model ionic liquid [bmim][BF4]: molecular dynamics simulations and comparison with NMR data. *The journal of physical chemistry. B*, *112*(26), 7826-36.

Müller M, Wolberg M, Schubert T, and Hummel W (2005): Enzyme-catalyzed regio- and enantioselective ketone reductions. *Advances in biochemical engineering/biotechnology*, *92*, 261-87.

Navarro A, Wu H-S, and Wang SS (2009): Engineering problems in protein crystallization. *Separation and Purification Technology*, *68*(2), 129-137.

Nicolis G, and Nicolis C (2003): Enhancement of the nucleation of protein crystals by the presence of an intermediate phase: a kinetic model. *Physica A: Statistical Mechanics and its Applications*, *323*, 139-154.

Pain RH (1963): the Molecular Weights of the Peptide Chains of Gamma-Globulin. *The Biochemical journal*, *88*, 234-9.

Peng ZG, Hidajat K, and Uddin MS (2005): Selective and sequential adsorption of bovine serum albumin and lysozyme from a binary mixture on nanosized magnetic particles. *Journal of colloid and interface science*, *281*(1), 11-7.

Penkova A, Pan W, Hodjaoglu F, and Vekilov PG (2006): Nucleation of protein crystals under the influence of solution shear flow. *Annals of the New York Academy of Sciences*, *1077*, 214-31.

Pfruender H, Amidjojo M, Kragl U, and Weuster-Botz D (2004): Efficient whole-cell biotransformation in a biphasic ionic liquid/water system. *Angewandte Chemie (International ed. in English)*, *43*(34), 4529-31.

Pfruender H, Jones R, and Weuster-Botz D (2006): Water immiscible ionic liquids as solvents for whole cell biocatalysis. *Journal of biotechnology*, *124*(1), 182-90.

Phillips DC (1967): The Hen Egg-White Lysozyme Molecule. *Proceedings of the National Academy of Sciences of the United States of America*, *57*(3), 484-495.

Pitts JE (1992): Crystallization by centrifugation. *Nature*, *355*, 117.

Przybycien TM, Pujar NS, and Steele LM (2004): Alternative bioseparation operations: life beyond packed-bed chromatography. *Current opinion in biotechnology*, *15*(5), 469-78.

Pusey ML, Paley MS, Turner MB, and Rogers RD (2007): Protein Crystallization Using Room Temperature Ionic Liquids. *Crystal Growth & Design*, *7*(4), 787-793.

Rao CK (2008): Who coined the terms "biotechnology" and "generic engineering", and when? *Current Science*, *95*(1), 1512-1513.

Reid C, and Rand RP (1997): Probing protein hydration and conformational states in solution. *Biophysical journal*, *72*(3), 1022-30.

Roberts MM, Heng JYY, and Williams DR (2010): Protein Crystallization by Forced Flow through Glass Capillaries: Enhanced Lysozyme Crystal Growth. *Crystal Growth & Design*, *10*(3), 1074-1083.

Roberts MWH, Ongkudon CM, Forde GM, and Danquah MK (2009): Versatility of polymethacrylate monoliths for chromatographic purification of biomolecules. *Journal of separation science*, *32*(15-16), 2485-94.

Rogers M, Hiraoka-Sutow M, Mak P, Mann F, and Lebreton B (2009): Development of a rapid sanitization solution for silica-based protein A affinity adsorbents. *Journal of chromatography. A*, *1216*(21), 4589-96.

Rosa PAJ, Azevedo AM, Sommerfeld S, Mutter M, Aires-Barros MR, and Bäcker W (2009): Application of aqueous two-phase systems to antibody purification: A multi-stage approach. *Journal of Biotechnology*, *139*(4), 306-313.

Rupp B (2010): *Biomolecular Crystallography: Principles, Practice, and Application to Structural Biology* (1st ed., pp. 1-809). New York: Garland Science, Taylor & Francis.

Salemme FR (1972): A free interface diffusion technique for the crystallization of proteins for X-ray crystallography. *Archives of Biochemistry and Biophysics*, *151*(2), 533-539.

Sanamaría-Holek I, Gadomski A, and Rubí JM (2011): Controlling protein crystal growth rate by means of temperature. *Journal of physics. Condensed matter : an Institute of Physics journal*, *23*(23), 235101.

Sate D, Janssen MHA, Stephens G, Sheldon RA, Seddon KR, and Lu JR (2007): Enzyme aggregation in ionic liquids studied by dynamic light scattering and small angle neutron scattering. *Green Chemistry*, *9*(8), 859.

Saxena A, Tripathi BP, Kumar M, and Shahi VK (2009): Membrane-based techniques for the separation and purification of proteins: an overview. *Advances in colloid and interface science*, *145*(1-2), 1-22.

Scharnagl C, Reif M, and Friedrich J (2005): Stability of proteins: temperature, pressure and the role of the solvent. *Biochimica et biophysica acta*, *1749*(2), 187-213.

Schlichtkrull J (1957): Insulin Crystals V. The Nucleation and Growth of Insulin Crystals. *Acta Chemica Scandinavica*, *11*(3), 439-460.

Schmidt S, Havekost D, Kaiser K, Kauling J, and Henzler H-J (2004): Kristallisation für die Aufarbeitung von Proteinen. *Chemie Ingenieur Technik*, *76*(6), 819-822.

Schmidt S, Havekost D, Kaiser K, Kauling J, and Henzler H-J (2005): Crystallization for the Downstream Processing of Proteins. *Engineering in Life Sciences*, *5*(3), 273-276.

Schroeder HW, and Cavacini L (2010): Structure and function of immunoglobulins. *The Journal of allergy and clinical immunology*, *125*(2 Suppl 2), S41-52.

Shenoy B, Wang Y, Shan W, and Margolin a L (2001): Stability of crystalline proteins. *Biotechnology and bioengineering*, *73*(5), 358-69.

Shimizu S, McLaren WM, and Matubayasi N (2006): The Hofmeister series and protein-salt interactions. *The Journal of chemical physics*, *124*(23), 234905.

Shukla AA, Hubbard B, Tressel T, Guhan S, and Low D (2007): Downstream processing of monoclonal antibodies--application of platform approaches. *Journal of chromatography. B, Analytical technologies in the biomedical and life sciences*, *848*(1), 28-39.

Shukla AA, and Thömmes J (2010): Recent advances in large-scale production of monoclonal antibodies and related proteins. *Trends in biotechnology*, *28*(5), 253-61.

Sim S-L, He T, Tscheliessnig A, Mueller M, Tan RBH, and Jungbauer A (2012): Protein precipitation by polyethylene glycol: a generalized model based on hydrodynamic radius. *Journal of biotechnology*, *157*(2), 315-9.

Stevens RC (2000): High-throughput protein crystallization. *Current opinion in structural biology*, *10*(5), 558-63.

Strohl WR, and Knight DM (2009): Discovery and development of biopharmaceuticals: current issues. *Current opinion in biotechnology*, *20*(6), 668-72.

Stura EA, Nemerow GR, and Wilson IA (1992): Strategies in the crystallization of glycoproteins and protein complexes. *Journal of Crystal Growth*, *122*(1-4), 273-285.

Sun L, Li J, Xu C, Yu F, Zhou H, Tang L, and He J (2010): The sandwich method for protein crystallization and its effect on crystal growth. *Acta Biochimica et Biophysica Sinica*, *42*(5), 332-336.

Tait S, White ET, and Litster JD (2009): A Study on Nucleation for Protein Crystallization in Mixed Vessels. *Crystal Growth & Design*, *9*(5), 2198-2206.

Takakura T, Ito T, Yagi S, Notsu Y, Itakura T, Nakamura T, Inagaki K, Esaki N, Hoffman RM, and Takimoto A (2006): High-level expression and bulk crystallization of recombinant L-methionine gamma-lyase, an anticancer agent. *Applied microbiology and biotechnology*, *70*(2), 183-92.

Takayama Y, and Nakasako M (2011): A few low-frequency normal modes predominantly contribute to conformational responses of hen egg white lysozyme in the tetragonal crystal to variations of molecular packing controlled by environmental humidity. *Biophysical chemistry*, *159*(2-3), 237-46.

Tenkanen M, Puls J, and Poutanen K (1992): Two major xylanases of Trichoderma reesei. *Enzyme and Microbial Technology*, *14*(7), 566-574.

Timasheff SN (2002): Protein-solvent preferential interactions, protein hydration, and the modulation of biochemical reactions by solvent components. *Proceedings of the National Academy of Sciences of the United States of America*, *99*(15), 9721-6.

Tscheliessnig A, Ong D, Lee J, Pan S, Satianegara G, Schriebl K, Choo A, and Jungbauer A (2009): Engineering of a two-step purification strategy for a panel of monoclonal immunoglobulin M directed against undifferentiated human embryonic stem cells. *Journal of chromatography. A*, *1216*(45), 7851-64.

Törrönen A, Rouvinen J, Ahlgren M, Harkki A, and Visuri K (1993): Crystallization and preliminary X-ray analysis of two major xylanases from Trichoderma reesei. *Journal of molecular biology*, *233*(2), 313-6.

Uniprot Consortium T (2012): Reorganizing the protein space at the Universal Protein Resource (UniProt). *Nucleic acids research*, *40*(Database issue), D71-5.

Vardar-Sukan F (1998): Foaming: Consequences, prevention and destruction. *Biotechnology Advances*, *16*(5-6), 913-948.

Vekilov PG (2003): Solvent entropy effects in the formation of protein solid phases. *Methods in enzymology*, *368*(1), 84-105.

Vekilov PG (2012): Phase diagrams and kinetics of phase transitions in protein solutions. *Journal of physics. Condensed matter : an Institute of Physics journal*, *24*(19), 193101.

Verma AS, Agrahari S, Rastogi S, and Singh A (2011): Biotechnology in the realm of history. *Journal of pharmacy & bioallied sciences*, *3*(3), 321-3.

Viikari L, Alapuranen M, Puranen T, Vehmaanperä J, and Siika-Aho M (2007): Thermostable enzymes in lignocellulose hydrolysis. *Advances in biochemical engineering/biotechnology*, *108*(June), 121-45.

Wang W, Nema S, and Teagarden D (2010): Protein aggregation--pathways and influencing factors. *International journal of pharmaceutics*, *390*(2), 89-99.

Wanka J, and Peukert W (2011): Optimized Production of Protein Crystals: From 1D Crystallization Slot towards 2D Supersaturation B22 Diagram. *Chemical Engineering & Technology*, *34*(4), 510-516.

Warren JC, Stowring L, and Morales MF (1966): The Effect of Structure-disrupting Ions on the Activity of Myosin and Other Enzymes. *The Journal of biological chemistry*, *241*(2), 309-316.

Watanabe N, Akiba T, Kanai R, and Harata K (2006): Structure of an orthorhombic form of xylanase II from Trichoderma reesei and analysis of thermal displacement. *Acta crystallographica. Section D, Biological crystallography*, *62*(Pt 7), 784-92.

Weaver KD, Vrikkis RM, Van Vorst MP, Trullinger J, Vijayaraghavan R, Foureau DM, McKillop IH, MacFarlane DR, Krueger JK, and Elliott GD (2012): Structure and function of proteins in hydrated choline dihydrogen phosphate ionic liquid. *Physical chemistry chemical physics : PCCP*, *14*(2), 790-801.

Weibels S, Syguda A, Herrmann C, and Weingärtner H (2012): Steering the enzymatic activity of proteins by ionic liquids. A case study of the enzyme kinetics of yeast alcohol dehydrogenase. *Physical chemistry chemical physics : PCCP*, *14*(13), 4635-9.

Weingärtner H, Cabrele C, and Herrmann C (2012): How ionic liquids can help to stabilize native proteins. *Physical chemistry chemical physics : PCCP*, *14*(2), 415-26.

Weuster-Botz D (2007): Process intensification of whole-cell biocatalysis with ionic liquids. *Chemical record (New York, N.Y.)*, *7*(6), 334-40.

Weuster-Botz D, Hekmat D, Puskeiler R, and Franco-Lara E (2007): Enabling technologies: fermentation and downstream processing. *White Biotechnology*, (October 2006), 205-247.

Wyckoff RWG, and Corey RB (1936): The Ultracentrifugal Crystallization of Tobacco Mosaic Virus Protein. *Science*, *84*(2188), 513.

Yang MX, Shenoy B, Disttler M, Patel R, McGrath M, Pechenov S, and Margolin AL (2003): Crystalline monoclonal antibodies for subcutaneous delivery. *Proceedings of the National Academy of Sciences of the United States of America*, *100*(12), 6934-9.

Yang Z (2009): Hofmeister effects: an explanation for the impact of ionic liquids on biocatalysis. *Journal of biotechnology*, *144*(1), 12-22.

Yap WB, Tey BT, Alitheen NBM, and Tan WS (2010): Purification of His-tagged hepatitis B core antigen from unclarified bacterial homogenate using immobilized metal affinity-expanded bed adsorption chromatography. *Journal of chromatography. A*, *1217*(21), 3473-80.

Yarden Y (2001): The EGFR family and its ligands in human cancer. signalling mechanisms and therapeutic opportunities. *European journal of cancer*, *37 Suppl 4*, S3-8.

Zappacosta S, Nisonoff A, and Mandy WJ (1968): Mechanism of cleavage of rabbit IgG in two stages by soluble papain and reducing agent. *Journal of immunology*, *100*(6), 1268-76.

Zhang Y, and Cremer PS (2006): Interactions between macromolecules and ions: The Hofmeister series. *Current opinion in chemical biology*, *10*(6), 658-63.

van Reis R, and Zydney A (2001): Membrane separations in biotechnology. *Current opinion in biotechnology*, *12*(2), 208-11.

8 Appendix

8.1 Abbreviations

2-HEAF	2-hydroxyethylammonium formate
AA	amino acid
AMTPS	aqueous micellar two-phase separation
AS	ammonium sulfate
ATPS	aqueous two-phase separation
CDHP	choline dihydrogenphosphate
CEC	cation exchange chromatography
CET	cetuximab
CIP	cleaning in place
CNT	classical nucleation theory
ddH$_2$O	bidistilled water
EBA	expanded bed adsorption
EGFR	epidermal growth factor receptor
Fab	antigen-binding antibody fragment
FAB	antigen-binding fragment of cetuximab
Fc	constant / crystallizable antibody fragment
GLU	glucose isomerase
HGMF	high-gradient magnetic fishing
HPLC	high-performance liquid chromatography
ID	inner diameter

IGF1	insulin-like growth factor I
IgG	immunoglobulin G
IgM	immunoglobulin M
IL	ionic liquid
LIP	lipase
LYS	lysozyme
MIR	mid infrared spectroscopy
PB	phosphate buffer
PDB	Protein Data Bank
PEG	polyethylene glycol
PESU	polyethersulfone
pI	isoelectric point
RTIL	room temperature ionic liquid
SC	sodium citrate
SDS-PAGE	sodium dodecyl sulfate polyacrylamide gel electrophoresis
SEC	size exclusion chromatography
UniProt	Universal Protein Resource
XYL	xylanase

8.2 Symbols and variables

A	CNT model coefficient A	s^{-1}
B	CNT model coefficient B	-
B_{22}	second virial coefficient	$mol\ mL\ g^{-2}$
c	concentration	$mol\ L^{-1}$, $g\ L^{-1}$
c_c	concentration inside dense liquid clusters	$mol\ L^{-1}$, $g\ L^{-1}$
c_{eq}	concentration at equilibrium	$mol\ L^{-1}$, $g\ L^{-1}$
crystallization yield	relative crystallization yield	-
ε	extinction coefficient	$mol\ L^{-1}\ cm^{-1}$
E	extinction	-
	or: Young's modulus	GPa
ΔG^0_{cryst}	change of the Gibbs free energy	$J\ mol^{-1}$
ΔG_2	energy barrier for nucleation inside dense liquid clusters	J
γ	surface free energy of the critical cluster	$J\ m^2$
ΔH^0_{cryst}	change of the enthalpy	$J\ mol^{-1}$
J	nucleation rate	$L^{-1}\ s^{-1}$
k_2	constant scaling the nucleation rate of crystals insite the clusters	$Pa\ g^{-1}\ K^{-1}$
k_B	Boltzmann constant	$J\ K^{-1}$
M	molar mass	$g\ mol^{-1}$
$\Delta\mu_c$	chemical potential of a protein molecule inside a dense liquid cluster	J
η	viscosity inside a dense liquid cluster	$Pa\ s$

r	size of the crystal nucleus	m
r_c	critical crystal nucleus size	m
ΔS^0_{cryst}	change of the entropy	J mol^{-1} K^{-1}
σ	thermodynamic supersaturation	-
T	temperature	K, °C
U_1	effective decay rate of dense liquid clusters	-
U_2	effective formation rate of dense liquid clusters	-
Ω	molecular protein volume	m^3

8.3   Material

8.3.1 Equipment

Table 8.1: Standard laboratory equipment.

Equipment	Name / Code	Manufacturer, location
Balance	Acculab VIC-123	Sartorius AG
Balance	ECON EC-411	Sartorius AG
Centrifuge	Rotixa 50 RS	Hettich, Tuttlingen, Germany
Chromatography	ÄKTApilot	GE Healthcare GmbH, Solingen, Germany
Cooling incubator	KB 53 and KB 115	Binder, Tuttlingen, Germany
Double distillation still	2108	Gesellschaft für Labortechnik mbH, Burgwedel, Germany
SDS-PAGE power supply	E802	Consort, Turnhout, Belgium
Freezer	Santo 604	AEG
Microliter pipettes	Transferpette S (1 µL, 10 µL, 20 µL, 100 µL, 200 µL, 1 mL, 10 mL)	Brand GmbH, Wertheim, Germany
pH-meter	S47 SevenMulti	Mettler Toledo
pH-electrode	InLab Micro	Mettler Toledo
Refrigerated centrifuge	5415 R	Eppendorf, Hamburg, Germany
SDS-PAGE chamber		OWL, Portsmouth, USA
UV/VIS spectrophotometer	GENESYS 10S	Thermo Fischer Scientific, Dreieich, Germany
Vortex	Vortex Genie 2	Scientific Industries, Bohemia, NY, USA

Table 8.2: Components of the Size Exclusion Chromatography (SEC) system.

Equipment	Name / Code	Manufacturer, location
Pump	S1110	Sykam, Eresing, Germany
Column	Superdex 200 10/300 GL	GE Healthcare GmbH, Solingen, Germany
Degaser	DEGAS	Shodex Europe, Munich, Germany
6-port 3-channel injection valve	-	Knauer, Berlin, Germany
Flow-Through absorption cell	178.010-QS, d = 10 mm	Hellma GmbH & Co. KG, Müllheim, Germany
Software	DHGenesysLogger	(own work)

Table 8.3: Components of the High Performance Liquid Chromatography (HPLC) system.

Equipment	Name / Code	Manufacturer, location
HPLC	Agilent 1000 Series	Agilent Technologies, Santa Clara, CA, USA
Quat. Pump	DE14918242	Agilent Technologies, Santa Clara, CA, USA
Autosampler	DE14918655	Agilent Technologies, Santa Clara, CA, USA
A/D-Converter	CN 00003423	Agilent Technologies, Santa Clara, CA, USA
Degasser	JP05033450	Agilent Technologies, Santa Clara, CA, USA
RI-Detector	1200 Series G1362A	Agilent Technologies, Santa Clara, CA, USA
UV-Detector	S 3300	Knauer, Berlin, Germany
Column	Aminex HPX-87H	Bio-rad Laboratories, Inc., Hercules, USA
Guard	HPLC Cation H Refill, 30*4.6MM	Bio-rad Laboratories, Inc., Hercules, USA
Software	A.05.01 + Rev E.01.02	Agilent Technologies, Santa Clara, CA, USA

Table 8.4: Components of the Cross-flow filtration system A.

Equipment	Name / Code	Manufacturer, location
Crossflow system	Sartoflow Slice 200 Benchtop System	Sartorius Stedim, Göttingen
PESU membrane	PESU-5 kD, 0.1 m² filter area	Sartorius Stedim, Göttingen
Scale	Talent TE 4100	Sartorius Stedim, Göttingen
Peristaltic pump	Tandem 1082	Sartorius Stedim, Göttingen

Table 8.5: Components of the Cross-flow filtration system B.

Equipment	Name / Code	Manufacturer, location
Pump	SartoJet HSE-U-72	Sartorius Stedim, Göttingen
Filter holder	Sartocon Slice	Sartorius Stedim, Göttingen
PESU membrane	PESU-5 kD; 0.1 m² filter area	Sartorius Stedim, Göttingen
Analog pressure gages	EN 837-1/0-4 bar	WIKA Alexander Wiegand SE & Co. KG, Klingenberg
Digital pressure gage	20100-100853-04	ifm electronic GmbH, Essen
Capacitative sensor	KQ6004	ifm electronic GmbH, Essen
Diaphragm valves	GEMÜ 601	GEMÜ GmbH & Co. KG, Ingelfingen-Criesbach

Table 8.6: Components of the Zeiss microscopy system.

Equipment	Name / Code	Manufacturer, location
Microscope	Axioplan	Carl Zeiss Microscopy GmbH, Jena
Lens A	Plan-Neofluar 10x/0.30; No. 440331	Carl Zeiss Microscopy GmbH, Jena
Lens B	Plan-Neofluar 2.5x/0.075; No. 440310	Carl Zeiss Microscopy GmbH, Jena
Camera	AxioCam ICc3	Carl Zeiss Microscopy GmbH, Jena
Software	AxioVision	Carl Zeiss Microscopy GmbH, Jena

Table 8.7: Components of the Nikon microscopy system.

Equipment	Name / Code	Manufacturer, location
Microscope	Eclipse 50i; No. MBA85020	Nikon Instruments Eurpoe BV, Amsterdam, The Netherlands
Lens A	Plan Chromat 4x/0.10; No. MRL00042	Nikon Instruments Eurpoe BV, Amsterdam, The Netherlands
Lens B	Plan Fluor 10x/0.3; No. MRH00101	Nikon Instruments Eurpoe BV, Amsterdam, The Netherlands
Camera	DS-2Mv; No. MQA12000	Nikon Instruments Eurpoe BV, Amsterdam, The Netherlands
Dual video port module	Y-IDP; No. MBB74105	Nikon Instruments Eurpoe BV, Amsterdam, The Netherlands
Software	NIS Elements (version: AR 3.2 64-bit)	Nikon Instruments Eurpoe BV, Amsterdam, The Netherlands

Table 8.8: Components of the 1 L-scale crystallization system.

Equipment	Name / Code	Manufacturer, location
Reaction vessel	107036314/2L	Rettberg GmbH, Göttingen, Germany
Pitched-bladed impeller	Z81315R007	IUL Instruments GmbH, Königswinter, Germany
Stepping motor	AS4118L1804-E	Nanotec Electronic GmbH & Co. KG, Feldkirchen, Germany
Motor control	SMCI33-1	Nanotec Electronic GmbH & Co. KG, Feldkirchen, Germany
Refrigerating circulator	1157P	VWR, Darmstadt, Germany
Software	DHCrystalControl	(own work)

Table 8.9: Components of the 100 mL-scale crystallization system.

Equipment	Name / Code	Manufacturer, location
Reaction vessel	11 21 60 136	Schott AG, Mainz, Germany
Stepping motor	ST2818L1006-B	Nanotec Electronic GmbH & Co. KG, Feldkirchen, Germany
Motor control	SMCI33-1	Nanotec Electronic GmbH & Co. KG, Feldkirchen, Germany
Refrigerating circulator	1157P	VWR, Darmstadt, Germany
Software	DHCrystalControl	(own work)

Table 8.10: Components of the 5 mL-scale crystallization system.

Equipment	Name / Code	Manufacturer, location
Reaction vessel	21 601 14 07	Schott AG, Mainz, Germany
Stepping motor	ST2019S0604-B	Nanotec Electronic GmbH & Co. KG, Feldkirchen, Germany
Motor control	SMCI33-1	Nanotec Electronic GmbH & Co. KG, Feldkirchen, Germany
Refrigerating circulator	1157P	VWR, Darmstadt, Germany
Software	DHCrystalControl	(own work)

8.3.2 Chemicals

Table 8.11: General chemicals.

Chemical	Purity	Manucafturer	No.
Acetic acid	100 %	Roth	3738
Acrylamide (aqueous 40 % acrylamide and bisacrylamide stock solution)		Roth	A516
Ammonium peroxydisulphate	≥ 98 %	Roth	9592
Ammonium sulfate	≥ 99.5 %	Roth	3746
Bismuth(III) subnitrate	98 %	Sigma-Aldrich	310646
Bromphenol blue		Merck	108122
Choline chloride	≥ 98 %	Sigma-Aldrich	C7527

Table 8.11: General chemicals (continued).

Chemical	Purity	Manucafturer	No.
Coomassie staining solution (Roti®-Blue)		Roth	A152
L-Cysteine chloride monohydrate	≥ 99 %	Roth	1694
di-Sodium hydrogen phosphate dodecahydrate	≥ 99 %	Roth	T106
EDTA	≥ 99 %	Roth	8040
Ethanol	≥ 99.9 %	Roth	P076
Glycerol	≥ 99.5 %	Roth	3783
Guanidine hydrochloride	≥ 99.5 %	Roth	0037
Gum arabic		Roth	4159
Hydrochloric acid	37 %	Roth	4625
β-Mercaptoethanol	≥ 99 %	Roth	4227
4-nitrophenyl palmitate		Sigma-Aldrich	N2752
PEG 200		Sigma-Aldrich	11309110
PEG 3 000		Sigma-Aldrich	11109094
PEG 10 000		Clariant	DEG4100252
PEG 20 000		Sigma-Aldrich	1411158
PEG 35 000		Clariant	DEG4046971
Potassium dihydrogen phosphate, anhydrous	≥ 99 %	Roth	P749
Potassium iodide	≥ 99.5 %	Sigma-Aldrich	30315
SDS-PAGE running buffer (10x)		Roth	3060
Sodium acetate trihydrate	≥ 99.5 %	Roth	6779
Sodium chloride	≥ 99 %	Roth	P029
Sodium dihydrogenphosphate monohydrate	≥ 98 %	Roth	K300
Sodium dodecyl sulfate		Merck	817034
Sodium hydroxide	≥ 99 %	Roth	6771
Sodium tetraborate decahydrate		Sigma-Aldrich	31457
TEMED		Roth	2367
tri-Sodium citrate dihydrate	≥ 99 %	Roth	3580
Tris(hydroxymethyl)amonimethane (TRIS)	≥ 99.9 %	Sigma-Aldrich	154563
Triton X-100		Roth	3051

Table 8.12: Proteins which were not crystallized. cooperation partner*: Merck KGaA, Darmstadt, Germany.

Protein	Manufacturer	No.
Albumin	Sigma-Aldrich, Taufkirchen	A3059-50G
Endonuclease	prov. by cooperation partner	-
Gammanorm	Octapharma	C909A860A
Papain	Sigma-Aldrich, Taufkirchen	76216-50MG

Table 8.13: Ionic liquids used in this work and their abbreviations, molecular formulae and molecular masses.

Ionic liquid	Details	Manuf.	No.
1-butyl-4-(dimethylamino)-pyridinium chloride	[bDMAP][Cl] $C_{11}H_{19}ClN_2$ 214.7 g mol^{-1}	Merck	IOLI-JE-1206
1-ethyl-4-(dimethylamino)-pyridinium chloride	[eDMAP][Cl] $C_9H_{15}ClN_2$ 186.7 g mol^{-1}	Merck	IOLI-JE-1209
1-methyl-4-(dimethylamino)-pyridinium chloride	[mDMAP][Cl] $C_8H_{13}ClN_2$ 172.7 g mol^{-1}	Merck	IOLI-JE-1210
2-hydroxyethylammonium formate	2-HEAF / IL 1.1 $C_3H_9NO_3$ 107.1 g mol^{-1}	Merck	IOLI-JE-1389
4-(2-hydroxyethyl)-morpholinium chloride	[(eOH)mmo][Cl] $C_6H_{14}ClO_2N$ 167.7 g mol^{-1}	Merck	IOLI-JE-1211
4-cyanomethylmorpholinium chloride	[(mCN)mmo][Cl] $C_6H_{11}ClON_2$ 162.6 g L^{-1}	Merck	IOLI-JE-1208
Bis-(2-methoxyethyl)-ammonium acetate	IL 2 $C_8H_{19}NO_4$ 193.2 g mol^{-1}	Bioniqs	006-102

Table 8.13: Ionic liquids used in this work and their abbreviations, molecular formulae and molecular masses (continued).

Ionic liquid	Details	Manuf.	No.
Choline dihydrogenphosphate	CDHP / IL 4 $C_5H_{16}NPO_5$ 201.2 g mol^{-1}	Merck	IOLI-JE-1388
Ethylammonium nitrate	EAN / IL 1.2 $C_2H_8N_2O_3$ 108.1 g mol^{-1}	IoLiTec	IL-0043
N,N-dimethylethynolammonium acetate	IL 3.2 $C_6H_{15}NO_3$ 149.2 g mol^{-1}	Bioniqs	111-102
N,N-dimethylethynolammonium glycolate	IL 3.1 $C_6H_{15}NO_4$ 165.2 g mol^{-1}	Bioniqs	111-112

8.3.3 Buffer compositions

Table 8.14: Solutions for the sodium docecyl sulfate polyacrylamide gel electrophoresis.

Substance	Concentration
Stacking gel buffer (2x)	
Sodium dodecyl sulfate (SDS)	0.4 % (w/v)
Tris-HCl pH 6.8	0.25 M
Separating gel buffer (4x)	
Sodium dodecyl sulfate (SDS)	0.8 % (w/v)
Tris-HCl pH 6.8	1.5 M
Laemmli buffer (5x)	
Bromphenol blue	0.05 % (w/v)
Glycerol	50 % (v/v)
β-Mercaptoethanol	5 % (v/v)
Running buffer (10x)	10 % (w/v)
Sodium dodecyl sulfate (SDS)	10 % (w/v)

Table 8.15: Solutions for the Coomassie staining.

Substance	Concentration
Fairbanks A	
Acetic acid	10 % (v/v)
Coomassie Brilliant Blue R-250	0.05 % (w/v)
Isopropanol	25 % (v/v)
Fairbanks B	
Acetic acid	10 % (v/v)
Coomassie Brilliant Blue R-250	0.005 % (w/v)
Isopropanol	10 % (v/v)
Fairbanks C	
Acetic acid	10 % (w/v)

Table 8.16: Solutions for the functional lipase assay.

Substance	Concentration
Solution A	
4-nitrophenyl palmitate	3 g L^{-1} in n-propanol
Solution B	
Gum Arabic	1 g L^{-1}
Tris-HCl pH 7.5	2.5 M
Triton X-100	5 g L^{-1}

Table 8.17: Solutions for the PEG determination using a modified Dragendorff reagent.

Substance	Concentration
Solution A	
Bismuth(III) subnitrate	16 g L^{-1} in 1 M HCl
Solution B	
Potassium iodide	400 g L^{-1}

8.4   Papain digestion of cetuximab

The Fab fragment of cetuximab (FAB) was generated by papain digestion of the antibody cetuximab. The papain digestion was characterized rudimentarily prior to the large-scale digestion. The results of an SDS-PAGE of samples taken during the papain digestion of 1 mg cetuximab are shown in Figure 8.1.
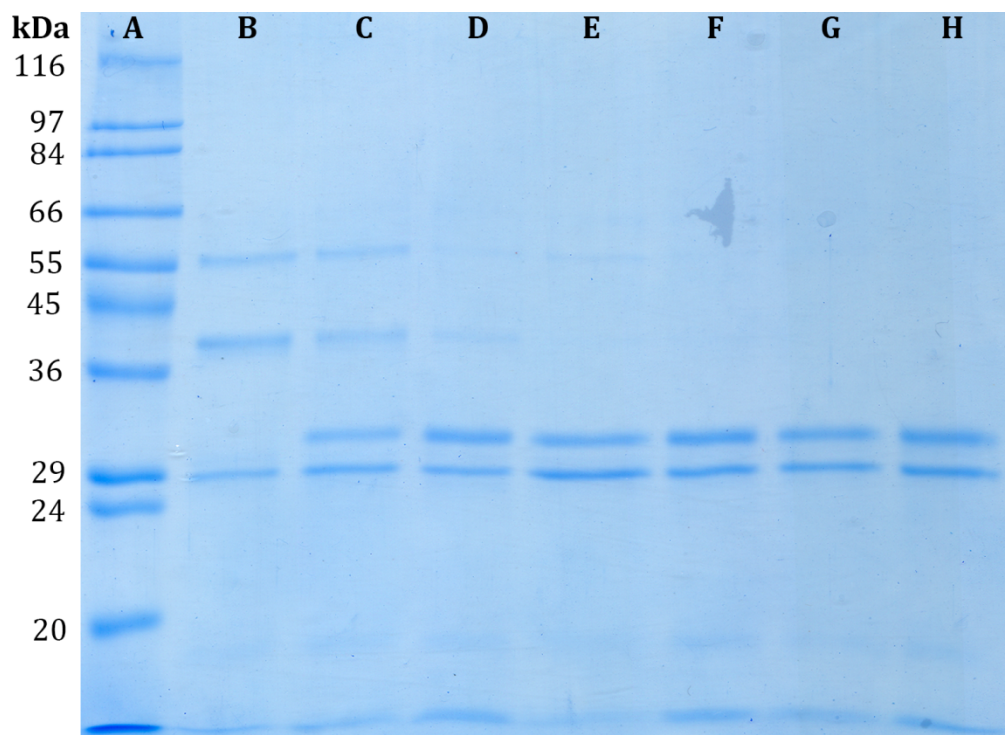
Figure 8.1: SDS-PAGE of a preliminary papain digestion of 1 mg cetuximab. **A)** Molecular weight marker; digest after **B)** 0 min, **C)** 20 min, **D)** 40 min, **E)** 60 min, **F)** 80 min, **G)** 100 min, and **H)** 120 min.

While the heavy chain (≈ 55 kDa) and intermediates (≈ 40 kDa) are present in the first samples, the digestion was complete after 60 min.

8.5 Quantification of crystallization agents

8.5.1 High Performance Liquid Chromatography (HPLC)

The components of the HPLC system are listed in Table 8.3. The oven temperature was 60 °C, 5 mM sulfuric acid were used as eluent phase and the eluent flow rate was 0.7 mL min^{-1}. The retention times of the substances under study are listed in .

Table 8.18: Retention times of the substances under study.

Substance	Retention time, min
Acetate	12.9
Citrate	7.2
Formate	12.0
2-Hydroxyethylammonium	19.2
Phosphate	7.6

8.5.2 PEG determination using a modified Dragendorff reagent method

Dragendorff reagent was prepared by mixing 2.5 mL of each solution A and solution B and adding ddH$_2$O to a volume 50 mL. 250 μL sample, 200 μL HCl (50 mM) and 50 μL Dragendorff reagent were mixed in a cuvette. After incubation at RT for 15 min, the measurement was performed via VIS-spectroscopy at 510 nm. The calibration curve recorded for PEG 10000 is shown in Figure 8.2.
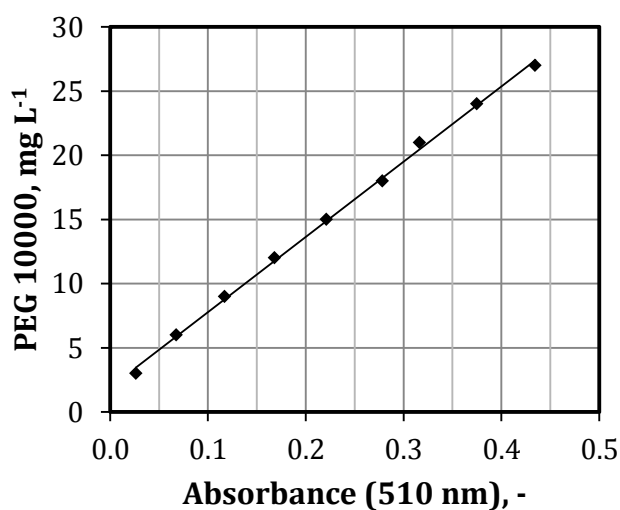
Figure 8.2: Calibration curve fort he determination of PEG 10000 using a modified Dragendorff reagent method. The line was obtained using linear regression (MS Excel): c_{PEG} = 58.6 mg L^{-1} · E + 1.9 mg L^{-1}.

8.5.3 Sodium chloride determination

The concentration of sodium chloride was determined using a modified protocol for a chloride test kit (Merck, Darmstadt, Germany). 300 µL sample were mixed with 150 µL reagent A and 30 µL reagent B. The composition of these reagents was not detailed in the description of the test kit. After incubation at RT for 10 min, the measurement was performed via VIS-spectroscopy at 492 nm. The calibration curve recorded for 0 - 50 g L^{-1} sodium chloride is depicted in Figure 8.3.
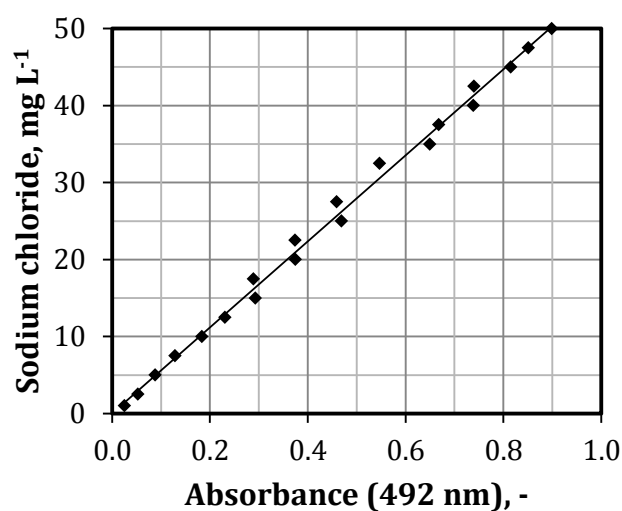
Figure 8.3: Calibration curve for the determination of NaCl using the modified protocol for the commercial chloride test kit. The line was obtained using linear regression (MS Excel): c_{NaCl} = 55.8 mg L^{-1} · E + 0.016 mg L^{-1}.

8.6 Protein sequences

Lysozyme (LYS)

```
KVFGRCELAA AMKRHGLDNY RGYSLGNWVC AAKFESNFNT QATNRNTDGS
TDYGILQINS RWWCNDGRTP GSRNLCNIPC SALLSSDITA SVNCAKKIVS
DGNGMNAWVA WRNRCKGTDV QAWIRGCRL
```

Lipase (LIP)

```
MRSSLVLFFV SAWTALASPI RREVSQDLFN QFNLFAQYSA AAYCGKNNDA
PAGTNITCTG NACPEVEKAD ATFLYSFEDS GVGDVTGFLA LDNTNKLIVL
SFRGSRSIEN WIGNLNFDLK EINDICSGCR GHDGFTSSWR SVADTLRQKV
EDAVREHPDY RVVFTGHSLG GALATVAGAD LRGNGYDIDV FSYGAPRVGN
RAFAEFLTVQ TGGTLYRITH TNDIVPRLPP REFGYSHSSP EYWIKSGTLV
PVTRNDIVKI EGIDATGGNN QPNIPDIPAH LWYFGLIGTC L
```

Xylanase (XYL)

```
QTIQPGTGYN NGYFYSYWND GHGGVTYTNG PGGQFSVNWS NSGNFVGGKG
WQPGTKNKVI NFSGSYNPNG NSYLSVYGWS RNPLIEYYIV ENFGTYNPST
GATKLGEVTS DGSVYDIYRT QRVNQPSIIG TATFYQYWSV RRNHRSSGSV
NTANHFNAWA QQGLTLGTMD YQIVAVEGYF SSGSASITVS
```

Glucose isomerase (GLU)

```
MNYQPTPEDR FTFGLWTVGW EGRDPFGDAT RRALDPVESV RRLAELGAHG
VTFHDDDLIP FGSSDSEREE HVKRFRQALD DTGMKVPMAT TNLFTHPVFK
DGGFTANDRD VRRYALRKTI RNIDLAVELG AETYVAWGGR EGAESGGAKD
VRDALDRMKE AFDLLGEYVT SQGYDIRFAI EPKPNEPRGD ILLPTVGHAL
AFIERLERPE LYGVNPEVGH EQMAGLNFPH GIAQALWAGK LFHIDLNGQN
GIKYDQDLRF GAGDLRAAFW LVDLLESAGY SGPRHFDFKP PRTEDFDGVW
ASAAGCMRNY LILKERAAAF RADPEVQEAL RASRLDELAR PTAADGLQAL
LDDRSAFEEF DVDAAAARGM AFERLDQLAM DHLLGARG
```

Cetuximab

Heavy chain

```
QVQLKQSGPG LVQPSQSLSI TCTVSGFSLT NYGVHWVRQS PGKGLEWLGV
IWSGGNTDYN TPFTSRLSIN KDNSKSQVFF KMNSLQSNDT AIYYCARALT
YYDYEFAYWG QGTLVTVSAA STKGPSVFPL APSSKSTSGG TAALGCLVKD
YFPEPVTVSW NSGALTSGVH TFPAVLQSSG LYSLSSVVTV PSSSLGTQTY
ICNVNHKPSN TKVDKRVEPK SPKSCDKTHT CPPCPAPELL GGPSVFLFPP
KPKDTLMISR TPEVTCVVVD VSHEDPEVKF NWYVDGVEVH NAKTKPREEQ
YNSTYRVVSV LTVLHQDWLN GKEYKCKVSN KALPAPIEKT ISKAKGQPRE
PQVYTLPPSR DELTKNQVSL TCLVKGFYPS DIAVEWESNG QPENNYKTTP
PVLDADGSFF LYSKLTVDKS RWQQGNVFSC SVMHEALHNH YTQKSLSLSP
GKFFFFFF
```

Light chain

```
DILLTQSPVI LSVSPGERVS FSCRASQSIG TNIHWYQQRT NGSPRLLIKY
ASESISGIPS RFSGSGSGTD FTLSINSVES EDIADYYCQQ NNNWPTTFGA
GTKLELKRTV AAPSVFIFPP SDEQLKSGTA SVVCLLNNFY PREAKVQWKV
DNALQSGNSQ ESVTEQDSKD STYSLSSTLT LSKADYEKHK VYACEVTHQG
LSSPVTKSFN RGA
```

Fab (FAB)

```
QVQLKQSGPG LVQPSQSLSI TCTVSGFSLT NYGVHWVRQS PGKGLEWLGV
IWSGGNTDYN TPFTSRLSIN KDNSKSQVFF KMNSLQSNDT AIYYCARALT
YYDYEFAYWG QGTLVTVSAA STKGPSVFPL APSSKSTSGG TAALGCLVKD
YFPEPVTVSW NSGALTSGVH TFPAVLQSSG LYSLSSVVTV PSSSLGTQTY
ICNVNHKPSN TKVDKRVEPK S
```

8.7 Technical drawings of the 5 mL- and 100 mL-crystallizers

8.7.1 Technical drawing of the 5 mL-scale crystallizer
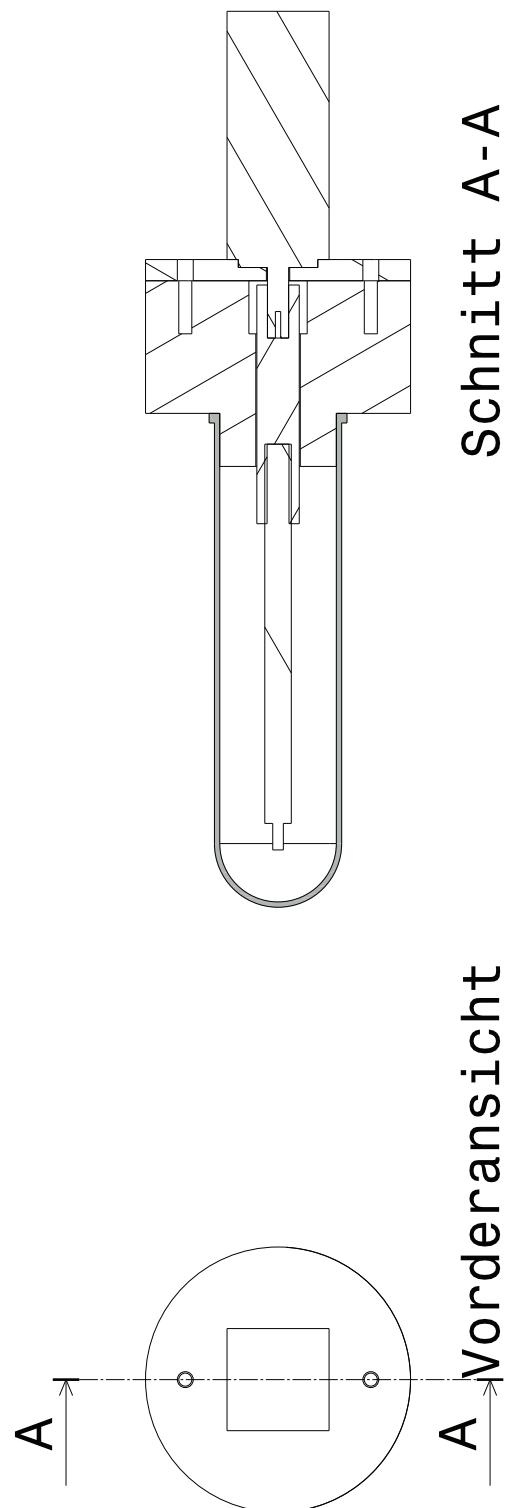
Figure 8.4: Technical drawing of the 5 mL-scale crystallizer.

8.7.2 Technical drawing of the 100 mL-scale crystallizer

SchnittansichtG-G
Maßstab: 1:2

I

H

Detail I
Maßstab: 2:1

G   G

Vorderansicht
Maßstab: 1:2

Detail H
Maßstab: 2:1
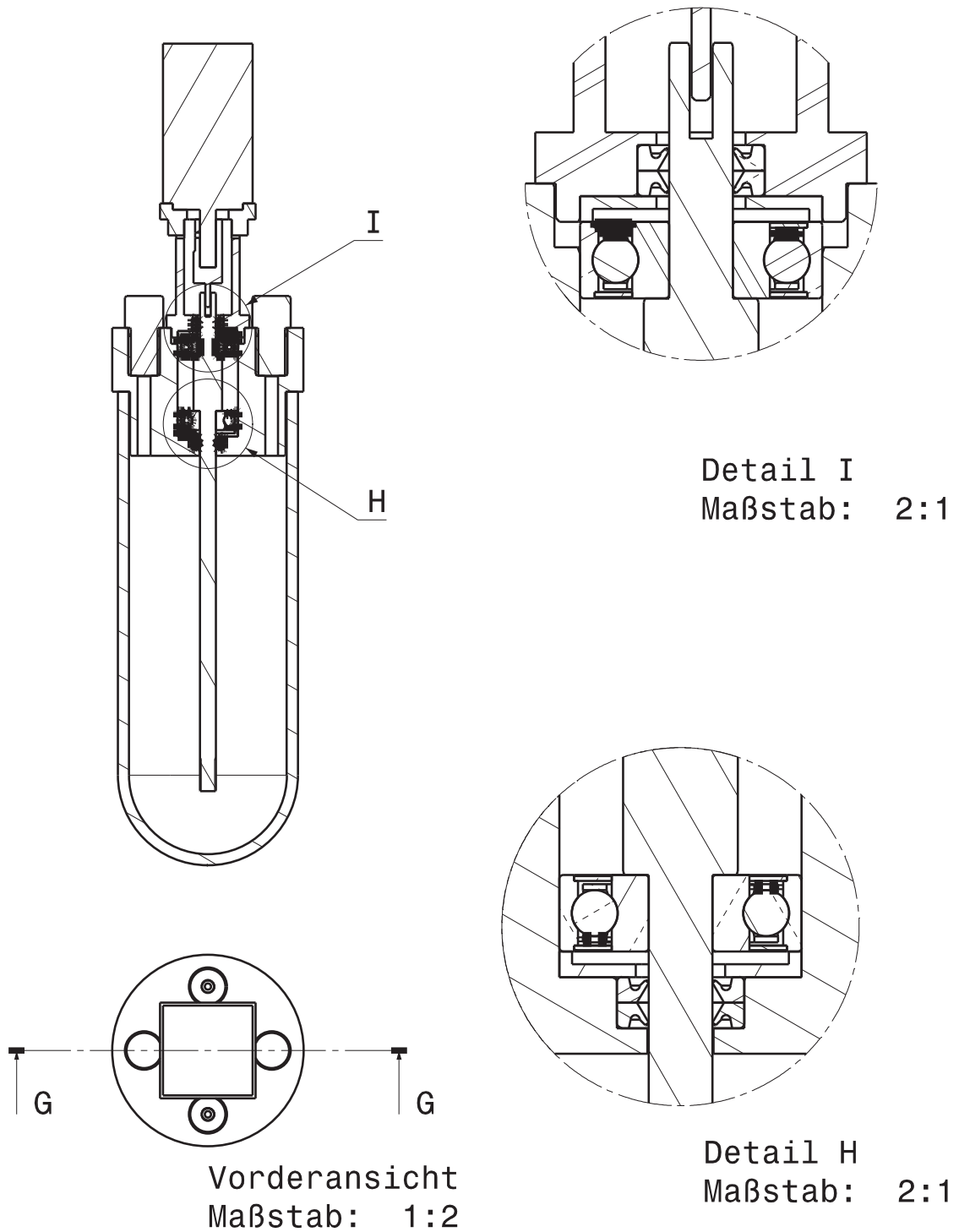
Figure 8.5: Technical drawing of the 100 mL-scale crystallizer.

SchnittansichtB-B

12

2

4.5

1

ϕ7

Isometrische Ansicht

Untersicht Rührerkopf

15

4.9

A

A

1

B

R3.5

B

45°

Vorderansicht Rührerkopf

M4

SchnittansichtA-A

120°

120°

Vorderansicht Rührerblatt

3.42

R4

R1

12.98

R14.26

120°

150°

Draufsicht Rührerblatt

1
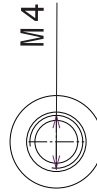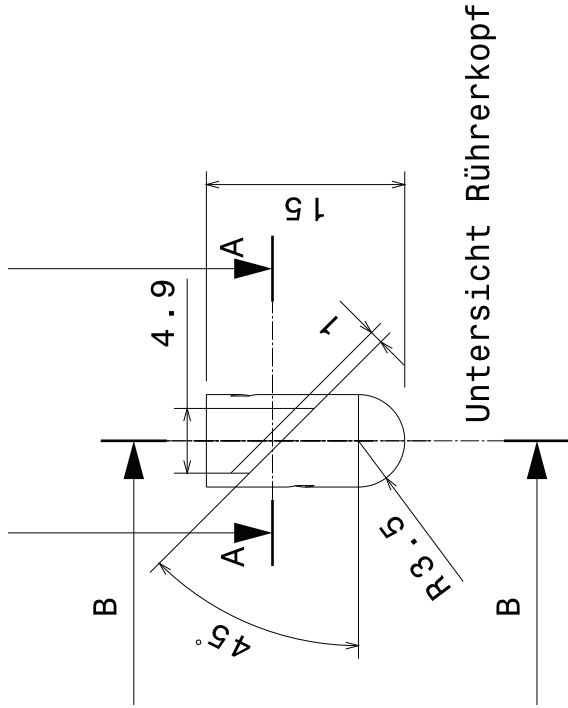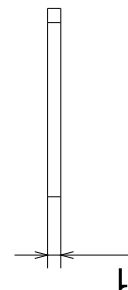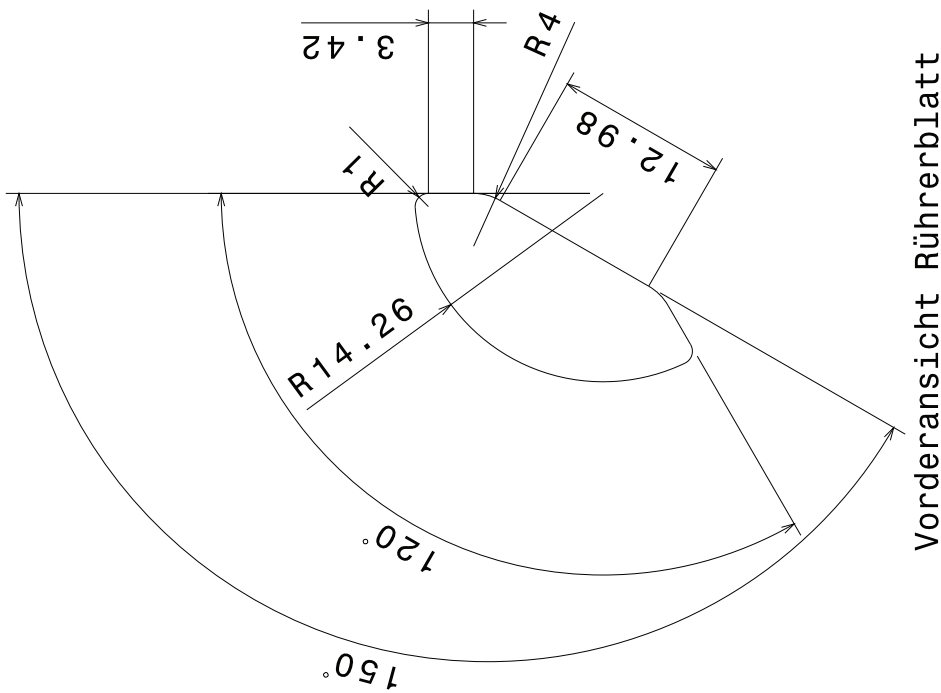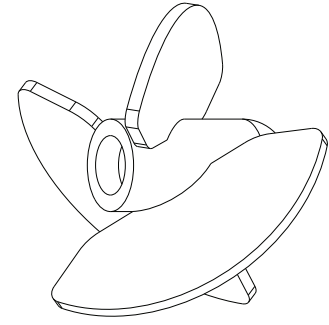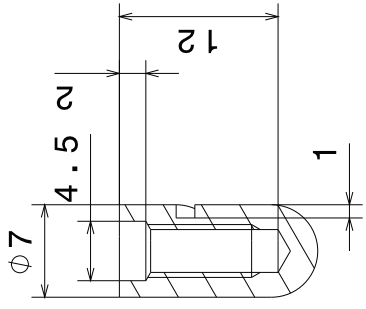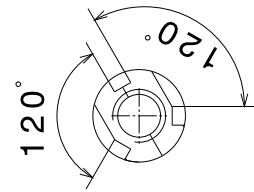
Figure 8.6: Technical drawing of the pitched-bladed impellers for the 100 mL-scale crystallizer.

8.8   List of Tables

8.9   List of Figures